

**Advanced Control Techniques for Grid-Interactive Smart Inverters under  
Asymmetrical Conditions**

by

Masoud Mohammadalizadeh Shabestary

A thesis submitted in partial fulfillment of the requirements for the degree of

Doctor of Philosophy

in

Energy Systems

Department of Electrical and Computer Engineering  
University of Alberta

© Masoud Mohammadalizadeh Shabestary, 2019

## **Abstract**

Grid-interactive smart inverters (GSIs) are becoming the main interface for integrating modern power units, such as renewable energies, energy storage systems, electric vehicles, distributed generation (DG) units, microgrids, and high-voltage direct-current transmission systems into smart power grids. Their expected high integration in future smart grids brings certain reliability and complexity challenges. Tackling these challenges with advanced control techniques can provide more efficient and optimal operation in future highly interconnected power grids. Riding through abnormalities while supporting host grids by smart inverters is one of these challenges which has attracted a lot of attention among system operators, regulatory organizations, manufacturing companies, and academia. This research project thus aims to present novel techniques in four stages for optimal and more reliable operation of GSIs, utilized in different configurations, under asymmetric grid conditions.

In the first stage, a comprehensive control scheme, with multiple objectives, is proposed for the optimal operation of a single GSI under unbalanced grid conditions. These optimal behaviors bring significant advantages to the emerging GSIs, empowering them to be more fault resilient and smartly responsive to abnormal grid conditions. They also provide noteworthy benefits to the host grid such as improving its stability, delivering maximum ancillary services, avoiding unnecessary outages, better complying with the grid interconnection codes, and increasing overall efficiency, reliability, and profitability. In the second stage, this

research proposes a regulation guideline for riding through asymmetric faults as well as dynamic flexible support of the grid. To date, most of the available grid codes only focus on the regulation of the DG operation under balanced faults due to the complexity, lacking the proper remedies for more common unbalanced conditions. Implementing in different test cases and using comparative analyses, the proposed regulation guideline and its unique control technique are proven to be very effective and superior to the state-of-the-art methods. They can thus be adopted by the updated versions of grid codes for more efficient integration of large GSIs and DG units. In the third stage, a novel voltage support scheme is proposed with improved accuracy in regulating the phase voltages within the pre-set safety limits, by (1) considering the zero-sequence voltage compensation, (2) considering the output active power and being adaptive to complex grid impedance, (3) augmenting the adjustable limited active power oscillation and the maximum active power delivery strategies. This empowers large DG units to provide their maximum asymmetric support to the grid without a negative impact on their performance. In the last stage of the thesis, the proposed techniques are extended for multiple GSIs structures: (1) parallel-operated grid-interactive inverters (e.g., in hybrid energy sources) and (2) multiple distributed inverters (e.g., in multi-DG active distribution networks).

The effectiveness of the proposed techniques is validated using simulation and experimental results. The proposed techniques facilitate the effective integration of renewable energy resources, via reliable GSIs, into smart power grids.

## Preface

This thesis is an original work by Masoud Shabestary. As detailed in the following, some chapters of this thesis have been published or submitted for publication as scholarly articles in which Professor Yasser Abdel-Rady I. Mohamed was the supervisory author and has contributed to concepts formation and the manuscript composition.

Materials in Chapter 2 have been published as two articles:

- M. M. Shabestary, and Y. A. I. Mohamed, "An Analytical Method to Obtain Maximum Allowable Grid Support by Using Grid-Connected Converters," in *IEEE Transactions on Sustainable Energy*, vol. 7, no. 4, pp. 1558-1571, Oct. 2016.
- M. M. Shabestary, and Y. A. I. Mohamed, "Analytical Expressions for Multi-objective Optimization of Converter-Based DG Operation Under Unbalanced Grid Conditions," in *IEEE Transactions on Power Electronics*, vol. 32, no. 9, pp. 7284-7296, Sept. 2017.

A version of Chapter 3 has been published as

- M. M. Shabestary, and Y. A. I. Mohamed, "Asymmetrical Ride-Through and Grid Support in Converter-Interfaced DG Units Under Unbalanced Conditions," in *IEEE Transactions on Industrial Electronics*, vol. 66, no. 2, pp. 1130-1141, Feb. 2019.

A version of Chapter 4 has been published as

- M. M. Shabestary, and Y. A. I. Mohamed, "Advanced Voltage Support and Active Power Flow Control in Grid-Connected Converters Under Unbalanced Conditions," in *IEEE Transactions on Power Electronics*, vol. 33, no. 2, pp. 1855-1864, Feb. 2018.

A version of Chapter 5 has been submitted as

- M. M. Shabestary, and Y. A. I. Mohamed, "Maximum Asymmetrical Support in Parallel-Operated Grid-Interactive Smart Inverters," *IEEE Transactions on Smart Grids*, Jan 2019.

A version of Chapter 6 has been submitted as

- M. M. Shabestary, and Y. A. I. Mohamed, "Decentralized Maximum Flexible Asymmetrical Support Tracking in Active Distribution Networks with Multiple DG Units," *IEEE Transactions on Smart Grids*, Dec 2018.

*This thesis work is dedicated to my wife, who has been a constant source of support and encouragement during the challenges of my graduate studies and life.*

*I am truly thankful for having you in my life.*

*This work is also dedicated to my parents, who have always inspired me and whose good examples have taught me to work hard for the things I aspire to achieve.*

## **Acknowledgment**

I would like to express my sincere appreciation to Prof. Yasser Abdel-Rady I. Mohamed for his great support and supervision during this research project. This research and dissertation would not have been possible without his continuous guidance.

Also, I would like to extend special thanks to my examining committee members, Prof. Yasser A. I. Mohamed, Prof. Venkata Dinavahi, and Prof. Yunwei (Ryan) Li for taking the time to review this thesis. I am also thankful to the faculty and staff members in the Department of Electrical and Computer Engineering at the University of Alberta who provided a pleasant working atmosphere for me during the past four years.

# Table of Contents

<b>ABSTRACT</b>	.....	<b>II</b>
<b>PREFACE</b>	.....	<b>IV</b>
<b>ACKNOWLEDGMENT</b>	.....	<b>VII</b>
<b>LIST OF ACRONYMS</b>	.....	<b>XII</b>
<b>LIST OF SYMBOLS</b>	.....	<b>XIII</b>
<b>CHAPTER 1</b>	<b>INTRODUCTION</b> .....	<b>1</b>
1.1	BACKGROUND.....	1
1.2	STATE-OF-THE-ART .....	3
1.3	MOTIVATIONS AND OBJECTIVES .....	5
1.4	THESIS OUTLINE .....	7
1.5	SUMMARY OF THE KEY CONTRIBUTIONS .....	10
<b>CHAPTER 2</b>	<b>MAXIMUM ASYMMETRIC SUPPORT (MAS) IN A GRID-INTERACTIVE SMART INVERTER</b> .....	<b>11</b>
2.1	INTRODUCTION .....	11
2.2	SYSTEM DESCRIPTION.....	12
2.3	PROPOSED MULTI-OBJECTIVELY OPTIMIZED CONTROL STRATEGIES .....	14
2.3.1	<i>Minimum Oscillation on the Active and Reactive Powers</i> .....	15
2.3.2	<i>Minimum Fault Current (MFC) Strategy</i> .....	16
2.3.3	<i>Maximum Allowable Active and Reactive Powers Strategies</i> .....	17
2.4	VOLTAGE SUPPORT STRATEGY .....	18
2.5	MAXIMUM ASYMMETRIC SUPPORT (MAS) SCHEME .....	20
2.6	SIMULATION RESULTS .....	21
2.6.2	<i>Test Case A: Performance Evaluation of MOP and MOQ Strategies</i> .....	22
2.6.3	<i>Test Case B: Performance Evaluation of VSS-MAP Strategy</i> .....	22

2.7	EXPERIMENTAL RESULTS.....	23
2.7.2	<i>Experimental Test Case A: MFC Strategy</i> .....	24
2.7.3	<i>Experimental Test Case B: MAQ Strategy</i> .....	25
2.7.4	<i>Experimental Test Case B: MAP Strategy</i> .....	27
2.8	CONCLUSION .....	27
<b>CHAPTER 3</b>	<b>ASYMMETRIC RIDE-THROUGH (ART) GUIDELINES.....</b>	<b>28</b>
3.1	INTRODUCTION .....	28
3.2	OVERVIEW OF LVRT CODES IN DIFFERENT COUNTRIES .....	29
3.2.1	<i>Reactive current injection (RCI)</i> .....	30
3.2.2	<i>Frequency Control and Active Power Restoration</i> .....	31
3.3	PROPOSED ASYMMETRIC RIDE-THROUGH (ART) GUIDELINES.....	32
3.4	OVERVIEW OF CONVENTIONAL VOLTAGE SUPPORT STRATEGIES UNDER UNBALANCED CONDITIONS.....	36
3.4.1	<i>Positive-Sequence Reactive Current Injection (PSRCI)</i> .....	37
3.4.2	<i>Voltage Support Based on the Maximum Allowable Reactive Power Delivery (MARPD)</i> .....	38
3.4.3	<i>Mixed Sequence Injection (MSI)</i> .....	38
3.4.4	<i>Positive-Negative Sequence Voltage Regulation (PNVR)</i> .....	38
3.5	COMPLIANCE OF THE CONVENTIONAL VOLTAGE SUPPORT STRATEGIES WITH THE PROPOSED ART GUIDELINES .....	40
3.6	PROPOSED ART-ADAPTIVE VOLTAGE SUPPORT .....	45
3.6.1	<i>Determination of Dynamic Reference Values for Minimum and Maximum Phase Voltage Magnitudes</i> .....	46
3.6.2	<i>Reactive Current Injection</i> .....	48
3.7	SIMULATION RESULTS .....	48
3.8	EXPERIMENTAL RESULTS .....	53
3.9	DISCUSSION .....	56
3.10	CONCLUSION .....	57

<b>CHAPTER 4</b>	<b>ADVANCED ASYMMETRIC VOLTAGE REGULATION AND MAS SCHEME IN A SINGLE GRID-INTERACTIVE SMART INVERTER.....</b>	<b>59</b>
4.1	INTRODUCTION .....	59
4.2	PROPOSED ZERO-SEQUENCE COMPENSATED ASYMMETRIC VOLTAGE REGULATION (ZCVS) SCHEME.....	60
4.3	PROPOSED COMPLEMENTARY STRATEGIES.....	63
4.3.1	ZCVS with LAPO Strategy .....	63
4.3.2	ZCVS with MAPD Strategy.....	64
4.4	SIMULATION RESULTS .....	67
4.4.2	Test Case A: Traditional VSS vs Proposed ZCVS Method .....	68
4.4.3	Test Case B: ZCVS with LAPO and MAPD strategies.....	69
4.4.4	Test Case C: ZCVS Method under Various X/R Ratios.....	73
4.5	EXPERIMENTAL RESULTS.....	75
4.6	CONCLUSION .....	75
<b>CHAPTER 5</b>	<b>PARALLEL MAS SCHEME IN MULTIPLE PARALLEL-OPERATED GRID- INTERACTIVE SMART INVERTERS .....</b>	<b>76</b>
5.1	INTRODUCTION .....	76
5.2	PARALLEL-OPERATED INVERTERS.....	77
5.3	SYSTEM DESCRIPTION.....	79
5.4	PLANE OF NEGATIVE REACTIVE VS. POSITIVE REACTIVE (NRPR).....	82
5.4.1	Allowable Current Areas in NRPR Plane .....	83
5.4.1	Allowable Flexible Voltage Support Areas .....	84
5.5	PROPOSED OPTIMIZED ASYMMETRIC SUPPORT BY PMAS.....	86
5.5.1	Stage I: Obtaining NRPR Equations.....	86
5.5.1	Stage II: AFSA Boundary Curves.....	87
5.5.2	Stage III: Convolution of Boundary Curves.....	90
5.5.3	Stage IV: Determination of the Optimal Values.....	90
5.6	SIMULATION RESULTS .....	94

5.7	CONCLUSION .....	97
<b>CHAPTER 6            DECENTRALIZED MAS SCHEME IN MULTIPLE DISTRIBUTED GRID- INTERACTIVE SMART INVERTERS .....</b>		
<b>98</b>		
6.1	INTRODUCTION .....	98
6.2	MULTI-DG ACTIVE DISTRIBUTION NETWORK.....	100
6.3	PROPOSED DECENTRALIZED MAXIMUM FLEXIBLE ASYMMETRICAL SUPPORT TRACKING SCHEME .....	102
6.4	IDENTIFIED CONSTRAINTS FOR MSPT METHOD .....	105
6.4.1	<i>Active Power Oscillation Limit (POL) Constraint</i> .....	106
6.4.2	<i>Peak-Current Limitation (PCL) Constraint</i> .....	108
6.4.3	<i>Allowable Flexible Voltage Support Areas</i> .....	109
6.4.1	<i>Simplified MSPT</i> .....	110
6.5	PROPOSED STRATEGIES TO DETERMINE MAXIMUM SUPPORT POINTS BY DSPM.....	111
6.5.1	<i>MSPT with Flexible Ratio between Positive- and Negative-Sequences (FRPN)</i> .....	112
6.5.2	<i>MSPT with Bounded Autonomous Moving Points (BAMP) Approach</i> .....	112
6.6	SIMULATION RESULTS .....	114
6.6.1	<i>Test Case A: Conventional vs Proposed</i> .....	114
6.6.2	<i>Test Case B: Proposed Scheme under Severe Conditions</i> .....	118
6.7	CONCLUSION .....	120
<b>CHAPTER 7            CONCLUSION AND FUTURE WORK.....</b>		
<b>122</b>		
7.1	THESIS ACHIEVEMENTS .....	122
7.2	FUTURE WORKS.....	124
7.3	EXPECTED SIGNIFICANCE .....	125
<b>REFERENCES .....</b>		<b>126</b>

# List of Acronyms

AC	Alternating Current
ART	Asymmetric Ride-Through
DC	Direct Current
DG	Distributed Generation
DMAS	Decentralized MAS
DOS	Duration of Support
GSI	Grid-interactive Smart Inverter
HVDC	High-Voltage Direct-Current
LVRT	Low-Voltage Ride Through
MAS	Maximum Asymmetric Support
MSI	Mixed Sequence Injection
PCC	Point of Common Coupling
PCL	Peak Current Limitation
PLL	Phase-Locked Loop
PMAS	Parallel MAS
PNVR	Positive- and Negative-Sequence Voltage Regulation
POL	Power Oscillation Limit
RCI	Reactive Current Injection
NRPR	Negative Reactive vs. Positive Reactive
ZCVS	Zero-sequence Compensated Voltage Support

# List of Symbols

## A. *Superscripts*

- + Positive sequence components
- Negative sequence components
- \* Variable reference value
- ~ Oscillatory terms

## B. *Subscripts*

- $p$  Active Power Component
- $q$  Reactive Power Component

## C. *Variables and parameters*

- $i_g$  Grid currents
- $i_l$  Inverter currents
- $V$  Voltage at the PCC
- $P^*$  Reference active power of inverter
- $Q^*$  Reference reactive power of inverter
- $V_g$  Grid voltage
- $C_f$  Capacitance of the ac filter
- $R_g$  Equivalent grid resistance
- $L_g$  Equivalent grid inductance
- $X$  Equivalent grid reactance
- $\omega_0$  Grid angular frequency.
- $K_i$  Integrator gain of the current controller compensator of inverter
- $K_p$  Proportional gain of the current controller compensator of inverter
- $K_{i,PLL}$  Integrator gain of the PLL
- $K_{p,PLL}$  Proportional gain of the PLL

# Chapter 1

## Introduction

### 1.1 Background

In the past decade, driven by the worldwide concerns about the harmful foot-prints of the fossil fuels along with the economic and political concerns, integration of renewable energy resources, such as wind turbines and photovoltaic arrays, combined with energy storage systems, into power systems has attracted increasing attention as a vital solution. In 2015, the International Energy Agency has reported that the energy sector contributes to almost two-thirds of all anthropogenic greenhouse gas emission due to the use of fossil fuels [1]. Thanks to development in power electronic technologies, large integration of renewable energies has been possible by utilizing popular voltage source converters in various applications. According to German and Danish Energy Agencies, the share of renewable energy will be increased to almost 35% by 2020 in these countries, and the long-term goal is to achieve 80% and 100% renewable energy share in the electricity sector, respectively, in Germany [2] and Denmark [3] by 2050. Some other indicators that show the rapid evolution in energy systems are more than 400 microgrid projects [4] and more than 70 large high-voltage direct-current (HVDC) projects worldwide [5]. Thus, the power electronic converters play a more crucial role than ever before in smooth transition from conventional synchronous-generator-based power systems (fuel dominant) to future converter-based highly-integrated energy systems (renewable dominant).

Conventional fossil-fuel-based power plants have large synchronous generators, capable of supporting the grid by several important ancillary services, such as providing a large amount of fault current which is of great importance to support grid voltage and activate protective relays. In contrast, emerging converter-interfaced power units, such as different types of renewable-based distributed generation (DG) units as well as grid-interactive microgrids and HVDC systems, have several challenges in supporting the grid stability. For example, converter-interfaced DG units can typically provide only 1–2 pu fault current depending on their semiconductor capabilities [6]. In addition, the control systems of converter-based units are sensitive to grid voltage deviations and thus increasing requirements have been imposed by transmission system operators for low-voltage ride-through (LVRT) and voltage support capabilities [7], [16], [41]-[42]. Numerous projects are consequently conducted worldwide to tackle the corresponding reliability and stability challenges in the coming power system era. “MIGRATE” project under the European Union framework [8], “Synchronous Condensers Application in Low Inertia Systems” in Denmark [9], and the “ProSmart” project in Norway [10] are just few examples of the extensive effort to address the grid reliability and stability concerns in future highly-integrated and low-inertia power systems.

During unbalanced conditions, the operation of converter-interfaced units is prone to even more undesirable functions, such as distortions on the output current and oscillations on the dc-link voltage and output power. These adverse situations can severely harm the operation of a power system and, if not managed properly, cause a cascading failure. A variety of control techniques, which are mainly based on the symmetric sequences, have thus been proposed to ride through grid faults by converter-interfaced units [11]-[16]. However, there are still different challenges remained which need further research and development such as improved operation of individual units and smart coordination between multiple units under the grid faults.

Grid-interactive smart inverters (GSIs) are becoming very popular both in research [66]-[68] and industry [69]-[70] which incorporate smart functionalities inside the grid-tied converters. These grid-tied converters are widely used for

integrating modern power units such as different types of renewable energies, energy storage systems, electric vehicles, solar roofs, DG units, hybrid microgrids, and HVDC systems [17]-[21]. Smart inverter functionalities refer to fast and reliable response of GSIs to grid abnormalities such as LVRT, voltage support, frequency ride-through, volt/var or volt/watt control, off-unity power factor, dynamic reactive current injection, etc. [66]-[70]. These functionalities can be achieved by central networked supervisory systems or advanced embedded control techniques. Expected high integration of smart inverters inside future energy systems brings unprecedented opportunities for optimized operation of energy systems and booming growth for clean technologies. Therefore, this research project focuses on proposing advanced control techniques for optimal operation of GSI units under asymmetric grid conditions.

## **1.2 State-of-the-Art**

For a decade, the proper operation of converter-based units under the grid faults, also known as the LVRT capabilities, is one of the hottest area in the literature among the power system studies. Numerous efforts have thus been carried out for improving the LVRT capabilities in converter-interfaced DG units [22]-[59], doubly-fed induction generators [60]-[62], and HVDC transmission systems [63]-[64]. The studies of the LVRT capabilities in the converter-interfaced DG units have mainly focused on the following five areas:

- quality of the injected current [11]-[16],
- reduction of oscillations on dc-link voltage and output active power [22]-[25],
- flexible oscillations on the output active and reactive powers [26]-[27],
- point of common coupling (PCC) voltage support schemes [26]-[53], and
- maximum allowable support to the grid [42], [51], [54].

Here, the recent accomplishments in each category are briefly discussed in order to give a glimpse into the state-of-the-art. The most recent work on the quality of the injected current under unbalanced grid faults [11] presents a model-based

control design to improve the dynamic performance of the grid-connected converters and enhance the fault current transients.

Reference [13] proposes a series of control strategies and corresponding circuit configurations which utilize the zero sequence components to enhance the power controllability and eliminate active power oscillations. For the flexible control of oscillations on the output active and reactive powers, different strategies based on symmetric-sequence components are proposed in [27], yielding an adaptive controllability that can manage multiple objectives and constraints. It is shown that active and reactive power oscillations can be independently regulated with two individually adaptable parameters. In a range of variation for these parameters, the amplitudes of oscillating power can be also slightly controlled, as well as the peak values of the output currents. For instance, the oscillating active power can be limited below a certain amount while the output currents are controlled to be as balanced as possible.

In the available literature, the voltage support schemes, by converter-interfaced DG units under unbalanced grid conditions, can be themselves categorized based on the following notions:

- voltage support based on the grid code requirements [36]-[40]
- voltage support based on the maximum allowable reactive power delivery [41]-[42]
- flexible voltage support based on the positive and negative sequence compensation [27], [43]-[45]
- phase voltage regulation by positive and negative sequence compensation [46]-[51]
- phase voltage regulation by positive, negative and zero-sequence compensation [52]-[53].

In [36]-[40], for supporting the PCC voltage under unbalanced grid faults, the idea is to follow the imposed rule by German E.ON grid code [65], requiring the reactive current injection proportional to the balanced voltage depth. This is a primitive solution because it over-simplifies the problem and does not consider

unbalanced fault characteristics and other parameters, such as grid impedance and over-voltage issues in unfaultry phases. In [42], it is proposed to utilize the entire available capacity of the converter to inject the reactive current for supporting the PCC voltage. This strategy also suffers from similar problems. However, the idea of the German grid code for balanced faults has been extended in [44] to consider unbalanced faults by proposing simultaneous positive and negative reactive current injection, respectively, proportional to the depth of the positive voltage component and raise of the negative voltage sequence. Although the strategies in this category (i.e., flexible positive and negative voltage support strategies [43]-[45]) aims to consider unbalance factor, they still lack taking into account grid impedance and over-voltages on unfaultry phases. To address these problems, the methods proposed in [46]-[51] shift the view toward regulating the phase voltages within the pre-set boundaries by positive and negative sequence control. These methods are revised in [52]-[53] to improve their accuracy by considering the zero-sequence compensation. Reference [53] presents the positive-, negative-, and zero-sequence voltage and current control schemes, with dynamically varying limits, in dq-frame for the converter-based DG units in order to compensate voltage unbalance in a microgrid.

References [42] and [55] overview the conventional reference current generation strategies and propose analytical approaches to provide their maximum allowable support capabilities considering the limitation on the peak value of the three-phase currents.

### **1.3 Motivations and Objectives**

Motivated by the aforementioned concerns, this research project focuses on proposing new solutions for improved performance of grid-connected smart inverters under unbalanced grid conditions and asymmetric short-term faults. In this regard, the followings are the main objectives of this research project.

**First stage:**

- comparative studies of the available control strategies under unbalanced conditions for evaluating their supporting capability,
- proposing maximum asymmetric support scheme based on the analytical studies,
- proposing a novel reference current generation scheme aiming to minimize the power oscillations and maximize the average active or reactive power delivery, considering the phase current limits,
- proposing a control technique to minimize the fault current with the existing set-points for the output active and reactive powers.

**Second stage:**

- proposing the comprehensive asymmetric ride-through (ART) regulation scheme,
- enforcing large DGs to properly regulate the phase voltages within the pre-set dynamic limits under short-term asymmetric low voltages,
- proposing an advanced dynamic voltage regulation method to accurately address the ART specifications.

**Third stage:**

- proposing a novel voltage support scheme with improved accuracy in regulating the phase voltages at the PCC within the pre-set safety limits, by considering the zero-sequence voltage component,
- considering the output active power in the improved asymmetrical voltage support and being adaptive to complex grid impedance (i.e. with resistive and inductive parts),
- augmenting the limited active power oscillation strategy to the proposed voltage support scheme, which provides an adjustable dc-link voltage oscillation setting while simultaneously supporting the host ac grid, even under severe unbalanced faults,

- augmenting the maximum active power delivery strategy to the proposed voltage support scheme to enable it with the maximum asymmetric support (MAS) capability.

**Fourth stage:**

- coordinating the maximum flexible asymmetrical voltage support and ride-through capability of parallel-operated multi inverter structure,
- maximizing the collective dynamic contribution of parallel-operated multi inverter structure in boosting the voltage and reducing the imbalance subject to the constraints of the plant and host system,
- keeping the active power injection of each unit intact during the support which leads to power/cost saving in the plant operation as well as host system stability enhancement.

**Fifth stage:**

- decentralized maximum flexible asymmetrical voltage support tracking in distributed multi inverter structure that does not need communication and central control unit,
- keeping the active power injection of each distributed unit intact during the support,
- introducing new concepts such allowable flexible support areas and support points trajectories represented in the *negative-reactive-current* vs. *positive-reactive-current* plane.

## **1.4 Thesis Outline**

The thesis is organized as follows (the contributions of each chapter are briefly presented here):

## ***Chapter 2: Maximum Asymmetric Support (MAS) in A Grid-Interactive Smart Inverter***

This chapter presents a novel reference current generation scheme with the ability to support the grid voltage by injecting optimal sets of positive/negative active/reactive currents. Analytical expressions are proposed in order to find the optimal values of the controlling parameters under any unbalanced grid voltage condition. The optimal performances can be obtained by achieving the following objectives: (1) compliance with the phase voltage limits, (2) maximized active and reactive power delivery, (3) minimized fault currents, and (4) reduced oscillations on the active and reactive powers. These optimal behaviors bring significant advantages to emerging GSIs, such as increasing the efficiency, lowering DC-link ripples, improving AC system stability, and avoiding equipment tripping.

## ***Chapter 3: Asymmetric Ride-Through (ART) Guidelines***

This chapter highlights the necessity of supporting the connection voltage by large DG units under short-term unbalanced voltage sags. To address this, a new regulation scheme, named ART scheme, is proposed. The proposed scheme enforces DG units to properly regulate the voltage within the dynamic limits for three important voltage parameters: positive-sequence, negative-sequence, and phase voltage magnitude. The main advantages of applying the ART scheme are avoiding unnecessary outages due to temporary unbalanced faults and enhancing the grid stability. As the second contribution, a dynamic voltage regulation method is also proposed to accurately address the specifications determined in the ART scheme.

## ***Chapter 4: Advanced Asymmetric Voltage Regulation and MAS Scheme in A Single Grid-Interactive Smart Inverter***

This chapter proposes an advanced voltage support scheme in a GSI, to accurately regulate the three-phase voltages of the connection point. The proposed scheme not only compensates the zero-sequence component but also considers the active power injection. Unlike the conventional methods, the proposed support method is adapted even in resistive distribution systems. Moreover, the adjustable

limited active power oscillation strategy is added to the proposed method. This feature limits the oscillation to a specified value which provides an adjustable DC-voltage oscillation setting while simultaneously supporting the AC host grid, even under severe unbalanced faults. Third, the MAS equations are formulated for the new method.

#### ***Chapter 5: Parallel MAS Scheme in Multiple Parallel-Operated Grid-Interactive Smart Inverters***

The analyses in this chapter show that the MAS techniques presented in the previous chapters are not sufficient to provide the overall optimal asymmetric support of the parallel-operated multi-inverter system. This paper thus proposes a new methodology to: (1) coordinate the asymmetrical ride-through and voltage support capabilities of different parallel-operated GSI units, (2) maximize the utilization of each unit and their overall collective contribution in boosting the positive-sequence voltage and reduction of the negative-sequence voltage subject to the constraints from both DG and grid points of views. The simulation tests on a parallel multi-inverter structure, i.e., the ABB 2.0 MVA central inverters, illustrate the promising results of the proposed algorithms.

#### ***Chapter 6: Decentralized MAS Scheme in Multiple Distributed Grid-Interactive Smart Inverters***

This chapter proposes a comprehensive autonomous coordination control scheme to achieve cooperative asymmetric low-voltage ride-through and grid support by multiple distributed GSI units in an active distribution network. In addition to the decentralized nature of the proposed coordination scheme, it provides three important features: 1) a maximized flexible asymmetrical voltage support that does not affect the active power injection of individual units at the time of the support, 2) maximum support point tracking of each unit considering current, voltage, and power constraints, and 3) wise dynamic support points movement. The proposed scheme is examined in a practical test system, adapted from Hydro One 27 kV medium-voltage active distribution network in Ontario, Canada. Test results

demonstrate significant improvements obtained from the proposed methodologies compared to the conventional techniques.

## **1.5 Summary of the Key Contributions**

The contributions of this thesis to the research field can be summarized as follows:

- 1) The MAS scheme is proposed by advanced control techniques with multi-objective optimization in a single inverter structure. The proposed MAS scheme has three fundamental criteria:
  - a. The asymmetric voltage is flexibly supported in positive and negative sequences.
  - b. The flexible voltage support has minimal impact on the output power (e.g., average value and oscillation amount).
  - c. The peak current limitation of the power electronic switches is respected.
- 2) The ART regulation guidelines are proposed enforcing large DGs to properly regulate the phase voltages within the pre-set dynamic limits under short-term asymmetric low voltages. Further, an advanced dynamic voltage regulation method is also suggested to accurately address the ART specifications.
- 3) Unique MAS techniques are proposed for multiple GSI units in the parallel structure which enables the maximum collaboration between the units in flexible and optimized asymmetric voltage support. This method is called parallel MAS (PMAS) technique.
- 4) Another unique MAS scheme is proposed for the autonomous coordination control of multiple GSI units in the distributed structure. This scheme is named decentralized MAS (DMAS). While achieving a superior coordination between the MAS performance of each GSI, the DMAS eliminates the dependency of the control system to communication infrastructure.

# Chapter 2

## Maximum Asymmetric Support (MAS) in A Grid-Interactive Smart Inverter

### 2.1 Introduction

Recently, riding through grid faults and supporting the grid under abnormal conditions by grid-interactive smart inverters (GSIs) have become increasingly attractive. This chapter presents a set of optimized reference current generation strategies with the ability to support the grid voltage by injecting a proper combination of positive/negative and active/reactive current components.

As the main contribution, this chapter utilizes a new control scheme with analytical expressions capable of finding the optimal values for four control parameters under any unbalanced grid voltage condition to achieve the following objectives:

- minimized oscillations on the active and reactive powers,
- boosted and semi-balanced phase voltages of the PCC,
- minimized inverter fault current, and
- maximized active and reactive power delivery.

To fully accomplish these objectives, the expressions of the boosted phase voltages, maximum oscillations on instantaneous active/reactive powers, and the

maximum phase currents under the unbalanced conditions must be found. Maximum allowable support scheme is also proposed to obtain the maximum allowable active or reactive powers which the inverter can deliver to the grid under unbalanced conditions (to support either the grid voltage or the grid frequency) without exceeding the phase current limit,  $I_{limit}$ . The mathematical equations of the control schemes under various conditions (i.e., various voltage dip characteristics, several system parameters, different operating points, etc.) are obtained and presented in the coming sections. Different simulation and experimental test cases are used to verify the accuracy and effectiveness of the proposed control schemes.

## 2.2 System Description

In this chapter, the flexible reference current generation strategy is initially presented for the GSI system, shown in Fig 2.1. Then, it will be utilized to build different control techniques. This flexible reference current generation strategy can flexibly contain positive/negative and active/reactive current components, offering valuable voltage support services with two controlling parameters,  $k_p$  and  $k_q$ , as well as set points for the average active and reactive powers,  $P^*$  and  $Q^*$ . The total reference current can be formulated by using four components as

$$\begin{aligned}
 i &= i_p^+ + i_p^- + i_q^+ + i_q^- \\
 i_p^+ &= k_p \frac{P^*}{(V^+)^2} v^+ = K_p^+ v^+, \quad i_p^- = (1 - k_p) \frac{P^*}{(V^-)^2} v^- = K_p^- v^- \\
 i_q^+ &= k_q \frac{Q^*}{(V^+)^2} v_{\perp}^+ = K_q^+ v_{\perp}^+, \quad i_q^- = (1 - k_q) \frac{Q^*}{(V^-)^2} v_{\perp}^- = K_q^- v_{\perp}^-
 \end{aligned} \tag{2.1}$$

Also, the voltage under single-phase unbalanced condition can be simplified as [42]

$$\begin{aligned}
 v^+ &= \begin{bmatrix} v_{\alpha}^+ \\ v_{\beta}^+ \end{bmatrix} = \begin{bmatrix} V^+ \cos(\omega t) \\ V^+ \sin(\omega t) \end{bmatrix}, \quad v^- = \begin{bmatrix} v_{\alpha}^- \\ v_{\beta}^- \end{bmatrix} = \begin{bmatrix} -V^- \cos(\omega t) \\ V^- \sin(\omega t) \end{bmatrix} \\
 v_{\perp}^+ &= \begin{bmatrix} v_{\perp\alpha}^+ \\ v_{\perp\beta}^+ \end{bmatrix} = \begin{bmatrix} -V^+ \sin(\omega t) \\ V^+ \cos(\omega t) \end{bmatrix}, \quad v_{\perp}^- = \begin{bmatrix} v_{\perp\alpha}^- \\ v_{\perp\beta}^- \end{bmatrix} = \begin{bmatrix} -V^- \sin(\omega t) \\ -V^- \cos(\omega t) \end{bmatrix}
 \end{aligned} \tag{2.2}$$

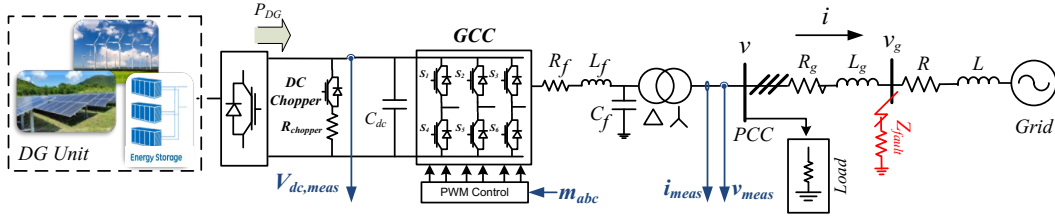


Figure 2.1 Circuit topology of the grid-interactive inverter.

In this section, the equations of oscillatory terms on active and reactive powers ( $\tilde{p}_{\max}$  and  $\tilde{q}_{\max}$ ) are obtained from reference current of Eq (2.1). The detailed derivation of the instantaneous active/reactive power is provided in Eq (2.3).

$$\begin{aligned}
 p &= v \cdot i = (v^+ + v^-) \cdot (i^+ + i^-) = \underbrace{v^+ \cdot i^+ + v^- \cdot i^-}_P + \underbrace{v^+ \cdot i^- + v^- \cdot i^+}_{\tilde{p}} \\
 &= P - \left[ P \times (1 - k_p) / n + P \times k_p \times n \right] \cos(2\omega t) - \left[ Q \times (1 - k_q) / n - Q \times k_q \times n \right] \sin(2\omega t) \\
 q &= v_{\perp} \cdot i = (v_{\perp}^+ + v_{\perp}^-) \cdot (i^+ + i^-) = \underbrace{v_{\perp}^+ \cdot i^+ + v_{\perp}^- \cdot i^-}_Q + \underbrace{v_{\perp}^+ \cdot i^- + v_{\perp}^- \cdot i^+}_{\tilde{q}} = Q + \tilde{q}_{s2} + \tilde{q}_{c2} \\
 &= Q + \left[ P \times (1 - k_p) / n - P \times k_p \times n \right] \sin(2\omega t) - \left[ Q \times (1 - k_q) / n + Q \times k_q \times n \right] \cos(2\omega t)
 \end{aligned} \tag{2.3}$$

where  $n$  is the ratio between the negative-sequence and positive-sequence voltages. The ability to analytically calculate the maximum power oscillations, i.e.  $\tilde{p}_{\max}$  and  $\tilde{q}_{\max}$ , in terms of the scalar parameters (i.e.,  $P$ ,  $Q$ ,  $k_p$ ,  $k_q$ , and  $n$ ) is very useful for proper controlling of the GSIs under generic voltage condition. Therefore, the expressions of  $\tilde{p}_{\max}$  and  $\tilde{q}_{\max}$  is obtained as

$$\begin{aligned}
 \tilde{p}_{\max} &= \sqrt{P^2 \left[ k_p n + (1 - k_p) n^{-1} \right]^2 + Q^2 \left[ k_q n - (1 - k_q) n^{-1} \right]^2} \\
 \tilde{q}_{\max} &= \sqrt{Q^2 \left[ k_q n + (1 - k_q) n^{-1} \right]^2 + P^2 \left[ k_p n - (1 - k_p) n^{-1} \right]^2}
 \end{aligned} \tag{2.4}$$

In this chapter, these equations are used to minimize the oscillations on active and reactive powers. By applying Eq (2.2) in (2.1), the injected current under the fault can be rewritten in the  $\alpha\beta$  frame:

$$\begin{aligned}
\begin{bmatrix} i_\alpha \\ i_\beta \end{bmatrix} &= \begin{bmatrix} i_{p,\alpha}^+ \\ i_{p,\beta}^+ \end{bmatrix} + \begin{bmatrix} i_{p,\alpha}^- \\ i_{p,\beta}^- \end{bmatrix} + \begin{bmatrix} i_{q,\alpha}^+ \\ i_{q,\beta}^+ \end{bmatrix} + \begin{bmatrix} i_{q,\alpha}^- \\ i_{q,\beta}^- \end{bmatrix} = \dots \\
&= \begin{bmatrix} [K_p^+ V^+ - K_p^- V^-] \cos(\omega t) - [K_q^+ V^+ + K_q^- V^-] \sin(\omega t) \\ [K_p^+ V^+ + K_p^- V^-] \sin(\omega t) + [K_q^+ V^+ - K_q^- V^-] \cos(\omega t) \end{bmatrix}
\end{aligned} \tag{2.5}$$

The  $\alpha\beta$  currents of Eq (2.5) are transformed into the  $abc$  currents by the transformation matrix. Therefore, the maximum currents in each phase can be obtained as

$$\begin{aligned}
\begin{bmatrix} I_{\max-a}^2 \\ I_{\max-b}^2 \\ I_{\max-c}^2 \end{bmatrix} &= \begin{bmatrix} (K_1)^2 + (K_2)^2 \\ (-\frac{1}{2} K_1 + \frac{\sqrt{3}}{2} K_4)^2 + (\frac{1}{2} K_2 + \frac{\sqrt{3}}{2} K_3)^2 \\ (-\frac{1}{2} K_1 - \frac{\sqrt{3}}{2} K_4)^2 + (\frac{1}{2} K_2 - \frac{\sqrt{3}}{2} K_3)^2 \end{bmatrix}, \text{ where} \\
\begin{cases} K_1 = K_p^+ V^+ - K_p^- V^- = \frac{P}{V^-} ((n+1)k_p - 1) \\ K_2 = K_q^+ V^+ + K_q^- V^- = \frac{Q}{V^-} ((n-1)k_q + 1) \\ K_3 = K_p^+ V^+ + K_p^- V^- = \frac{P}{V^-} ((n-1)k_p + 1) \\ K_4 = K_q^+ V^+ - K_q^- V^- = \frac{Q}{V^-} ((n+1)k_q - 1) \end{cases}
\end{aligned} \tag{2.6}$$

### 2.3 Proposed Multi-Objectively Optimized Control Strategies

In this section, five strategies are initially proposed:

- 1) minimized active power oscillation,
- 2) minimized reactive power oscillation,
- 3) minimized fault current,
- 4) maximum allowable active power injection, and
- 5) maximum allowable reactive power injection.

It is suggested that some of these objectives can be combined to simultaneously benefit their advantages. In the next section, an advanced strategy will be also proposed which not only provides the maximum allowable active power injection but also aims to regulate the phase voltages within the desired limits.

### 2.3.1 Minimum Oscillation on the Active and Reactive Powers

By taking the derivative of Eq (2.3) in terms of  $k_p$  and  $k_q$ , and finding the extreme point by enforcing the derivatives to be zero, the following expression can be easily obtained for the minimum oscillations on the instantaneous active and reactive powers:

$$\begin{aligned} \tilde{p}_{\max} \text{ is minimum when } & \begin{cases} k_p = 1/(1-n^2) \\ k_q = 1/(1+n^2) \end{cases}, \\ \tilde{q}_{\max} \text{ is minimum when } & \begin{cases} k_p = 1/(1+n^2) \\ k_q = 1/(1-n^2) \end{cases} \end{aligned} \quad (2.7).$$

These strategies are called minimum oscillation on the active (or MOP) and reactive (or MOQ) powers. For an efficient power delivery, the  $k_p$  and  $k_q$  values are set to be only between 0 and 1 [13], [49]. Since Eq (2.7) gives a  $k_p$  (or  $k_q$ ) value greater than 1, it can be changed to  $k_p=1$ . In this case, only positive sequence active currents will be injected while the reactive currents will contain both positive and negative components based on  $1/(1+n^2)$ . However,  $k_p$  (or  $k_q$ ) can be set to be  $1/(1-n^2)$  in certain applications when minimizing the active (or reactive) power oscillations is critical. To improve the MOP strategy,  $P^*$  or  $Q^*$  can be obtained by using the proposed MAP or MAQ expressions, presented in next sections, respectively. Therefore, the objectives of both strategies, e.g., MOP and MAQ, can be simultaneously accomplished. Similarly, MOQ can be also combined with MAP strategies in order to achieve double objectives.

### 2.3.2 Minimum Fault Current (MFC) Strategy

To obtain the minimum fault currents, Eq (2.6) should be considered. According to Eq (2.6), the maximum phase current can be one of the three expressions. For the proposed MFC scheme, the reference values for the active and reactive powers can be determined from the operating mode controllers (either PV or PQ modes) or from the grid code requirements. Also, the value of  $k_q$  can be obtained from the voltage support scheme introduced in the next section. Therefore, the minimum point of each expression of Eq (2.6) should be obtained by taking their derivatives with respect to  $k_p$ :

$$\begin{aligned}
 I_{a-\min} \Rightarrow k_{p,a} &= \frac{1}{n+1}, & I_{b-\min} \Rightarrow k_{p,b} &= \frac{P \times (2-n) + \sqrt{3}nQ \times (2k_q - 1)}{2P \times (n^2 - n + 1)} \\
 I_{c-\min} \Rightarrow k_{p,c} &= \frac{P \times (2-n) - \sqrt{3}nQ \times (2k_q - 1)}{2P \times (n^2 - n + 1)}
 \end{aligned} \tag{2.8}$$

However, only Eq (2.8) cannot fully ensure that the obtained  $k_p$  will always minimize  $I_{max}$  in Eq (2.6) because these equations minimize only their corresponding currents, i.e.,  $I_{max-a}$ ,  $I_{max-b}$ , and  $I_{max-c}$ . Therefore, it is suggested in this chapter that, in addition to the three  $k_p$ s obtained in Eq (2.8), three other  $k_p$ s should be also considered to find the optimum value,  $k_{p,opt}$ . Two of these  $k_p$ s are the intersections of the magnitude curve of  $I_a(k_p)$  with the magnitude curves of  $I_b(k_p)$  and  $I_c(k_p)$ . Therefore, the equations of  $I_a$  and  $I_b$ , as well as  $I_a$  and  $I_c$  are taken to be equal in order to find  $k_{p,ab}$  and  $k_{p,ac}$ , respectively.

$$\begin{aligned}
 I_a(k_p) = I_b(k_p) \Rightarrow k_{p,ab} &= \frac{-b + \sqrt{b^2 - 4ac}}{2a} \begin{cases} a = 3nP^2 \\ b = -3nP^2 + \sqrt{3}nPQ(2k_q - 1) \\ c = 3nk_qQ^2(1 - k_q) - \sqrt{3}nPQk_q \end{cases} \\
 I_a(k_p) = I_c(k_p) \Rightarrow k_{p,ac} &= \frac{-b + \sqrt{b^2 - 4ac}}{2a} \begin{cases} a = 3nP^2 \\ b = -3nP^2 - \sqrt{3}nPQ(2k_q - 1) \\ c = 3nk_qQ^2(1 - k_q) + \sqrt{3}nPQk_q \end{cases}
 \end{aligned} \tag{2.9}$$

Since  $k_p$  is bounded to 1,  $k_{p,l}=1$  should be also considered in order to find the minimum phase currents and optimal  $k_p$  value, i.e.  $I_{max,opt}$  and  $k_{p,opt}$ . Therefore, the

three phase currents are calculated for six possible  $k_p$ s in order to find the minimum  $I_{max}$ . This chapter suggests that the  $k_{p,opt}$ , can be calculated under any operating and fault condition for any  $P$ ,  $Q$ ,  $V^+$ , and  $V^-$  values.

### 2.3.3 Maximum Allowable Active and Reactive Powers Strategies

Applying the maximum allowable active power (MAP) strategy provides the maximum active power to the grid for assisting the frequency stability while simultaneously respects the phase current limits. The required equations of  $P_{MAP}$  should be obtained such that they guarantee none of the phase currents under the abnormal condition passes the pre-set limits,  $I_{max}$ . In this strategy, the reference value for  $Q$  is determined either by the V-Q droop control or grid code requirements. By using the  $I_{max}$  equations of Eq (2.6), three possible active power values can be obtained as

$$\begin{bmatrix} P_1 \\ P_2 \\ P_3 \end{bmatrix} = \begin{bmatrix} \frac{V^- \sqrt{I_{max}^2 - K_2^2}}{k_p n + k_p - 1} \\ \left( -b + \sqrt{b^2 - 4ac} \right) / 2a \\ \left( b + \sqrt{b^2 - 4ac} \right) / 2a \end{bmatrix}, \quad \text{where}$$

$$\begin{cases} a = \frac{3}{V^-} (k_p (n-1) + 1)^2 + \frac{1}{V^-} (k_p (n+1) - 1)^2 \\ b = 2\sqrt{3} \left[ \frac{K_4}{V^-} (k_p (n+1) - 1) - \frac{K_2}{V^-} (k_p (n-1) + 1) \right] \\ c = K_2^2 + 3K_4^2 - 4I_{max}^2 \end{cases} \quad (2.10).$$

In order to have all of the three-phase currents of Eq (2.6) lower than the pre-set  $I_{max}$  value,  $P_{MAP}^*$  should comply with  $P_{MAP}^* = \min(P_1, P_2, P_3)$ .

Similarly, the maximum allowable reactive power (i.e. MAQ strategy) aims to provide reference value of  $Q_{MAQ}^*$  such that all phase currents remain bounded with the current limit. The reference value of  $P$  is determined by other controllers

in the GSI (e.g., by maximum power point tracking), and the  $Q_{MAQ}^*$  expressions can be obtained by using the  $I_{max}$  equations of Eq (2.6):

$$\begin{bmatrix} Q_1 \\ Q_2 \\ Q_3 \end{bmatrix} = \begin{bmatrix} \frac{V^- \sqrt{I_{max}^2 - K_1^2}}{k_q n - k_q + 1} \\ \left( -b + \sqrt{b^2 - 4ac} \right) / 2a \\ \left( b + \sqrt{b^2 - 4ac} \right) / 2a \end{bmatrix}, \text{ where} \quad (2.11).$$

$$\begin{cases} a = \frac{3}{V^-} (k_q (n+1) - 1)^2 + \frac{1}{V^-} (k_q (n-1) + 1)^2 \\ b = 2\sqrt{3} \left[ \frac{K_3}{V^-} (k_q (n-1) + 1) - \frac{K_1}{V^-} (k_q (n+1) - 1) \right] \\ c = K_1^2 + 3K_3^2 - 4I_{max}^2 \end{cases}$$

To satisfy  $\min(I_a, I_b, I_c) \leq I_{max}$ ,  $Q_{MAQ}^*$  can be obtained as  $Q_{MAQ}^* = \min(Q_1, Q_2, Q_3)$ .

## 2.4 Voltage Support Strategy

Supporting the PCC voltage by using DG units is another objective proposed in this chapter. If the DG plant rated power and the grid impedance are not small, then, under the moderate sags, the three-phase voltages can be regulated at the desired range between  $V_{min}$  and  $V_{max}$ . In [49], the proposed scheme has been applied only in the STATCOM application, where the reference current contains only the reactive components. The principal objective in the voltage support is to avoid the over-voltage and under-voltage at the PCC whenever possible. However, a proper solution can be found in this range in order to satisfy other objectives as well. Unlike [49], this chapter considers the active components of the current. The PCC voltage support strategy (VSS) can be extracted as a function of the grid voltage and the injected positive and negative currents:

$$v = v^+ + v^- = \begin{bmatrix} v_\alpha^+ + v_\alpha^- \\ v_\beta^+ + v_\beta^- \end{bmatrix} = \begin{bmatrix} v_{g\alpha}^+ + v_{g\alpha}^- + L_g \frac{d(i_\alpha^+ + i_\alpha^-)}{dt} + R_g (i_\alpha^+ + i_\alpha^-) \\ v_{g\beta}^+ + v_{g\beta}^- + L_g \frac{d(i_\beta^+ + i_\beta^-)}{dt} + R_g (i_\beta^+ + i_\beta^-) \end{bmatrix} \quad (2.12).$$

Applying Eq (2.6) and (2.2) in (2.12) gives the following:

$$\begin{bmatrix} (V^+ - V^-) \cos(\omega t) \\ (V^+ + V^-) \sin(\omega t) \end{bmatrix} = \begin{bmatrix} (V_g^+ - V_g^-) \cos(\omega t - \delta) \\ (V_g^+ + V_g^-) \sin(\omega t - \delta) \end{bmatrix} + \begin{bmatrix} \omega L_g (-K_1 \sin(\omega t) + K_2 \cos(\omega t)) \\ \omega L_g (-K_3 \sin(\omega t) + K_4 \cos(\omega t)) \end{bmatrix} + \begin{bmatrix} R_g (K_1 \cos(\omega t) + K_2 \sin(\omega t)) \\ R_g (K_3 \cos(\omega t) + K_4 \sin(\omega t)) \end{bmatrix} \quad (2.13).$$

In practical applications,  $\delta$  is small and can be neglected for the simplicity in the analytical solution. Then, the positive and negative components of (2.13) can be separated as

$$\begin{bmatrix} V^+ \\ V^- \end{bmatrix} - \begin{bmatrix} V_g^+ \\ V_g^- \end{bmatrix} = \begin{bmatrix} \omega L_g I_q^+ \\ -\omega L_g I_q^- \end{bmatrix} + \begin{bmatrix} R_g I_p^+ \\ R_g I_p^- \end{bmatrix} \quad (2.14).$$

The maximum and minimum phase voltages can be determined simply by

$$V_{abc-\min} = \min(V_a, V_b, V_c) = \sqrt{(V^+)^2 + (V^-)^2 + 2(V^+)(V^-)\lambda_{\min}}, \text{ where}$$

$$V_{abc-\max} = \max(V_a, V_b, V_c) = \sqrt{(V^+)^2 + (V^-)^2 + 2(V^+)(V^-)\lambda_{\max}}$$

$$\lambda_{\min} = \min\left(\cos(\gamma), \cos\left(\gamma - \frac{2\pi}{3}\right), \cos\left(\gamma + \frac{2\pi}{3}\right)\right),$$

$$\lambda_{\max} = \max\left(\cos(\gamma), \cos\left(\gamma - \frac{2\pi}{3}\right), \cos\left(\gamma + \frac{2\pi}{3}\right)\right) \quad (2.15).$$

Then the reference values for the maximum and minimum phase voltages can be determined so that the phase voltages are regulated within the explained thresholds. The reference values for  $V^+$  and  $V^-$  can be calculated as

$$\begin{aligned}
V_{ref}^+ &= \sqrt{\frac{\lambda_{\max} V_{\min}^2 - \lambda_{\min} V_{\max}^2 + \sqrt{(\lambda_{\max} V_{\min}^2 - \lambda_{\min} V_{\max}^2)^2 - (V_{\min}^2 - V_{\max}^2)^2}}{2(\lambda_{\max} - \lambda_{\min})}} \\
V_{ref}^- &= \sqrt{\frac{\lambda_{\max} V_{\min}^2 - \lambda_{\min} V_{\max}^2 - \sqrt{(\lambda_{\max} V_{\min}^2 - \lambda_{\min} V_{\max}^2)^2 - (V_{\min}^2 - V_{\max}^2)^2}}{(\lambda_{\max} - \lambda_{\min})}}
\end{aligned} \tag{2.16}.$$

By using Eq (2.16), the reference values for the desired positive and negative sequences of the voltage are obtained. Then,  $V^+$  and  $V^-$  in (2.14) are replaced with the reference values obtained from (2.16). Moreover, positive and negative sequences of the grid voltage can be estimated from the PCC measurements. Therefore, (2.14) can be rewritten as

$$\begin{aligned}
I_p^+ &= \frac{R}{X^2 + R^2} \times \Delta V_{ref}^+, \quad I_p^- = \frac{R}{X^2 + R^2} \times \Delta V_{ref}^-, \\
I_q^+ &= \frac{X}{X^2 + R^2} \times \Delta V_{ref}^+, \quad I_q^- = \frac{-X}{X^2 + R^2} \times \Delta V_{ref}^-
\end{aligned} \tag{2.17}.$$

For an inductive grid, (2.17) can be simplified as

$$I_p^+ = I_p^- = 0, \quad I_q^+ = \frac{\Delta V_{ref}^+}{X}, \quad I_q^- = \frac{-\Delta V_{ref}^-}{X} \tag{2.18}.$$

## 2.5 Maximum Asymmetric Support (MAS) Scheme

This thesis proposes a new supportive scheme under unbalanced grid conditions which combines the control strategies introduced in the previous sections. This scheme is named maximum asymmetric support (MAS) and denotes a set of strategies that empowers GSIs to flexibly support the asymmetric voltage up to their maximum capability, e.g., supporting both positive- and negative-sequence voltages by a GSI while retaining its maximum power delivery capability with respect to its peak-current limitation.

A simple example of the MAS scheme can be the combination of the proposed VSS and MAP strategies in the previous sections. Hence, the objectives of both strategies are simultaneously accomplished:

- 1) regulating the phase voltages within the pre-specified boundaries,
- 2) injecting the maximum active power, and
- 3) respecting the pre-defined current limit,  $I_{max}$ .

If the X/R ratio of the system is high, the active current components of Eq (2.17), i.e.,  $I_p^+$  and  $I_p^-$ , do not contribute significantly in regulating the voltage. Consequently, the voltage support should be completely accomplished by the reactive currents, and the active current components can be used to inject the maximum allowable active power with respect to the current limitation.

## 2.6 Simulation Results

Fig 2.1 illustrates the circuit topology of a GSI-interfaced DG unit (210 kVA, 690 V, and 60 Hz). A dc power supply can be used to emulate the renewable energy resources and storage in the dc-link [13], [49]. A type B fault (phase A to ground) occurs with a significant voltage dip on phase *A* as indicated in Fig 2.2(a). System parameters are reported in Table 2.1.

**TABLE 2.1 Simulation Test System Parameters**

$Z_g$ (m $\Omega$ )	$7 + j2\pi f \times 90e-3$	$V_{DC}$ (V)	1200
$Z$ (m $\Omega$ )	1	$V_{L-L, RMS}$ (V)	690
$Z_f$ (m $\Omega$ )	0.8	$f$ (Hz)	60
$I_{rate}$ (A)	200	$S$ (kVA)	210
$Kp-cc$	0.05	$Ki-cc$	1
$Kp-pll$	180	$Ki-pll$	3200

### 2.6.2 Test Case A: Performance Evaluation of MOP and MOQ Strategies

In normal operation,  $k_p$  and  $k_q$  both are set to be 1, and consequently, pure positive sequence current injection is applied. Between  $t_1=0.3\text{s}$  and  $t_2=0.6\text{s}$ , a moderate voltage dip happens where  $V_a = 0.5$  pu., and a solid one-phase fault is emulated after  $t_2=0.6\text{s}$ . Here,  $P$  and  $Q$  are set to be 100 kW and 30 kVAR.  $k_p$  and  $k_q$  are obtained according to Eq (2.7). According to 0, the oscillations on the active and reactive powers are eliminated after applying the MOP and MOQ strategies, respectively.

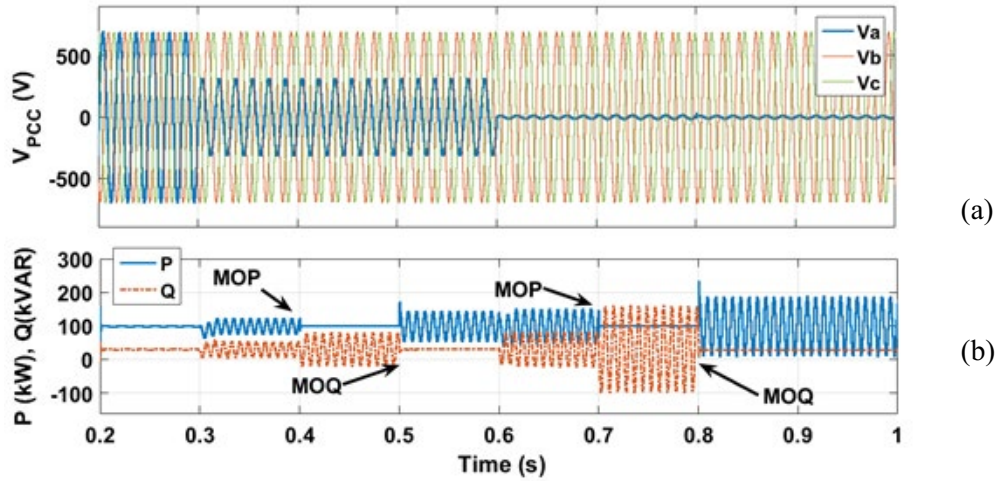


Figure 2.2 Simulation results of MOP and MOQ Strategies: (a) PCC voltage, and (b) active/reactive powers.

### 2.6.3 Test Case B: Performance Evaluation of VSS-MAP Strategy

This test case shows the performance of the proposed VSS-MAP strategy. Four different voltage sags occur for one phase of the grid voltage in  $t=0.1, 0.25, 0.4, 0.55$  s, respectively. To clearly illustrate the performance of the proposed VSS method, a 0.05 delay is considered after all the fault occurrences in order to compare the results before and after applying the VSS strategy. Fig 2.3 shows that by applying this strategy, all three phases are regulated in the desired range of  $V_{min}=0.9$  pu and  $V_{max}=1.1$  pu. In  $t=0.4$  s, the voltage sag in phase A is 0.25pu (0.15 pu below  $V_{min}$ ), so boosting  $V_a$  with 0.15 pu by using only the positive reactive current will cause overvoltage in the other two phases. In order to tackle overvoltage in the other

two phases, the proposed VSS strategy is applied to inject the required negative reactive current as well as the positive reactive current (see Fig 2.3(b)). In addition to showing the applied VSS strategy, Fig 2.3 demonstrates that the MAP strategy has also determined the maximum active power where the three phase currents are under the pre-set limitation, i.e.,  $I_{max}=200$  A. Therefore, the objectives of both strategies are simultaneously accomplished in this test case: (i) the phase voltages have been regulated within the pre-specified boundaries, (ii) the maximum active power has been injected to support the grid, and (iii) all three-phase currents are limited to the pre-specified current limitation,  $I_{max}$ .

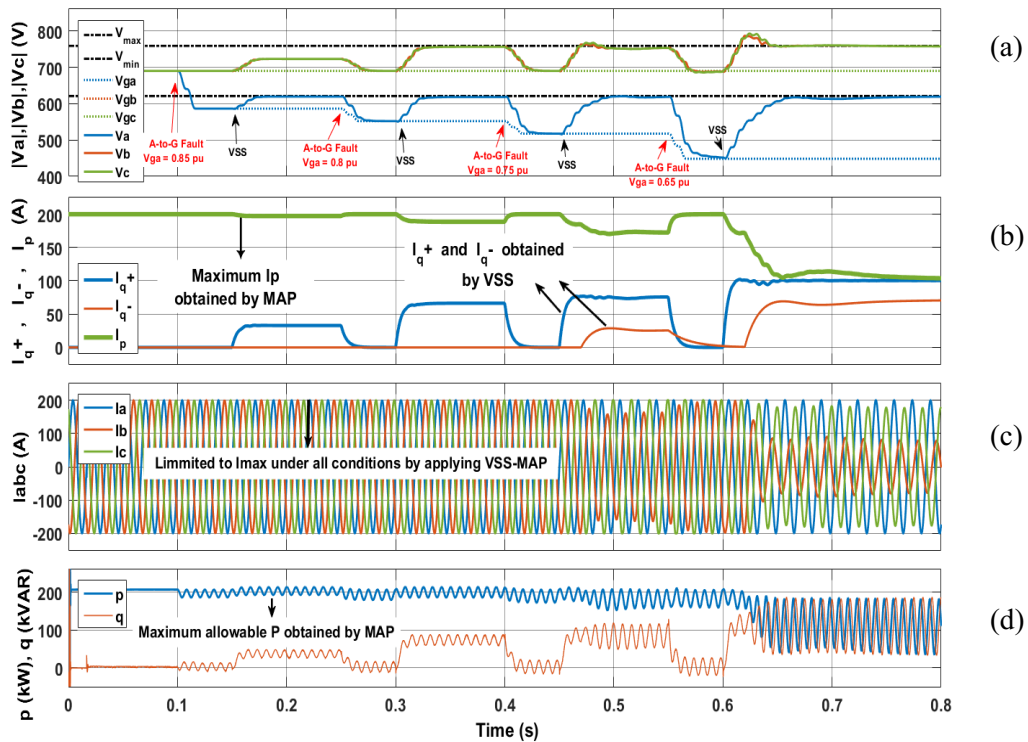


Figure 2.3 Simulation results of VSS-MAP Strategy: (a) magnitude of phase voltages, (b) positive/negative and active/reactive components of currents, (c) phase currents, and (d) active/reactive powers.

## 2.7 Experimental Results

To verify the analytical expressions, the experimental test system, shown in Fig 2.4, is also employed. This system contains a voltage source converter connected to the

grid and operated in the PQ mode. A Semistack intelligent power module consisting of gate drives and six insulated gate bipolar transistors (IGBTs) is used to implement the GSI. The switching frequency is 10 kHz. The converter is interfaced to a dSPACE1104 control card via a CMOS/TTL interfacing circuit. The converter is connected to a 60-Hz, 110-V (phase-voltage) three-phase grid via a three-phase transformer. Other parameters are reported in [51]. The proposed schemes are implemented on the dSPACE for switching-signal generation.

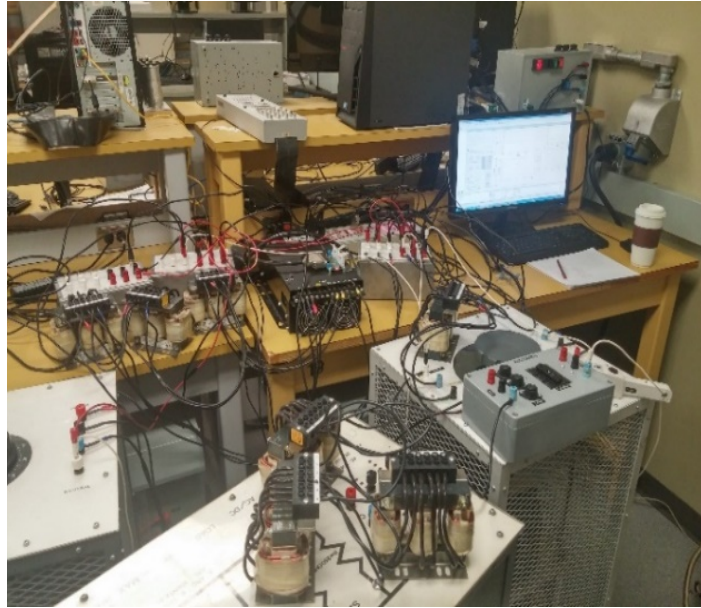


Figure 2.4 Experimental test setup.

### 2.7.2 Experimental Test Case A: MFC Strategy

This test case shows the results of the MFC strategy. In this case,  $P=100$  W and  $Q=175$  VAR are injected by the GSI. Again, a similar phase-to-ground fault occurs at  $t=2.6$  s. In this test case,  $k_q$  is taken to be 0.8 after the fault occurrence. After it, the phase currents increase up to 9.5 A. At  $t=11$  s, the MFC strategy is activated. The activation changes the value of the  $k_p$  from 1 to 0.79 in order to minimize the maximum phase current. Using the MFC strategy, the optimum  $k_p$  value is obtained by having three known parameters (i.e.,  $P=100$  W,  $Q=175$  VAR, and  $k_q=0.8$ ) and the fault characteristics. The MFC strategy reduces the phase currents to 8 A, as Fig 2.5(b) illustrates.

### 2.7.3 Experimental Test Case B: MAQ Strategy

This test examines the effectiveness of the proposed MAQ. Here,  $P=150\text{W}$  is injected. A similar phase-to-ground fault occurs in  $t=1.5\text{ s}$ . Under the fault, the voltage profile drops from  $30\text{V}$  to  $25\text{V}$  (%16.6 voltage drop). At  $t=4.3\text{ s}$ , the MAQ scheme is triggered with the predefined  $I_{limit}=10\text{A}$ , as shown in Fig 5. In practical applications, this scheme can be triggered automatically and immediately after the fault. However, it is configured manually in this test to show the results before and after applying the MAQ. According to Fig 2.6 (a), the PCC voltage is increased to  $29\text{V}$  after applying the MAQ. Also, the injected currents are limited to  $10\text{A}$ , as indicated in Fig 2.6(b).

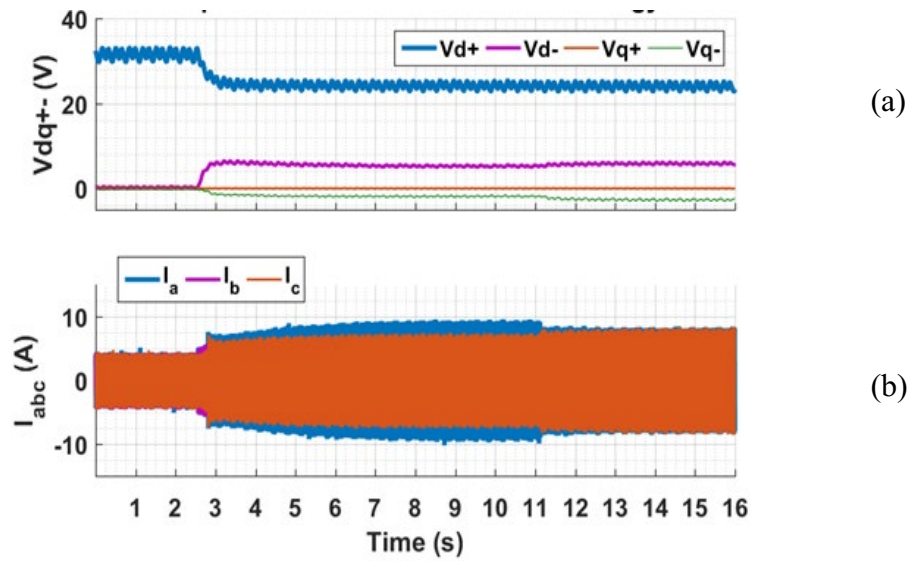


Figure 2.5 Experimental results of the MFC strategy: (a) faulted voltage, (b) currents.

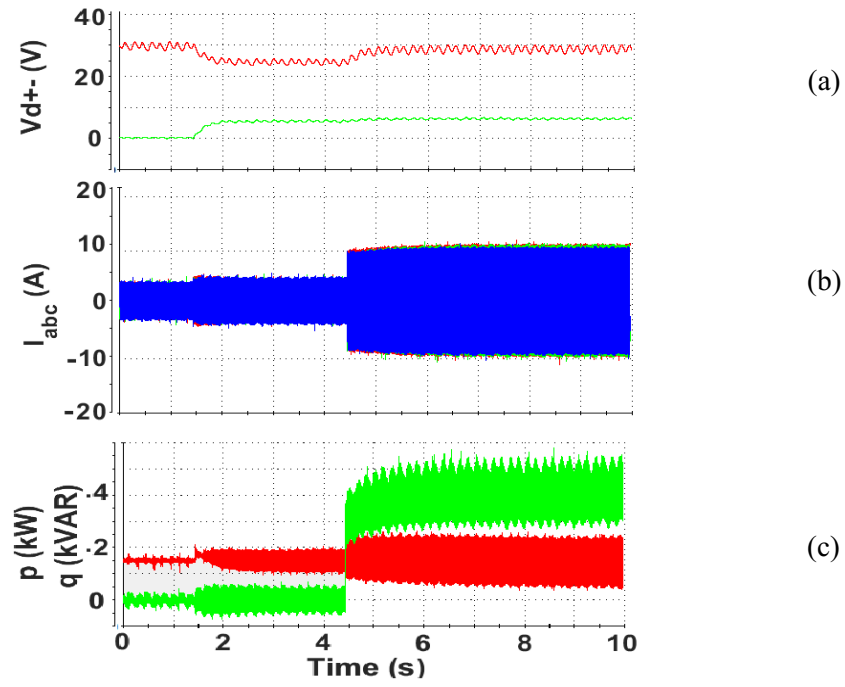


Figure 2.6 Experimental results of MAQ: (a) faulted voltage, (b) phase currents, (c) active and reactive powers.

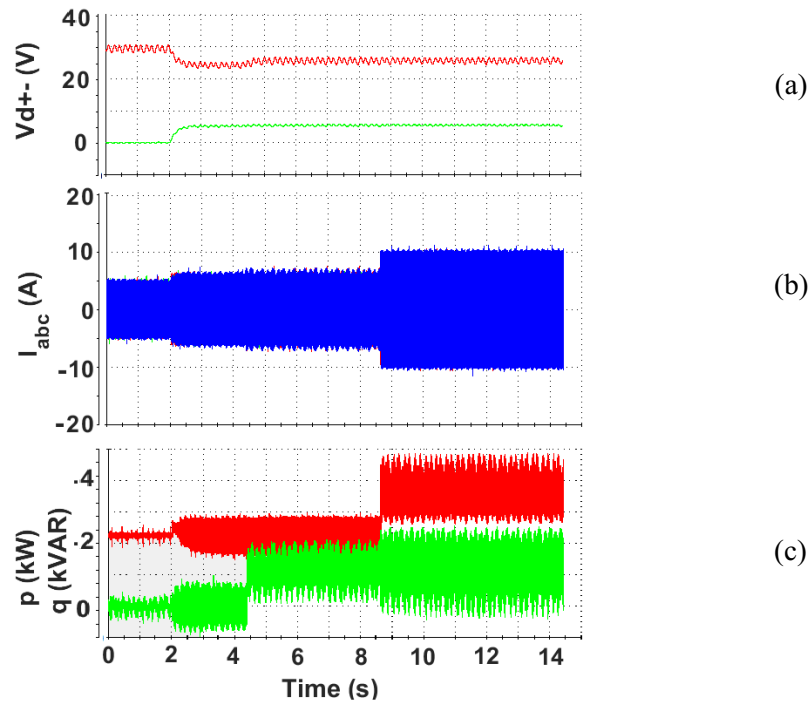


Figure 2.7 Experimental results of MAP: (a) faulted voltage, (b) phase currents, (c) active and reactive powers.

### 2.7.4 Experimental Test Case B: MAP Strategy

This test case provides the grid code requirement for the  $Q$  injection during the low-voltage and investigates the application of the MAP strategy. In this test case,  $P=225W$  is initially injected by the GSI, as indicated in Fig 2.7(c). Similarly, a phase-to-ground fault occurs in  $t=2$ . This fault causes the PCC voltage to drop from 30V to 25V. At  $t=4.3s$ , the reactive power imposed by the grid code requirement is injected. This injection causes the PCC voltage to increase to 26V, as shown in Fig 2.7(a). At  $t=8.6s$ , the MAP strategy is activated to inject the maximum allowable active power with respect to  $I_{limit}=10A$ . As shown in Fig 2.7(b), the abc currents are limited to 10A under the unbalanced fault and after applying MAP scheme.

## 2.8 Conclusion

This chapter presented multi-objectively optimized reference current generation schemes by injecting a proper set of positive/negative active/reactive currents using four controlling parameters. Analytical expressions were proposed in order to find the optimal values of these parameters under generic grid voltage condition. The proposed schemes aim to regulate the three phase voltages, minimize power oscillations, minimize fault currents, and maximize power delivery, under low voltage and unbalanced conditions. Depending on the available controlling parameters, two or three of these objectives can be achieved simultaneously, but not all of them since there are only four controlling parameters. This multi-objective optimized operation has substantial advantages in the increasing integration of GSIs, such as improving the efficiency, lowering DC-link ripples, increasing AC system stability, complying with stringent grid codes, and avoiding equipment tripping. The successful results of the proposed schemes were verified using simulation and experimental test results.

# Chapter 3

## Asymmetric Ride-Through (ART)

### Guidelines

#### 3.1 Introduction

The integration of renewable energy resources and DG units is remarkably increasing with no signs of slowing down. For more than a decade, system operators have been updating their grid codes to address the reliability concerns of such integrated grids [71]-[74]. First, this chapter briefly overviews the LVRT requirements and trends in different countries [72]-[83]. Then, a new scheme, called asymmetric ride-through (ART), is proposed in this chapter to enhance the system reliability under the short-term unbalanced faults. The ART scheme aims to enforce large DG units not only ride-through the asymmetrical grid faults, but also support the grid by proper measures. Based on the proposed scheme, DG units are required to withstand the short-term unbalanced low-voltages under certain circumstances. In the ART scheme, specific dynamic boundaries are developed for three voltage parameters (i.e., positive-sequence, negative-sequence, and magnitudes of phase voltages). If a DG with a proper voltage support strategy can meet the proposed requirements for these three voltage parameters, it will have a successful ART performance. The proposed regulation scheme can be very

beneficial for the growing integration of DG units as well as other converter-interfaced units such as grid-interactive micro-grids, and HVDC systems.

In section 3.4, this chapter also overviews the voltage support strategies (VSSs), under unbalanced conditions, presented in the recent works [36]-[53]. These strategies are categorized into four groups and briefly discussed. The compliance of the reviewed four VSS groups [36]-[53] with the proposed ART scheme is studied in section 3.5. Then, a new ART-adaptive voltage support (ART-VS) method is proposed to enable DG units to meet the ART requirements. The proposed ART-VS method has the following advantages:

- 1) supporting the phase voltages under any unbalanced faults to the maximum capability of the DG,
- 2) preventing phase voltages from exceeding the boundaries proposed in the ART scheme by proper combination of voltage boost and unbalance reduction,
- 3) being adaptive to the dynamic ART boundaries, and
- 4) extending the tolerable fault time with successful ART performance.

By applying the proposed ART-VS method, phase voltages are time-varyingly regulated inside the dynamic boundaries introduced in the ART scheme, leading to successful ride-through. The effectiveness of the proposed ART scheme and ART-VS control method is validated by simulation and experimental test cases.

## **3.2 Overview of LVRT Codes in Different Countries**

In the early 2000s, the LVRT requirements were initially mandated by grid codes of the countries with high wind penetration levels such as Germany [65], Denmark [75], Spain [76] and other European countries [77]-[78]. Grid code development in other parts of the world usually follows Europe. In 2011, Chinese grid code eventually mandated wind power plants to meet a set of interconnection standards [79]. To increase the amount of wind generation and enhance grid performance, China currently has plans to continuously update and improve its grid

code. In Canada, several interconnection requirements have been developed by different transmission system operators [80]. In the United States, there are also several regulatory institutions that study and shape national interconnection standards, such as U.S. Federal Energy Regulatory Commission and North American Electric Reliability Corporation. In compliance with these national standards, regional reliability organizations have established their grid codes. Two prominent examples are the projects conducted by Independent System Operator–New England in 2009 [81] and the Electric Reliability Council of Texas in 2010 [82] which both have high wind installation targets for the future. As for the future, more changes and improvements are expected for the grid codes in the United States.

Typically, most grid codes require DG units to remain connected a minimum of 150ms [80], during balanced and unbalanced faults. This period can, however, vary based on the system characteristics (e.g., 400ms in Australian grid code [72] and 625ms in Ireland grid code [78]) and different voltage sags (e.g., 700ms in France grid code for voltage sags less than 0.5 p.u. [80]).

### **3.2.1 Reactive current injection (RCI)**

The RCI under grid faults is another requirement identified by some grid codes to provide the necessary support at the point of connection. In some countries, such as Brazil with lower wind integration, the transmission system operator does not stipulate yet the need of RCI during faults. However, system operators in some countries (i.e., Germany [65], Denmark [75], England [77], Ireland [78], and Spain [76]) impose RCI requirements for the large DG interconnections to support the grid reliability under grid faults. The primary grid codes on LVRT [65], [75]-[78] mainly focused on the interconnection requirements under balanced grid faults. However, the most recent grid code, published in 2015 in Germany [83], has even considered the negative-sequence current injection during unbalanced faults. In this regard, recent studies [59], [84] have also proposed the new LVRT methods with the negative RCI during unbalanced faults. These developments and continuous updates in interconnection requirements and increasing demand for

high penetration of DGs clearly show the necessity of grid codes evolution into more effective versions. The interconnection codes in different countries should improve to achieve two crucial objectives at the same time:

- 1) increasing the penetration level of clean and renewable energy resources, and
- 2) enhancing the stability and reliability of the highly-integrated grid.

This chapter thus proposes an extended version of the LVRT curves for the proper operation of DG units under short-term unbalanced grid faults.

### **3.2.2 Frequency Control and Active Power Restoration**

Frequency and active power control, under the grid faults, refer to the ability of DG units to regulate their power output to a defined level either by disconnecting or proper control [80]. The grid codes of Germany, Ireland, Nordic [86], and Denmark demand DG units to have the ability of active power curtailment. Generally, most grid codes require high capacity DG units to provide frequency response and contribute to the regulation of system frequency. The Irish [78] and Danish [75] codes demand active power control according to the frequency response curves. According to the German code [65], DG units must reduce their active power with a gradient of 40% (of the available power) per Hz when the frequency exceeds the value 50.2 Hz. The British code requires wind power plants to supply primary and secondary frequency control as well as over-frequency control. The Hydro-Quebec grid code [90] requires the wind power plants (with rated power greater than 10 MW) to have a frequency support control system. The timeframe for active power restoration varies in different grid codes. According to British [77] and Irish [78] codes, the active power must be rapidly restored to at least 90% of the pre-fault available value within 1s after the voltage recovery. While the German grid code requires restoration with a rate at least equal to 20% of the nominal output power (reaching 100% in 5s after voltage recovery) [65]. The requirement severity on the active power restoration corresponds to the grid strength. For example, grid codes in weak systems demand faster active power recovery to the pre-fault values

which is crucial for their system stability. It should be noted that the contribution of this chapter is to propose advanced RCI requirements; and the active power restoration and frequency control are not the main scope of this chapter. Therefore, the timeframes of the active power restoration prescribed in the existing grid codes can also be adopted by the proposed ART scheme in this chapter.

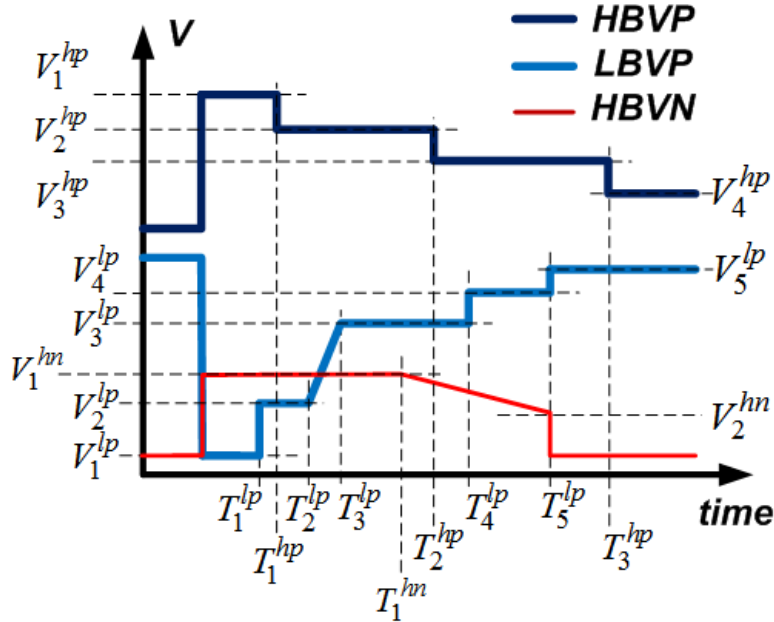


Figure 3.1 General schematic of the proposed ART boundary curves for the positive-sequence, negative-sequence, and phase-voltage magnitudes at the PCC of a DG unit.

### 3.3 Proposed Asymmetric Ride-Through (ART)

#### Guidelines

It is proposed in this paper to extend the LVRT curves by specifying certain regulation curves for proper operation of DG units under short-term unbalanced grid faults. In other words, the proper performance of DG units is defined in terms of the three important voltage terms at the PCC using three proposed ART curves illustrated in Fig 3.1. The first curve, named LBVP, defines a lower boundary for the positive-sequence voltage value,  $V_p$ , (under unbalanced grid faults) that is similar to the LVRT curves which typically define boundaries for the RMS values of the voltage at the PCC. Therefore, five time parameters ( $T_1^{lp}, T_2^{lp}, \dots, T_5^{lp}$ ) and five

voltage parameters ( $V_1^{lp}, V_2^{lp}, \dots, V_5^{lp}$ ) have been embedded in the proposed LBVP curve to be able to capture the specifications from 23 different grid codes [72]-[80]. For instance, only two  $T^{lp}$  and two  $V^{lp}$  parameters are enough to adopt the LBVP curve of Fig 3.1 from the LVRT codes of Germany [65] and Ireland [78]. However, adopting from some other codes requires more parameters. For instance, three  $T^{lp}$  and three  $V^{lp}$  parameters are required to adopt LBVP curve from the French and Italian codes [80].

The second proposed curve, named HBVN, defines a higher boundary for the negative-sequence voltage value,  $V_n$ , at the PCC. The HBVN curve is important since it prescribes DG units to support the grid by balancing the phase voltages and reducing the negative-sequence component. To present a simple yet effective boundary for the negative-sequence voltage, the proposed HBVN curve is designed adaptive to the first curve, i.e., LBVP, as demonstrated in Fig 3.1. Thus, it only comprises one time parameter ( $T_1^{hn}$ ) and two voltage parameters ( $V_1^{hn}, V_2^{hn}$ ). The third proposed curve, named HBVP, determines the higher boundary for the phase voltage peaks at the PCC. This curve is beneficial to regulate the maximum tolerable voltage magnitudes based on the system and DG unit characteristics and avoid over-voltages. The HBVP curve is designed to be able to capture the specifications of the over-voltage regulations in different codes. Thus, it has three time parameters ( $T_1^{hp}, T_2^{hp}, T_3^{hp}$ ) and four voltage parameters ( $V_1^{hp}, V_2^{hp}, \dots, V_4^{hp}$ ) as shown in Fig 3.1.

As stated earlier, three proposed ART curves aim to extend the concept of the existing LVRT curves to better regulate the operation of the grid-connected converters under asymmetric short-term faults for increasing the reliability in future's highly integrated power systems. Therefore, the following requirements are proposed in this chapter for a successful ART scheme, according to Fig 3.1:

- 1)  $V_p$  is (or can be regulated) above the LBVP curve
- 2)  $V_n$  remains (or can be regulated) under the HBVN curve, and

- 3) for unbalanced faults, none of the phase voltage magnitudes exceeds the HBVP curve.

If the applied VSS in the grid-connected converter-based unit can satisfy all three requirements, the unit can stay connected to the grid to avoid cascaded outages and support the system reliability. Three proposed ART curves contain 11 voltage parameters and 9 time parameters in total. These 20 parameters, not only, make the ART scheme comprehensive and capable of adopting from the existing codes; but also, provides a proper specific regulation for asymmetric faults. Therefore, each grid code, based on its system characteristics and requirements, can suggest specific ART curves similar (or in addition) to its already-established LVRT curve.

Based on the general curves of Fig 3.1, two examples of the ART curves are proposed in this chapter. Fig 3.2 illustrates the first proposed curve, named ART-1, which comprises two stages, i.e., withstanding (immediately after the fault) and recovery stages. The duration of the first stage in the ART-1 is suggested to be 150ms after the fault occurrence. This value can vary based on the specification of each grid. However, since most grid codes have the first stage duration of 150ms in their LVRT curves, it is also suggested here for the ART-1 scheme. If the fault lasts more than 150ms and one of the followings happens:

- the magnitude of the positive-sequence voltage goes under the LBVP curve, or
- the magnitude of the negative-sequence voltage goes above the HBVN curve, or
- one of the phase voltage magnitudes goes above the HBVP,

the DG has two options:

- disconnecting from the grid, or
- remaining connected to the grid and supporting the PCC voltage (as much as it can) to satisfy the ART requirements.

Here, the goal is to keep the voltage magnitudes within the prescribed boundaries of the ART scheme as much as possible by boosting the positive-sequence voltage and reducing the negative-sequence value. Without any support, when one of the voltage terms passes the corresponding ART curve, it is no longer necessary to stay connected; but it is still preferred that the DG utilizes its available capacity to further stand connected by regulating its voltage parameters within the prescribed ART boundaries. The more one DG can support the PCC to stay within the prescribed ART boundaries, the more reliability the host grid can have. For the simplicity, 20 ART parameters of Fig 3.1 are aggregated in six voltage parameters and three time parameters (as shown with the suggested values in Fig 3.2). Fig 3.3 also shows another proposed example for riding through asymmetrical faults, named as ART-2. According to ART-2 curves, the faults with  $V_p$  down to zero should be tolerated up to 150ms. Also, the voltage sags with a  $V_p$  value more than 0.5p.u. should be endured up to 2s. The values of eight voltage parameters and four time parameters in ART-2 curves are proposed as shown in Fig 3.3.

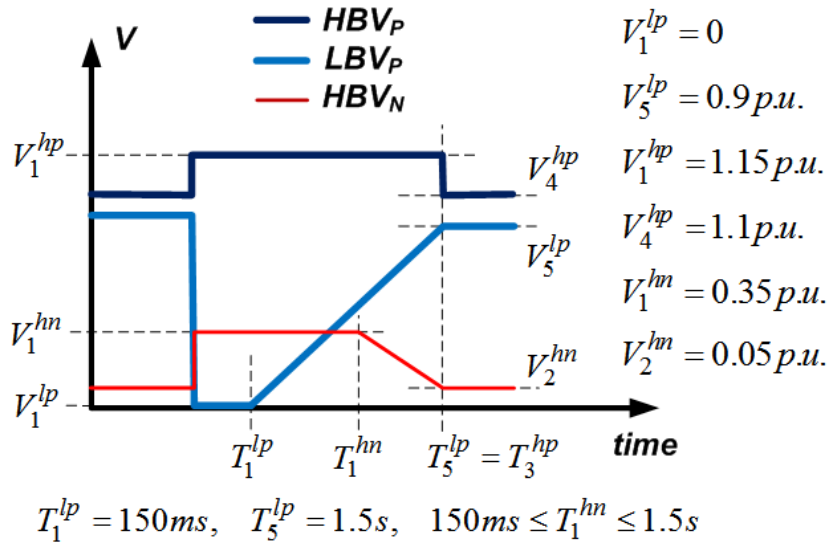


Figure 3.2 Proposed ART-1 curves.

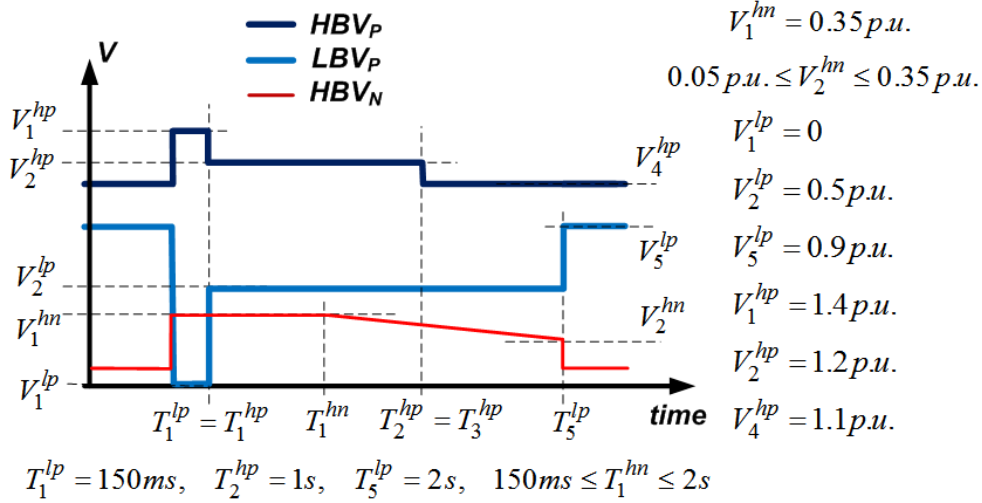


Figure 3.3 Proposed ART-2 curves.

### 3.4 Overview of Conventional Voltage Support Strategies under Unbalanced Conditions

This chapter overviews the VSSs under unbalanced conditions, presented in the recent works [36]-[53]. These strategies are categorized into four groups and briefly discussed. The compliance of the reviewed four VSS groups [36]-[53] with the proposed ART scheme is studied in section 3.5.

Fig 2.1 illustrated the diagram of a DG unit interfaced with a grid-connected converter. For any unbalanced condition, the positive and negative sequence voltage vectors can be written in the  $\alpha\beta$  frame as

$$v^+ = \begin{bmatrix} v_\alpha^+ \\ v_\beta^+ \end{bmatrix} = \begin{bmatrix} V^+ \cos(\omega t + \delta^+) \\ V^+ \sin(\omega t + \delta^+) \end{bmatrix}, v^- = \begin{bmatrix} v_\alpha^- \\ v_\beta^- \end{bmatrix} = \begin{bmatrix} V^- \cos(\omega t + \delta^-) \\ -V^- \sin(\omega t + \delta^-) \end{bmatrix} \quad (3.1).$$

To exploit a flexible and supportive performance from a DG unit, its injected reactive current vector,  $i_q$ , can be divided into positive and negative sequences as

$$i = i_p + i_q^+ + i_q^- \quad \text{or}$$

$$\begin{aligned}
i = \begin{bmatrix} i_\alpha \\ i_\beta \end{bmatrix} &= \begin{bmatrix} I_p \cos(\omega t + \delta^+) \\ I_p \sin(\omega t + \delta^+) \end{bmatrix} \\
&+ \begin{bmatrix} I_q^+ \sin(\omega t + \delta^+) \\ -I_q^+ \cos(\omega t + \delta^+) \end{bmatrix} + \begin{bmatrix} -I_q^- \sin(\omega t + \delta^-) \\ -I_q^- \cos(\omega t + \delta^-) \end{bmatrix}
\end{aligned} \tag{3.2},$$

where the superscripts “+”/“-” and subscripts “p”/“q” denote the positive/negative and active/reactive components, respectively. The mathematical expressions of the ac-side voltages are

$$v = v^+ + v^- = \begin{bmatrix} v_\alpha^+ \\ v_\beta^+ \end{bmatrix} + \begin{bmatrix} v_\alpha^- \\ v_\beta^- \end{bmatrix} = \begin{bmatrix} v_{g\alpha}^+ \\ v_{g\beta}^+ \end{bmatrix} + \begin{bmatrix} v_{g\alpha}^- \\ v_{g\beta}^- \end{bmatrix} + L_g \frac{d}{dt} \begin{bmatrix} i_\alpha \\ i_\beta \end{bmatrix} + R_g \begin{bmatrix} i_\alpha \\ i_\beta \end{bmatrix} \tag{3.3},$$

where the subscript “g” represents the grid components. In the following subsections, different voltage support techniques introduced in the literature [36]-[53] for DG units under unbalanced conditions are presented in four categories.

### 3.4.1 Positive-Sequence Reactive Current Injection (PSRCI)

The German grid code, E.ON [65] forces wind farms to support grid voltage with additional reactive current only during a three-phase symmetrical voltage dip, amounting to at least 2% of the rated current for each percent of the voltage dip. The symmetrical voltage dip is defined as the magnitude of the balanced three-phase voltage drop at the low-voltage side of the interconnection transformer. Similarly, references [36]-[39] tried to present some strategies to apply this rule in the case of asymmetrical faults. Therefore, the reference value for the reactive current, , can be generated by [65]

$$I_{q^+,PSRCI}^{ref} = 2 \times \frac{V_{nom} - V_p}{V_{nom}} \times I_{max} \tag{3.4},$$

where  $V_{nom}$  is the nominal voltage, and  $I_{max}$  is the rated current of the inverter.

### 3.4.2 Voltage Support Based on the Maximum Allowable Reactive Power Delivery (MARPD)

The grid codes in Britain [77] and Ireland [78] denote that wind power plants must deliver their maximum reactive current only during a symmetrical voltage dip. Similar to Britain and Ireland grid codes [77]-[78], references [41]-[42] presented the MARPD for unbalanced grid conditions. Using the MARPD strategy, the GSI injects the maximum reactive power and respects the phase currents limit under unbalanced faults by reactive current command of

$$I_{q^+,MARPD}^{ref} = \sqrt{I_{\max}^2 - I_p^2} \quad (3.5),$$

where  $I_p$  is the reference value of the active current. The detailed derivation of maximum available reactive currents can be found in [41]-[42].

### 3.4.3 Mixed Sequence Injection (MSI)

References [43]-[45] suggested some strategies which are based on the injection of both positive and negative currents to support the connection voltage by a combination of boosting and equalizing the phase voltage magnitudes. According to [44], both positive and negative sequence reactive currents are injected under unbalanced faults. The reference values for Eq (3.2) can thus be obtained as

$$I_{q^+,MSI}^{ref} = k^+ \times \frac{V_1 - V_p}{V_{nom}} \times I_{\max}, \quad I_{q^-,MSI}^{ref} = k^- \times \frac{V_2 - V_n}{V_{nom}} \times I_{\max} \quad (3.6),$$

where the recommended values for four parameters of (6) are , p.u., and p.u. [44].

### 3.4.4 Positive-Negative Sequence Voltage Regulation (PNVR)

In the most recent literature [46]-[53], the voltage regulation strategies aim to determine proper reactive current reference values to regulate the phase voltage magnitudes within the desired margin under unbalanced conditions. The magnitudes of the phase voltages in terms of the magnitudes of positive and negative sequence voltages are obtained by the following expressions:

$$\begin{aligned}
V_a &= \sqrt{(V_p)^2 + (V_n)^2 + 2(V_p)(V_n)\cos(\gamma) + (V^0)\cos(\phi^0)} \\
V_b &= \sqrt{(V_p)^2 + (V_n)^2 + 2(V_p)(V_n)\cos(\gamma)\cos(\gamma - \frac{2\pi}{3}) + (V^0)\cos(\phi^0 + \frac{2\pi}{3})} \quad (3.7), \\
V_c &= \sqrt{(V_p)^2 + (V_n)^2 + 2(V_p)(V_n)\cos(\gamma)\cos(\gamma + \frac{2\pi}{3}) + (V^0)\cos(\phi^0 - \frac{2\pi}{3})}
\end{aligned}$$

where  $V_a$ ,  $V_b$ , and  $V_c$  are magnitudes of the phase voltages, and  $\gamma = \delta^+ - \delta^-$ ,  $\gamma^0 = \delta^0 - \delta^+$ . References [46]-[51] neglect the zero sequence voltage terms and simplifies the problem. Then, the reference values for the positive and negative voltage values are obtained in [49] as

$$\begin{aligned}
(V_{ref}^+)^2 &= \frac{xV_y^2 - yV_x^2 + \sqrt{(xV_y^2 - yV_x^2)^2 - (V_y^2 - V_x^2)^2}}{2(x-y)} \\
(V_{ref}^-)^2 &= \frac{xV_y^2 - yV_x^2 - \sqrt{(xV_y^2 - yV_x^2)^2 - (V_y^2 - V_x^2)^2}}{2(x-y)} \quad (3.8),
\end{aligned}$$

where,

$$\begin{aligned}
V_y &= V_{\min}, \\
V_x &= \min(V_{\max}, V_{\min} + \max\{V_a, V_b, V_c\} - \min\{V_a, V_b, V_c\}) \\
y &= \min(\cos(\gamma), \cos(\gamma - \frac{2\pi}{3}), \cos(\gamma + \frac{2\pi}{3})), \\
x &= \max(\cos(\gamma), \cos(\gamma - \frac{2\pi}{3}), \cos(\gamma + \frac{2\pi}{3}))
\end{aligned} \quad (3.9).$$

Finally, the reference values of Eq (3.10) are determined:

$$I_{q^+,PNVR}^{ref} = (V_{ref}^+ - V_g^+) / X_g, \quad I_{q^-,PNVR}^{ref} = (V_g^- - V_{ref}^-) / X_g \quad (3.10),$$

where  $X_g$  is the equivalent line impedance (i.e.  $X_g = \omega L_g$ ). Eq (3.10) provides the voltage regulation based on the positive and negative sequence voltage values, and it is named PNVR in this chapter. The positive and negative reactive currents that fulfill the voltage support method need an estimate of the line inductance. In [46], [49], the PNVR strategy was only applied to the STATCOM application where

the reference current only consists of the reactive components. Also, the PNVR strategy is only suggested for the inductive grids. However, the effects of the inverter active power and line resistance in regulating the voltage are considered in [52].

### **3.5 Compliance of the Conventional Voltage Support Strategies with the Proposed ART Guidelines**

This section examines the capability of the conventional voltage support techniques [36]-[53] in satisfying the ART requirements. The test system is shown in Fig 2.1 (with the parameters listed in Table 3.2). To demonstrate the performance of these strategies considering the proposed ART requirements, a short-term unbalanced (double-phase) fault of Fig 3.4 is implemented. According to ART-1 with  $t = 1s$ , the DG is required to withstand at least 0.75s after the fault occurrence since all three criteria are met until this time (see Fig 3.4(a)). After 0.75s, it is preferred that the DG utilizes its available capacity to further stand connected by regulating its voltage parameters within the ART boundaries. If the ART-2 scheme is imposed in this case, the DG is only required to withstand the unbalanced fault up to 150ms after the occurrence since the positive voltage goes to the area where disconnection is allowed by ART-2 (see Fig 3.4(b)). However, it is preferred that the DG uses a proper technique to regulate the voltage terms within the ART curves.

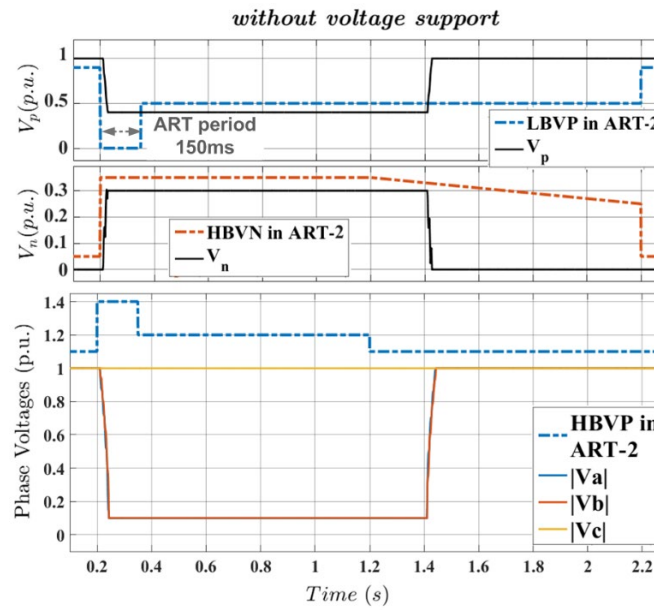
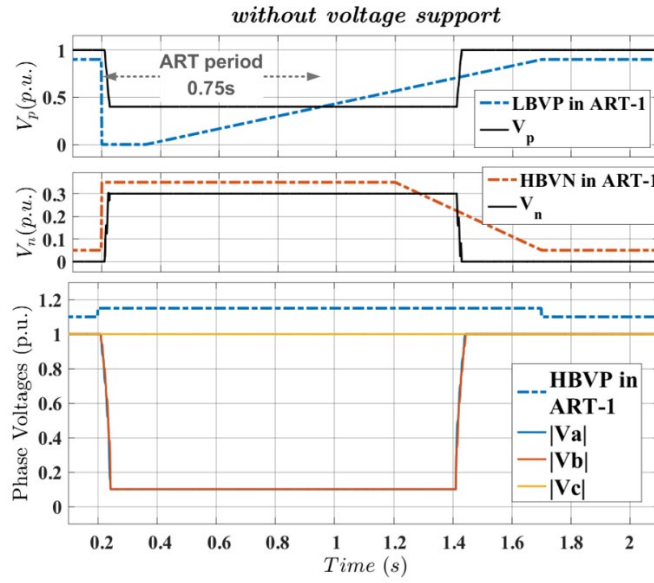
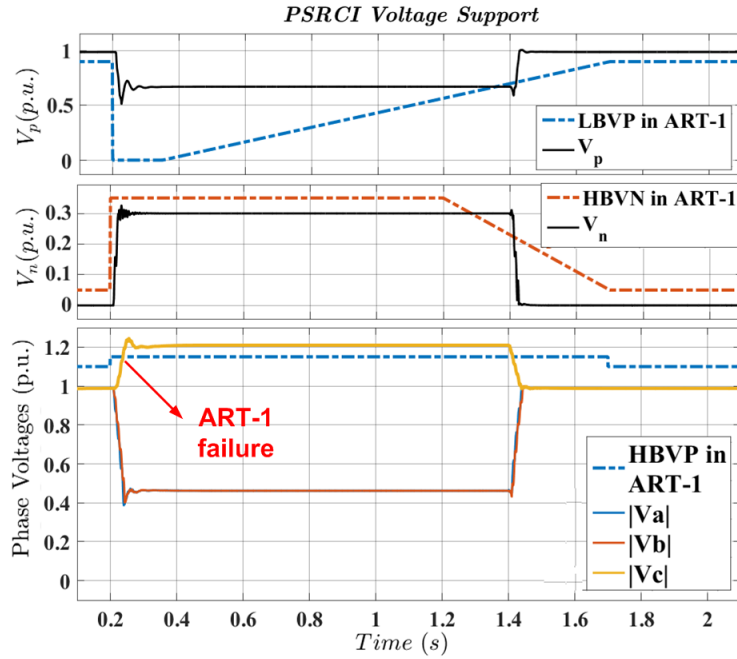
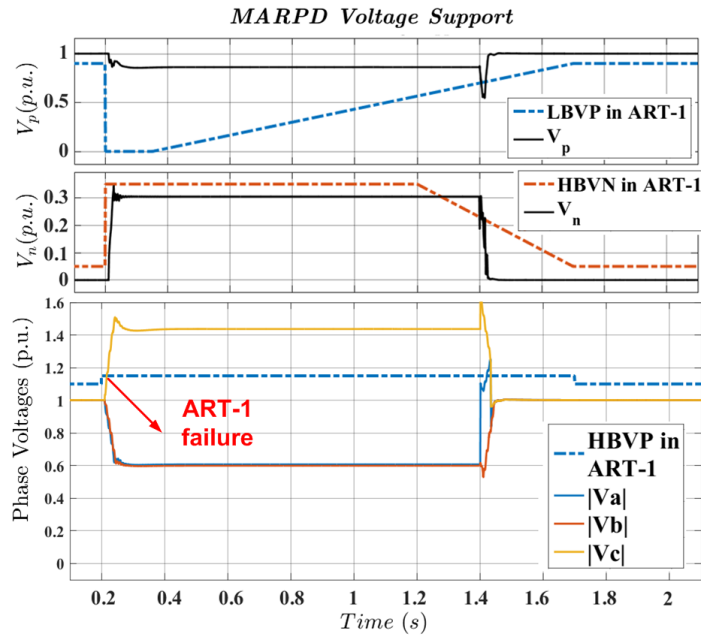


Figure 3.4 Test Case A: two-phase fault scenario when (a) ART-1 scheme, or (b) ART-2 scheme is applied.



(a)



(b)

Figure 3.5 Test Case A: ART-1 scheme with conventional VSSs: (a) PSRCI [36]-[39], (b) MARPD [41]-[42].

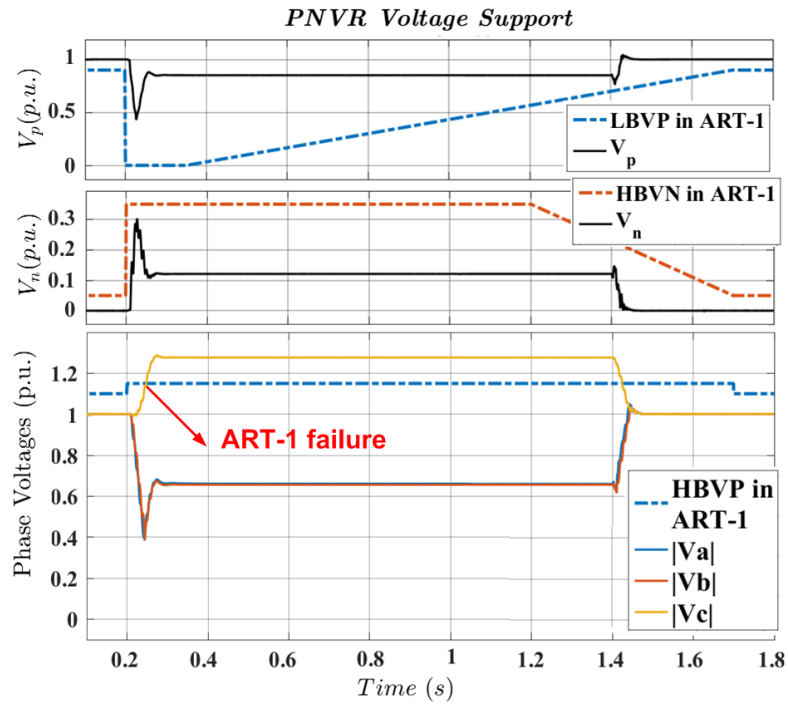
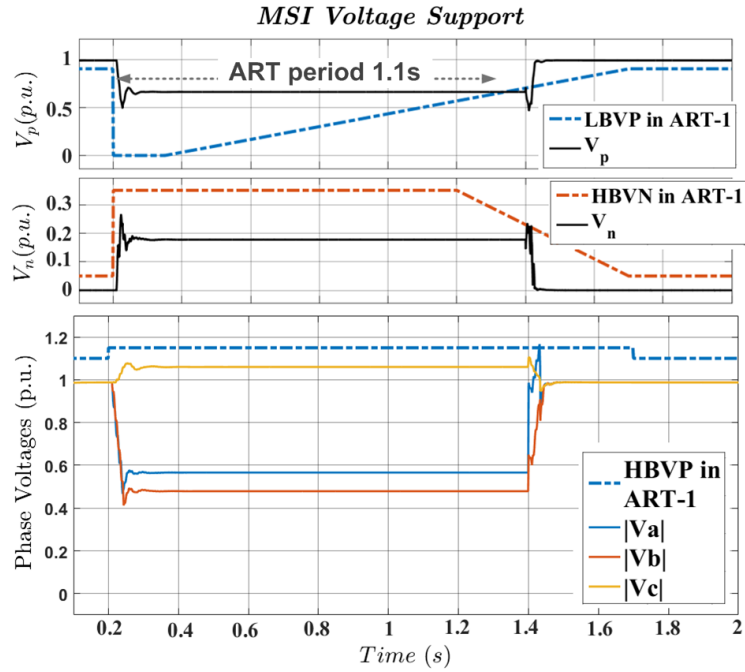


Figure 3.6 Test Case A: ART-1 scheme with conventional VSSs: (a) MSI [43]-[45], and (b) PNVR [46]-[53].

Fig 3.5 and 3.6 demonstrate the performance of the four conventional VSSs under the unbalanced condition of Fig 3.4 when the ART-1 scheme is imposed. According to Fig 3.5, none of the strategies can fully ride-through the unbalanced fault until the fault clearance. As expected, Fig 3.5(a) shows that the PSRCI strategy only supports the positive sequence voltage. This strategy suffers from the lack of negative-sequence reactive current injection. Therefore, the un-faulted phase experiences an overvoltage, there is a high unbalance between the phases, and the negative sequence voltage remains high. According to Fig 3.5-(b), the MARPD strategy has an almost similar performance. As expected, the MARPD strategy uses all the reactive current capacity and causes a higher boost in all phases in comparison with the PSRCI results. Not only this higher reactive current does not help the voltages properly but also it worsens the situation by creating higher overvoltage in the un-faulted phase. As Fig 3.6-(a) shows, although the negative and positive sequence voltages are appropriately controlled by the PNVR, this strategy is not successful in avoiding the overvoltage on the un-faulted phase. The MSI has better results than the other three strategies, as indicated in Fig 3.6-(b). All phase voltages stay under the ART-1 boundary, and the positive sequence voltage is compensated above the proposed boundary until 1.1s after the fault. Therefore, the MSI is the only strategy that could regulate the voltage terms within the recommended boundaries more than 0.75s (which is the required time imposed by the ART-1 for this fault case).

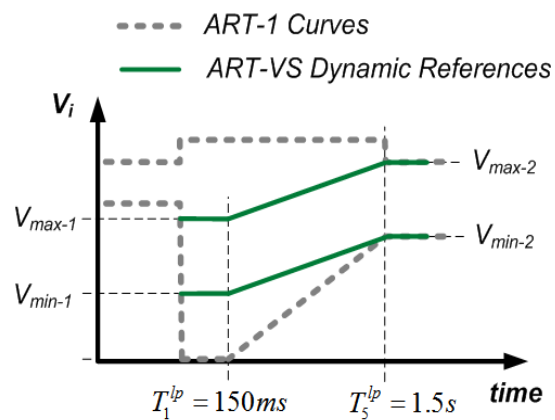


Figure 3.7 Proposed ART-VS dynamic reference setting for  $V_{max}$  and  $V_{min}$ .

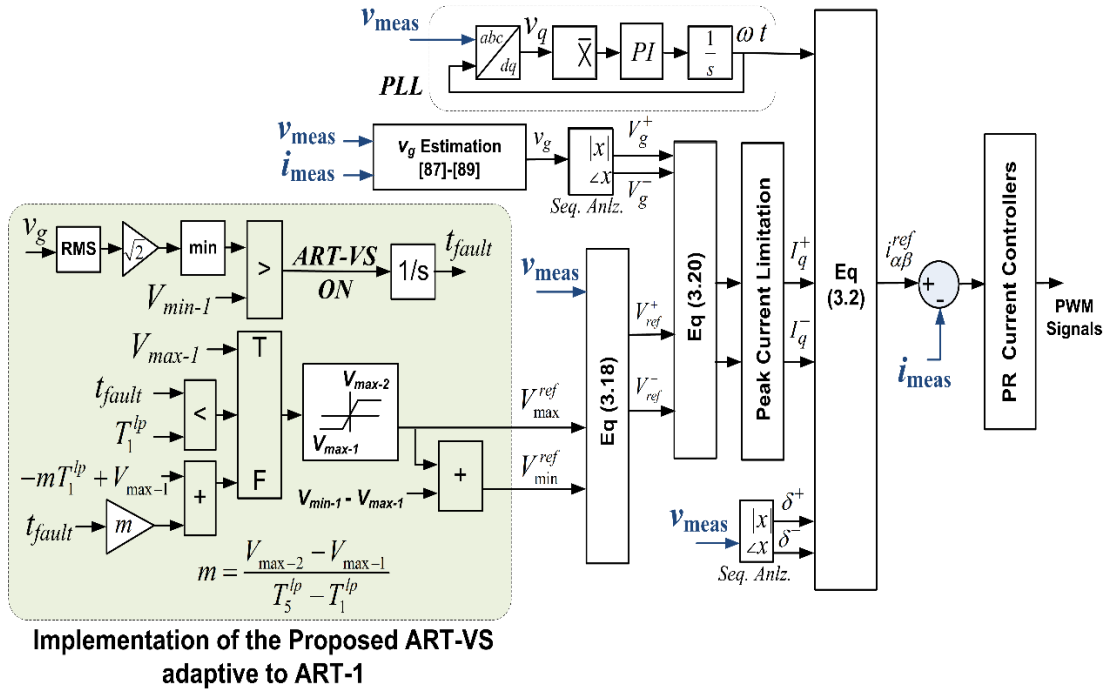


Figure 3.8 Proposed ART-VS control blocks.

### 3.6 Proposed ART-Adaptive Voltage Support

As examined in the previous section, the existing VSSs in the literature are not able to completely fulfill the three criteria proposed in the ART scheme. Sometimes they fail before the required time of staying connected, and sometimes they do not have preferable performance after the required time. Therefore, an advanced voltage support method is proposed in this chapter, named ART-VS. The proposed ART-VS method has two significant advantages:

- 1) it is adaptive to the proposed ART curves, and
- 2) its reference values (for the phase voltage magnitudes) can dynamically vary during and after the fault to provide the superior voltage regulation and riding-through capabilities.

The proposed adaptive and dynamic setting of the reference values for the minimum and maximum phase voltage magnitudes are based on the system characteristics, and they dynamically change during the ART period as

illustrated in Fig 3.7. This setting consists of four parameters,  $V_{min-1}$ ,  $V_{min-2}$ ,  $V_{max-1}$ , and  $V_{max-2}$ . These parameters can be determined based on the system characteristics:

- 1) line impedance,  $X_g$ ,
- 2) type, depth, and duration of the worst unbalanced fault that is needed to be ridden through, and
- 3) peak currents of the power electronic switches.

The grid voltage is estimated by the local measurements and using the following equation:

$$v_g = v - R_g i - L_g \frac{di}{dt} \quad (3.11).$$

### 3.6.1 Determination of Dynamic Reference Values for Minimum and Maximum Phase Voltage Magnitudes

In the proposed ART-VS method, the desired operation is to regulate the all three-phase voltage magnitudes such that the minimum and maximum phase voltage magnitudes,  $V_{min}$  and  $V_{max}$ , are dynamically regulated adaptive to the proposed ART curves. If the rated power of the DG unit and the connecting line impedance are not small, this objective can be accomplished by reference values indicated in Fig 3.7 for  $V_{min}$  and  $V_{max}$ . For example, in the studied case of the previous section, where  $X_g=0.5$  p.u. and  $I_{max}=1$  p.u., the four parameters of Fig 3.7 can be pre-determined as follows.

#### Determination of $V_{min-1}$ :

The following equation shows how much boost in one phase is expected based on the reactive current injection in that phase and the line impedance.

$$\Delta V_i = X I_{i,q} \quad i: \text{faulted phase, } a, b, \text{ or } c \quad (3.12).$$

Therefore, if the maximum current limit is assumed 1 p.u. and  $X$  is 0.5p.u. the following voltage boost in the faulted voltage can be expected:

$$\Delta V_i \leq X I_{i,q} = 0.5 \text{ p.u.} \rightarrow V_{min-1} - V_i \leq 0.5 \text{ p.u.} \quad (3.13).$$

From Eq (3.13) and considering the demand of the ART-1 scheme which is tolerating the unbalanced faults even down to the zero at the withstanding stage (see Fig 3.1), a proper  $V_{min-1}$  can be selected as

$$V_{min-1} \leq 0.5 \text{ p.u.} \quad (3.14).$$

#### **Determination of Vmax-1:**

Utilizing the negative reactive current in Eq (3.2), the overvoltage on the un-faulted phase can be avoided; and simultaneously, the negative sequence voltage and unbalance factor can be reduced by proper setting of  $V_{max-1}$ . Therefore, the maximum reduction on un-faulted phase can be formulated, and  $V_{max-1}$  can be determined as

$$|\Delta V_j| \leq XI_{j,q} = 0.5 \text{ p.u.} \rightarrow V_j - V_{max-1} \leq 0.5 \text{ p.u.} \quad (3.15).$$

*j: unfaulted phase, a, b, or c*

In the normal cases, the un-faulted phase voltage is typically 1 p.u.. Thus,

$$0.5 \text{ p.u.} \leq V_{max-1} \leq 1 \text{ p.u.} \quad (3.16).$$

#### **Determination of Vmax-2 and Vmin-2:**

Depending on the selected ART scheme, the value of  $V_{max-2}$  and  $V_{min-2}$  are determined. For example, for the ART-1 and ART-2 schemes presented in Figs. 2 and 3,  $V_{max-2}$  and  $V_{min-2}$  are obtained 1.1p.u. and 0.9p.u., respectively. Also, for the simplicity, the following expression can be set

$$V_{min-2} - V_{min-1} = V_{max-2} - V_{max-1} \quad (3.17).$$

Then,  $V_{min-1}$  and  $V_{max-1}$  can be found based on (14), (16), and (17). For example, if  $V_{min-1}=0.5\text{p.u.}$  is chosen from Eq (3.14),  $V_{max-1}$  is obtained 0.7p.u. based on (3.17) and the values of  $V_{max-2}=1.1 \text{ p.u.}$  and  $V_{min-2}=0.9\text{p.u.}$ .

### 3.6.2 Reactive Current Injection

The dynamic reference values of minimum and maximum phase voltage magnitudes,  $V_{\min}^{ref}$  and  $V_{\max}^{ref}$ , that are introduced in the previous sub-section and shown in Fig 3.7, are used to calculate the proper dynamic set-points for the proposed ART-VS method. From (3.7), the maximum and minimum phase voltage magnitudes can be determined by

$$\begin{aligned} V_{\min} &= \sqrt{(V^+)^2 + (V^-)^2 + 2(V^+)(V^-)y + (V^0)\lambda_{\min}^0} \\ V_{\max} &= \sqrt{(V^+)^2 + (V^-)^2 + 2(V^+)(V^-)x + (V^0)\lambda_{\max}^0} \end{aligned} \quad (3.18),$$

where  $\lambda_{\min}^0$  and  $\lambda_{\max}^0$  can be found as follows

$$\begin{cases} \text{if } y = \cos\left(\gamma + k_1 \frac{2\pi}{3}\right) \rightarrow \lambda_{\min}^0 = \cos\left(\gamma^0 + k_1 \frac{2\pi}{3}\right) \\ \text{if } x = \cos\left(\gamma + k_2 \frac{2\pi}{3}\right) \rightarrow \lambda_{\max}^0 = \cos\left(\gamma^0 + k_2 \frac{2\pi}{3}\right) \end{cases} \quad (3.19),$$

where  $k_1$  and  $k_2$  can take 0, 1, and -1 values, respectively, for phases a, b, and c. Applying  $V_{\min}^{ref}$  and  $V_{\max}^{ref}$  from Fig 3.7 in (3.18), the dynamic values for the  $V_{ref}^+$  and  $V_{ref}^-$  can be solved. It is worth mentioning that Chapter 4 discusses solving the  $V_{ref}^+$  and  $V_{ref}^-$  equation while considering the zero-sequence compensation.

Finally, the required reactive current references in the proposed ART-VS method can be set as

$$I_{q^+, ART-VS}^{ref} = \frac{V_{ref}^+ - V_g^+}{X_g}, \quad I_{q^-, ART-VS}^{ref} = \frac{V_g^- - V_{ref}^-}{X_g} \quad (3.20).$$

## 3.7 Simulation Results

As presented in section 3.5, none of the four conventional voltage support groups could fully ride through the asymmetric fault of test case A. However, the proposed ART-VS method provides the adaptive and dynamic voltage regulation. As Fig 3.9 illustrates, the ART-VS method regulates the values of  $V_p$ ,  $V_n$ , and phase voltage

magnitudes within the ART-1 boundaries and satisfies all three requirements presented in section 3.3. Therefore, the DG unit experiences a successful ride-through under this unbalanced fault. To further show the effectiveness of the proposed ART-VS method, four other simulation test cases are examined in this section. The fault characteristics of all test cases are reported in Table 3.1. Table 3.4 presents the results of the conventional strategies and the proposed ART-VS method. According to this table, the PSRCI and MARPD strategies suffer from the lack of negative voltage support. Furthermore, the PNVR and MSI strategies show better performances. According to TABLE 3.3, the MSI gives proper results in regulating the phase voltage peaks and insufficient performance in reducing the unbalance factor. On the other hand, the PNVR is successful in reducing the negative-sequence voltage and ineffective in regulating the peak values. Thus, these two strategies are unable to fully satisfy the three requirements defined by the ART-1 scheme. In contrast, the proposed ART-VS method successfully satisfies all three requirements in all cases.

Fig 3.10 shows the comparison between the results of the PSRCI and ART-VS strategies under the time-varying asymmetric fault of the test case E. In this test case, both faulted phases experience time-varying voltage dip. As Fig 3.10(a) shows, the phase voltage of the un-faulted phase, in the PSRCI strategy, exceeds the HBVP boundary. However, Fig 3.10(b) shows that the ART-VS method satisfies the three requirements and provides the successful ART performance.

**TABLE 3.1 Fault Characteristics of Five Test Cases**

	Faulty phases (p.u.)	$V_p$ (p.u.)	$V_n$ (p.u.)
Test Case A	$V_a = V_b = 0.1$	0.4	0.3
Test Case B	$V_a = 0$	0.67	0.33
Test Case C	$V_a = V_b = 0$	0.33	0.33
Test Case D	$V_a = 0, V_b = 0.5$	0.5	0.29
Test Case E	$V_a(t) = -0.5t+0.6$ $V_b(t) = 0.75t+0.1$	$V_p(t) = 0.08t+0.57$	

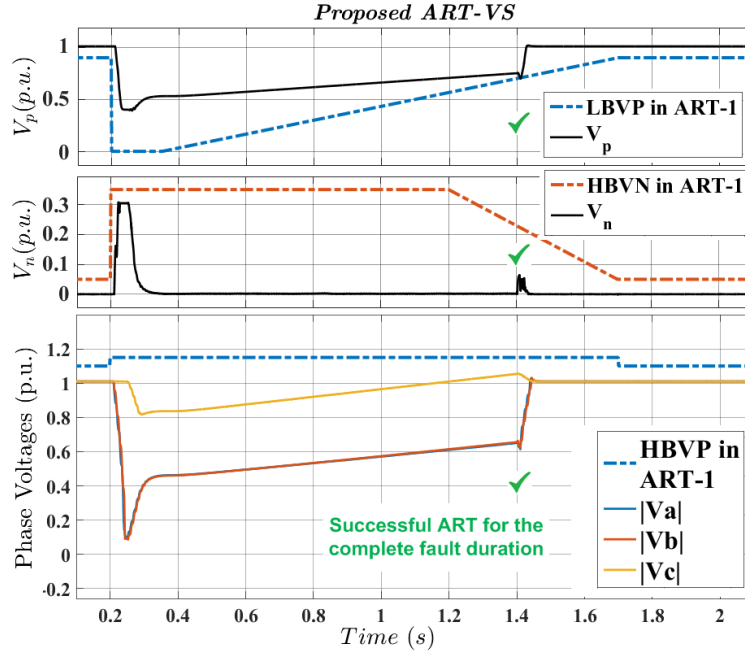


Figure 3.9 Test Case A: Voltage support by the proposed ART-VS.

**TABLE 3.2** Simulation Test System Parameters

$Z_g$	$j0.48 \Omega$	$V_{DC}$	1500 V
$S$	1.0 MVA	$V_{L-L, RMS}$	690 V
$I_{max}$	200 A	$f$	60 Hz

**TABLE 3.3** Experimental Test System Parameters

$I_{max}$	20 A (peak)	$V_g$	208 V
$L_g$	2.7 mH	$f$	60 Hz
$V_{min-1}$	125 V	$V_{min-2}$	187 V
$V_{max-1}$	166 V	$V_{max-2}$	229 V
$T_1^{hn}$	0.5 s	$V_2^{hn}$	2 V

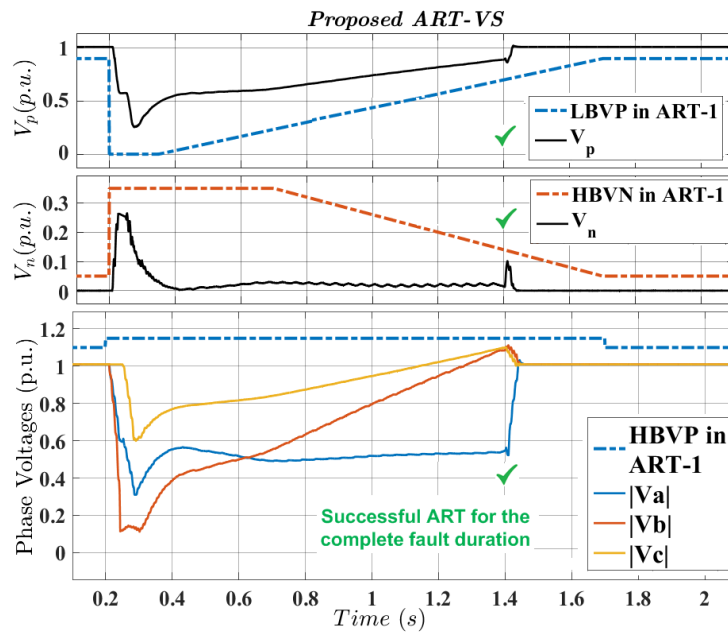
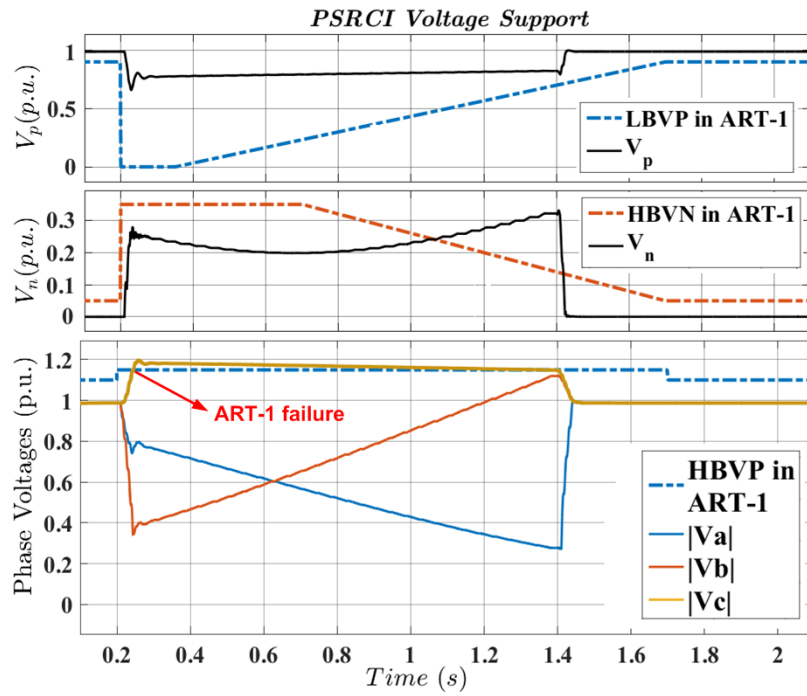


Figure 3.10 Test Case E: voltage support results by (a) conventional PSRCI strategy and (b) proposed ART-VS method.

**TABLE 3.4 Results of the Four Conventional Voltage Support Techniques [36]-[53] and the Proposed ART-VS Method**

	Strategy	LBVP	HBVN	HBVP
Test Case B	PSRCI	✓	×	✓
	MARPD	-	×	×
	MSI	✓	-	✓
	PNVR	✓	✓	×
	ART-VS	✓	✓	✓
Test Case C	PSRCI	✓	×	-
	MARPD	✓	×	×
	MSI	✓	×	✓
	PNVR	✓	✓	×
	ART-VS	✓	✓	✓
Test Case D	PSRCI	✓	×	-
	MARPD	✓	×	×
	MSI	✓	-	✓
	PNVR	✓	✓	×
	ART-VS	✓	✓	✓
Test Case E	PSRCI	✓	-	×
	MARPD	-	×	×
	MSI	✓	×	✓
	PNVR	✓	✓	×
	ART-VS	✓	✓	✓

### 3.8 Experimental Results

To further verify the effectiveness of the proposed schemes, a laboratory-scale test system is also employed. The test system contains a voltage source converter connected to an ac grid via impedances and a transformer. A Semistack intelligent power module, shown in Fig 3.11, is used which includes gate drives, six insulated-gate bipolar transistors, and protection circuit. The switching frequency of the transistors is 10 kHz, showing the computational efficiency of the proposed control technique. The converter is controlled by a dSPACE1104 card via a CMOS/TTL interfacing circuit, and is connected to a 60-Hz, 110-V (phase-voltage) grid. The software code is generated by using the Real-Time Toolbox under a MATLAB/Simulink environment for PWM signals generation. The parameters are listed in Table 3.3. The unbalanced faults are realized using circuit breakers and different fault impedances for each phase, as indicated for the without support case in Fig 3.12. Fig 3.13 and Fig 3.14, respectively, show the results of the conventional MSI strategy and the proposed ART-VS method, under the fault indicated in Fig 3.12. Bottom figures in Fig 3.13 and Fig 3.14 indicate the reference values of the positive- and negative-sequence reactive currents obtained by the MSI and ART-VS strategies. As Fig 3.13 reveals, the MSI method fails to satisfy the first two recommendations in the ART-1 scheme. However, the ART-VS method demonstrates successful performance in terms of all three criteria of the ART-1 scheme as indicated in Fig 3.14.

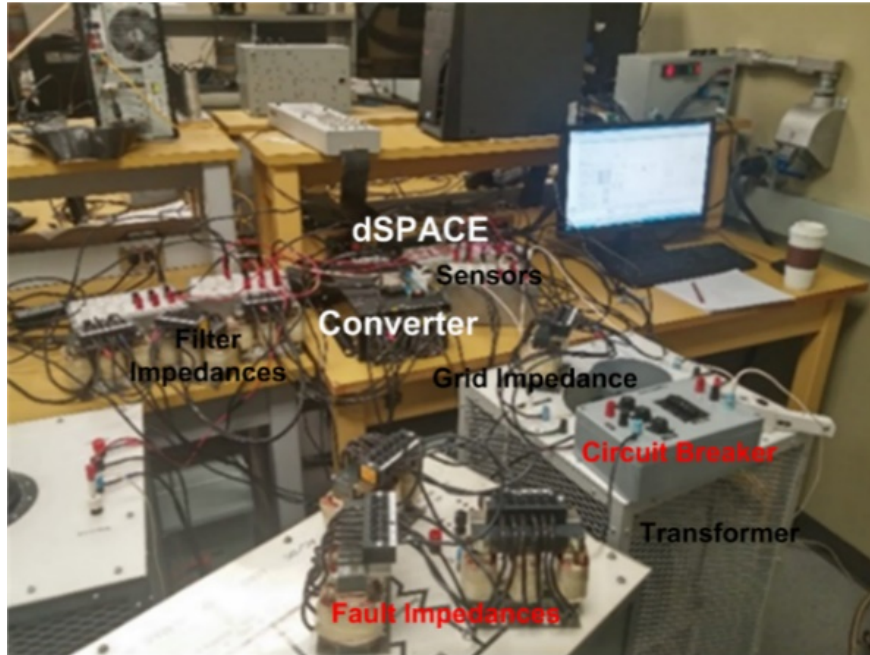


Figure 3.11 Scaled-down test setup.

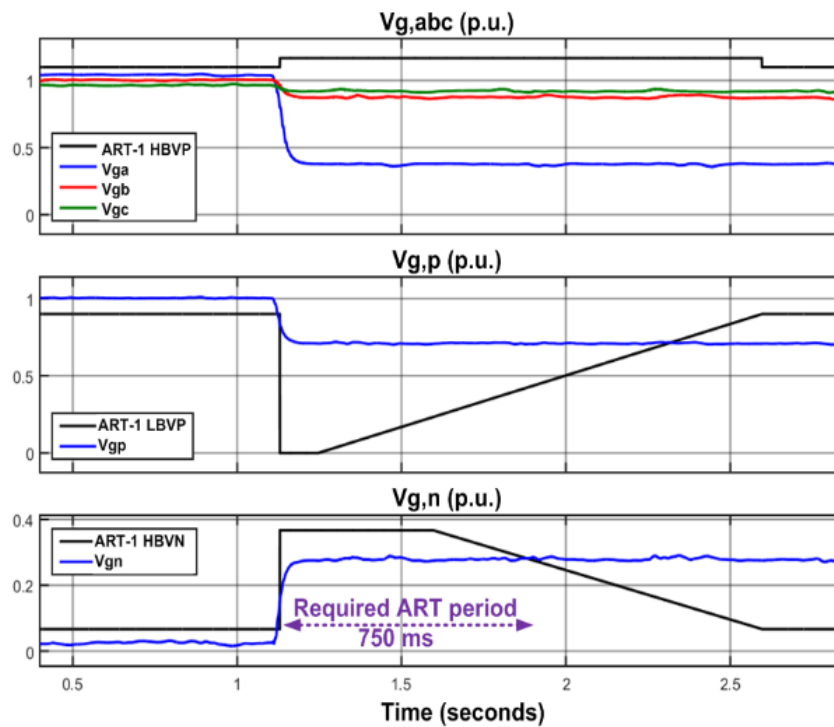


Figure 3.12 Experimental Test: without support.

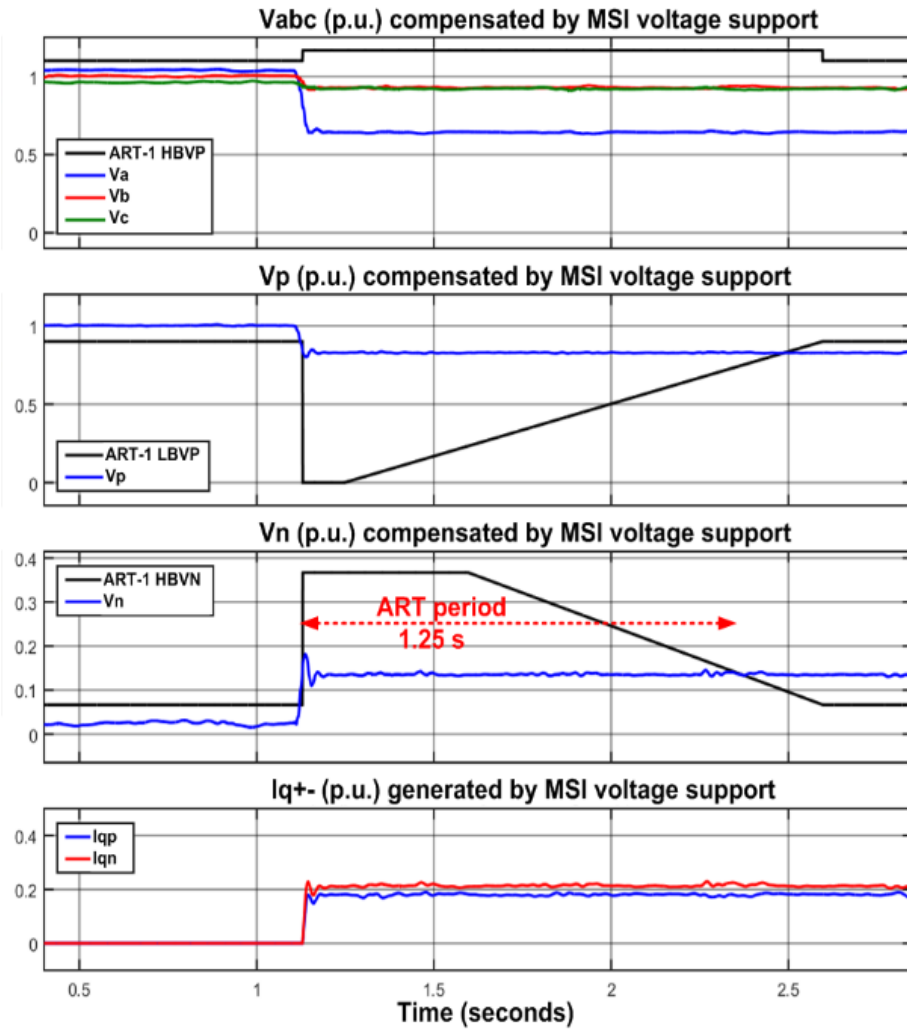


Figure 3.13 Experimental Test: (a) voltage without support, (b) voltage and current components with MSI,

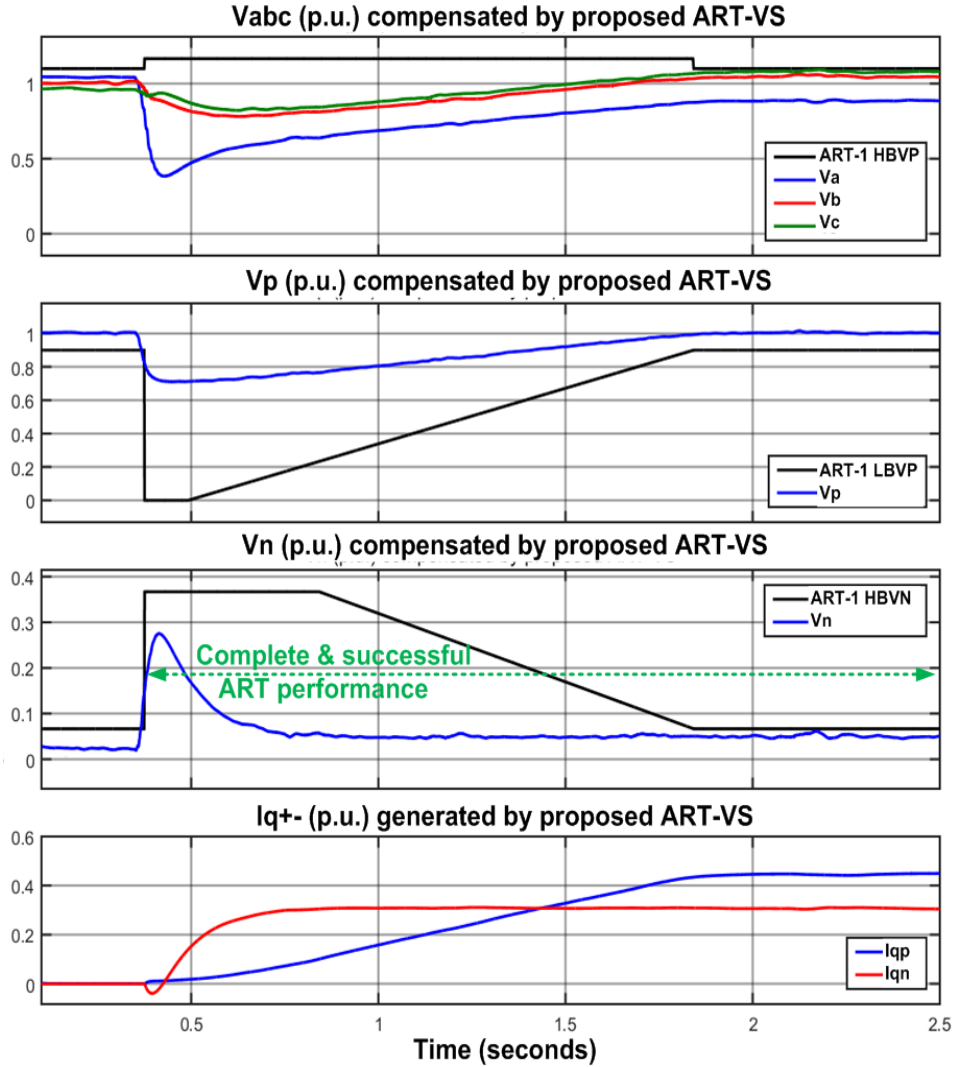


Figure 3.14 Experimental Test: voltage and current components with proposed ART-VS

### 3.9 Discussion

The proposed ART curves in section 3.3 can be prescribed for any type of DG units including converter-interfaced distributed energy resources (e.g., permanent magnet synchronous generators or photovoltaic), directly-connected generating units (e.g., squirrel cage induction generators), or doubly-fed induction generators. Although the main application of the proposed ART curves is high capacity wind power plants, they can be implemented for DG units with any energy resource such as wind, solar, wave, geothermal, etc. The proposed curves can also be imposed for the proper operation of HVDC systems and grid-interactive microgrids.

Furthermore, the proposed ART-VS method in section 3.6 can be applied to any converter-interfaced applications such as different types of converter-interfaced DG units [41]-[42], grid-interactive converter-interfaced microgrids [59], and converter-interfaced HVDC systems [44]. Since the voltage support in most cases is obtained using the reactive current, the nature of the energy source (that is responsible for generating the active power) does not affect the effectiveness of the proposed ART-VS method. To fulfill the ART-VS method, it is needed to estimate the line impedance. This impedance can be estimated online [87]-[89]; and be updated inside the proposed ART-VS control loops. Also, the equivalent grid voltage can be simply obtained by a Kirchhoff voltage law equation and local measurements. Since a symmetrical fault can be considered as a simple case of the generic asymmetrical conditions (with the negative-sequence voltage value equal to zero), all analyses in this chapter remain intact. The proposed ART curves and ART-VS control method can thus be simply applied under the three-phase grid faults.

The specification on the active power limitation during the fault and its restoration after the fault is an important area which needs similar comparative research. These specifications vary in different grid codes based on system characteristics such as grid strength. Although the imposed specifications on active power restoration by different grid codes can be adopted by the proposed ART regulation scheme, it is an interesting area for future research on specific requirements of active power restoration (from the system operator point of view) under unbalanced grid faults.

### **3.10 Conclusion**

This chapter presented three contributions. First, the LVRT along with the reactive current injection and active power restoration requirements in different grid codes were overviewed. Also, the existing voltage support strategies in the literature, under unbalanced grid faults, were reviewed and categorized. Second, the LVRT curves were extended for short-term unbalanced faults, and the asymmetric ride-

through (ART) curves were proposed. The ART scheme prescribes proper specifications on the regulation of the phase voltage magnitudes and the positive- and negative-sequence voltages. This chapter showed that even the most recent voltage support strategies in the literature are not able to fully comply with the suggested ART specifications. As a third contribution, a new dynamic and adaptive voltage regulation method was proposed, named ART-adaptive voltage support. The proposed adaptive voltage support method helps the connection voltage under any unbalanced voltage sag by

- 1) regulating all phase voltages inside the ART boundaries within the dynamic margins,
- 2) boosting the positive-sequence voltage value,
- 3) reducing the voltage unbalance factor, and
- 4) being adaptive to different grid codes.

The results of the proposed ART scheme and ART-adaptive voltage support were successfully verified by simulation and experimental test cases.

# Chapter 4

## Advanced Asymmetric Voltage Regulation and MAS Scheme in A Single Grid-Interactive Smart Inverter

### 4.1 Introduction

This chapter proposes a MAS scheme with an advanced asymmetric voltage regulation strategy. Under most grid faults, the accuracy of the traditional VSSs is severely affected due to the existence of the zero-sequence voltage component. References [47]-[48] aim to regulate the positive and negative sequences of the PCC voltage. However, it is more desirable to control the phase voltage magnitudes [46], [49]. Conventional VSSs under unbalanced conditions [46]-[51] generally suffer from three drawbacks:

- 1) none of them considers the zero-sequence voltage component.
- 2) the methods presented in [47]-[49] have been studied only in the STATCOM applications where the active power is assumed zero.
- 3) the methods suggested in [46], [48]-[50] have been only applied in inductive grids, i.e., assuming very high X/R ratio.

Therefore, this chapter proposes an advanced VSS in a GSI unit, called zero-sequence compensated voltage support (ZCVS) to address the aforementioned three issues. It has the following advantages compared to the existing VSSs:

- 1) It fully compensates the zero-sequence component and accurately regulates the phase voltages within the pre-set safety limits under unbalanced fault conditions. The safety voltage limits are typically imposed by grid codes for uninterrupted operation of GSIs.
- 2) Unlike most of the traditional methods, the proposed ZCVS is adapted with any complex grid impedance, e.g. resistive and inductive distribution systems.
- 3) The active power transferred by the GSI is also considered. The MAP equations for the ZCVS is also formulated. Therefore, this technique can be considered as a MAS scheme.

The delivered active power may, however, become highly oscillatory under severe unbalanced conditions. This chapter also proposes an analytical technique to limit the active power oscillations (LAPO) and enhance dc-bus voltage stabilization while, simultaneously, the GSI is supporting the ac host grid. Both of the last two strategies, i.e., MAP and LAPO, can be simultaneously augmented to the proposed ZCVS strategy.

## **4.2 Proposed Zero-sequence Compensated Voltage Support (ZCVS) Scheme**

The basic requirement in the voltage support is to avoid the over-voltage and under-voltage at the PCC whenever possible. Eq (3.3) can be expanded as

$$\begin{aligned} & \left[ \begin{aligned} & (V^+ - V_g^+) \cos(\omega t + \delta^+) + (V^- - V_g^-) \cos(\omega t + \delta^-) \\ & (V^+ - V_g^+) \sin(\omega t + \delta^+) - (V^- - V_g^-) \sin(\omega t + \delta^-) \end{aligned} \right] = \\ & \left[ \begin{aligned} & (L_g \omega I_q^+ + R_g I_p^+) \cos(\omega t + \delta^+) + (R_g I_p^- - L_g \omega I_q^-) \cos(\omega t + \delta^-) \\ & (L_g \omega I_q^+ + R_g I_p^+) \sin(\omega t + \delta^+) - (R_g I_p^- - L_g \omega I_q^-) \sin(\omega t + \delta^-) \end{aligned} \right] \end{aligned} \quad (4.1),$$

where  $\delta^+$  and  $\delta^-$  are angles of the positive and negative sequences of the voltage.

If the following expressions are satisfied:

$$\frac{I_p^+}{I_q^+} = \frac{R_g}{L_g \omega}, \quad \frac{I_p^-}{I_q^-} = -\frac{R_g}{L_g \omega} \quad (4.2);$$

then, the positive and negative components of (4.1) result in

$$V^+ - V_g^+ = L_g \omega I_q^+ + R_g I_p^+, \quad V^- - V_g^- = R_g I_p^- - L_g \omega I_q^- \quad (4.3).$$

To comply with voltage limits, a combination of positive/negative and active/reactive currents (i.e.,  $I_p^+$ ,  $I_p^-$ ,  $I_q^+$ , and  $I_q^-$ ) should be injected into an inductive-resistive grid to support the grid voltage. The magnitudes of the phase voltages can be obtained in terms of the magnitudes of positive and negative sequence voltages by Eq (3.7). From Eq (3.7), the maximum and minimum phase voltages with zero-sequence consideration can be determined by

$$\begin{aligned} V_{\min} &= \min(V_a, V_b, V_c) = \sqrt{(V^+)^2 + (V^-)^2 + 2(V^+)(V^-)\lambda_{\min} + (V^0)\lambda_{\min}^0} \\ V_{\max} &= \max(V_a, V_b, V_c) = \sqrt{(V^+)^2 + (V^-)^2 + 2(V^+)(V^-)\lambda_{\max} + (V^0)\lambda_{\max}^0} \end{aligned} \quad (4.4),$$

where  $\lambda_{\min}$ ,  $\lambda_{\max}$ ,  $\lambda_{\min}^0$ , and  $\lambda_{\max}^0$  can be found as follows:

$$\begin{cases} \lambda_a = \cos(\gamma) \\ \lambda_b = \cos(\gamma - \frac{2\pi}{3}) \\ \lambda_c = \cos(\gamma + \frac{2\pi}{3}) \end{cases} \rightarrow \begin{cases} \lambda_{\min} = \min(\lambda_a, \lambda_b, \lambda_c) \\ \lambda_{\max} = \max(\lambda_a, \lambda_b, \lambda_c) \end{cases}$$

$$\begin{cases}
\text{if } \lambda_{\min} = \lambda_a \rightarrow \lambda_{\min}^0 = \cos(\gamma^0) \\
\text{if } \lambda_{\min} = \lambda_b \rightarrow \lambda_{\min}^0 = \cos(\gamma^0 - \frac{2\pi}{3}) \\
\text{if } \lambda_{\min} = \lambda_c \rightarrow \lambda_{\min}^0 = \cos(\gamma^0 + \frac{2\pi}{3}) \\
\text{if } \lambda_{\max} = \lambda_a \rightarrow \lambda_{\max}^0 = \cos(\gamma^0) \\
\text{if } \lambda_{\max} = \lambda_b \rightarrow \lambda_{\max}^0 = \cos(\gamma^0 - \frac{2\pi}{3}) \\
\text{if } \lambda_{\max} = \lambda_c \rightarrow \lambda_{\max}^0 = \cos(\gamma^0 + \frac{2\pi}{3})
\end{cases} \quad (4.5),$$

where  $\gamma = \delta^+ - \delta^-$  and  $\gamma^0 = \delta^0 - \delta^+$ . After applying proper  $V_{\min}^{ref}$  and  $V_{\max}^{ref}$  in (4.4), the reference values of  $V_{ref}^+$  and  $V_{ref}^-$  can be solved as

$$\begin{cases}
(V_{ref}^+)^2 = \frac{-B + \sqrt{B^2 - 4A^2}}{2}, & V_{ref}^- = \frac{A}{V_{ref}^+} \\
A = \frac{V_H - V_L}{2(\lambda_{\max} - \lambda_{\min})} \\
B = 2A \times \lambda_{\max} - V_H \\
V_L = (V_{\min}^{ref} - V^0 \lambda_{\min}^0)^2 \\
V_H = (V_{\max}^{ref} - V^0 \lambda_{\max}^0)^2
\end{cases} \quad (4.6).$$

A general solution (applicable in grids with any  $X/R$  ratio) is to apply the results of (4.6) in (4.3) as

$$\begin{aligned}
I_p^+ &= \frac{R_g}{X_g^2 + R_g^2} \times \Delta V_{ref}^+, & I_p^- &= \frac{R_g}{X_g^2 + R_g^2} \times \Delta V_{ref}^-, \\
I_q^+ &= \frac{X_g}{X_g^2 + R_g^2} \times \Delta V_{ref}^+, & I_q^- &= \frac{-X_g}{X_g^2 + R_g^2} \times \Delta V_{ref}^-.
\end{aligned} \quad (4.7),$$

where expressions of (4.2) are also satisfied. According to (4.7), the active components do not contribute in supporting the voltage in an inductive grid. In this case, they can be utilized to fulfill complementary objectives discussed in the next section (i.e., MAP strategy). Fig 4.1 shows the control diagram of the proposed ZCVS scheme.

### 4.3 Proposed Complementary Strategies

For an inductive grid, the positive and negative sequences of the reactive current component were obtained for regulating the phase voltages. In this section, two complementary strategies are proposed to be applied to the active components of the current. These strategies can be also obtained for the resistive grids and grids with any X/R value if the active and reactive components are replaced or (4.2) is satisfied.

#### 4.3.1 ZCVS with LAPO Strategy

In severe unbalanced conditions, the required negative reactive component of the current obtained by ZCVS may become high. Negative-sequence current and voltage components give rise to large oscillations in the active power. Therefore, the LAPO strategy is proposed to obtain a limit for the negative reactive current component which prevents exceeding the pre-set maximum allowable active power oscillation. Using the instantaneous power theory, the output active and reactive powers of the GSI is calculated by Eq (2.3). Using Eq (2.3) gives the magnitude of the oscillations on the active power as

$$\tilde{P} = \sqrt{(V^- I_p^+ + V^+ I_p^-)^2 + (V^- I_q^+ - V^+ I_q^-)^2} \quad (4.8).$$

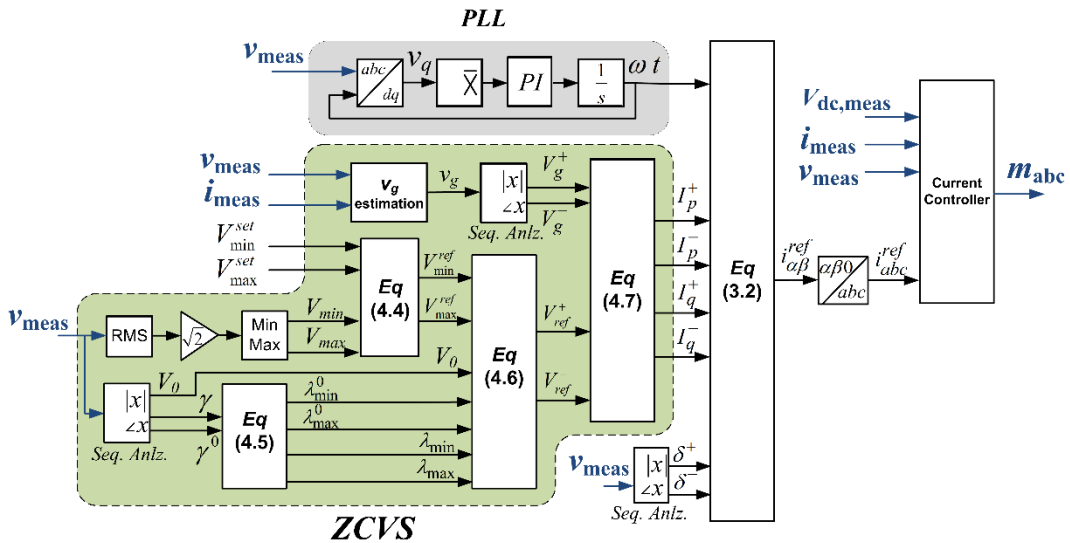


Figure 4.1 Proposed voltage support scheme

Using (4.8), the equation of the maximum negative reactive current can also be obtained which limits the oscillation magnitude of the active power to the pre-set value:

$$I_{q, LAPO}^- = \frac{\sqrt{\tilde{P}_{\max}^{set 2} - (V^- I_p^+ + V^+ I_p^-)^2} + V^- I_q^+}{V^+} \quad (4.9).$$

Fig 4.2 shows the control diagram of the ZCVS scheme with LAPO strategy. LAPO may slightly affect the operation of the ZCVS. However, the GSI operator can flexibly compromise between the full ZCVS and the limited oscillation on active power, by using these analytical expressions.

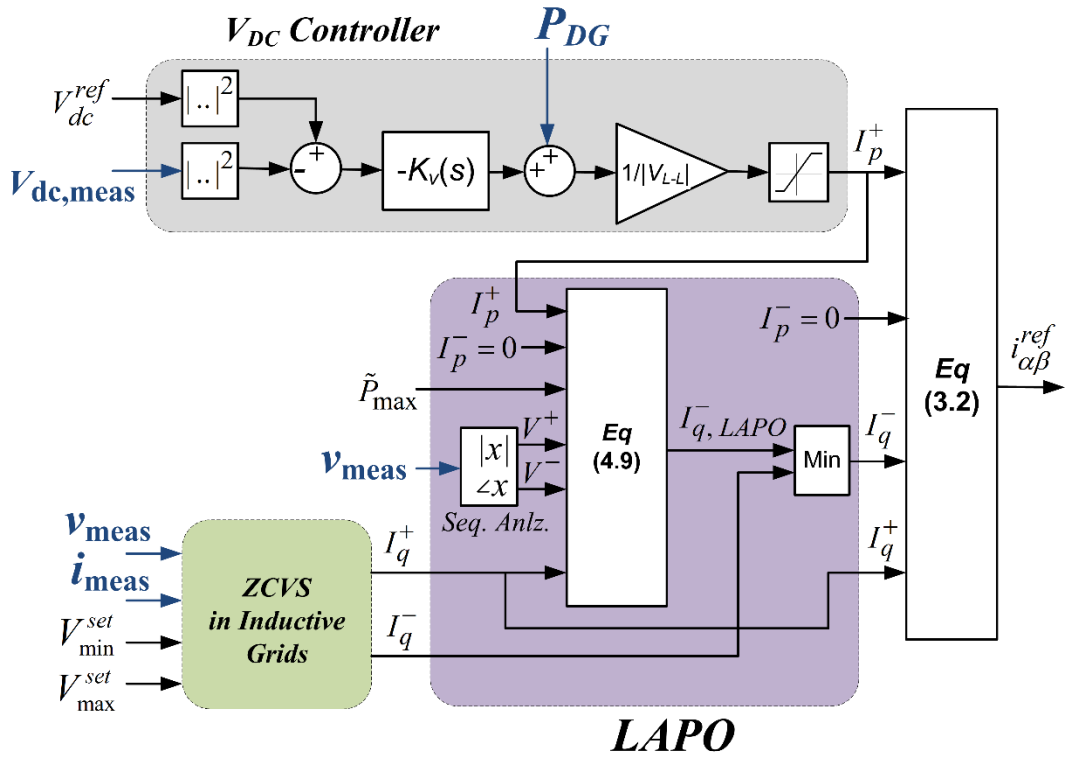


Figure 4.2 Proposed control diagram to limit the active power oscillations

### 4.3.2 ZCVS with MAPD Strategy

Augmenting the MAPD technique to ZCVS method ensures four simultaneous objectives: *i*) riding through abnormal conditions, *ii*) regulating the phase voltages,

iii), delivering the maximum allowable active power to the grid and iv) respecting the current limitations. This section finds the MAPD equation to achieve the aforementioned goals in an inductive grid. In this strategy,  $I_q^+$  and  $I_q^-$  are already obtained by (4.7) to provide the proposed voltage support. The value of  $I_p^-$  is also set to zero in order to allocate all the available current capacity to  $I_p^+$ . Then, (2.5) can be rewritten as

$$\begin{bmatrix} i_\alpha \\ i_\beta \end{bmatrix} = \begin{bmatrix} \left( I_p^+ + I_q^- \sin \gamma \right) \cos(\omega t + \delta^+) + \left( I_q^+ - I_q^- \cos \gamma \right) \sin(\omega t + \delta^+) \\ \left( I_p^+ - I_q^- \sin \gamma \right) \sin(\omega t + \delta^+) - \left( I_q^+ + I_q^- \cos \gamma \right) \cos(\omega t + \delta^+) \end{bmatrix} \quad (4.10).$$

The  $\alpha\beta$  currents of (4.10) are transformed into the  $abc$  currents, and the magnitude of the phase currents will be obtained as

$$\begin{bmatrix} I_a^2 \\ I_b^2 \\ I_c^2 \end{bmatrix} = \begin{bmatrix} (I_{\alpha c})^2 + (I_{\alpha s})^2 \\ \left( -\frac{1}{2} I_{\alpha c} + \frac{\sqrt{3}}{2} I_{\beta c} \right)^2 + \left( \frac{1}{2} I_{\alpha s} + \frac{\sqrt{3}}{2} I_{\beta s} \right)^2 \\ \left( -\frac{1}{2} I_{\alpha c} - \frac{\sqrt{3}}{2} I_{\beta c} \right)^2 + \left( \frac{1}{2} I_{\alpha s} - \frac{\sqrt{3}}{2} I_{\beta s} \right)^2 \end{bmatrix} \quad (4.11),$$

where

$$I_{\alpha c} = I_p^+ + I_q^- \sin \gamma, \quad I_{\alpha s} = I_q^+ - I_q^- \cos \gamma, \quad I_{\beta s} = I_p^+ - I_q^- \sin \gamma, \quad I_{\beta c} = -\left( I_q^+ + I_q^- \cos \gamma \right) \quad (4.12).$$

Then, the phase current magnitudes under the fault can be found by

$$\begin{aligned} I_a^2 &= \left( I_p^+ + I_q^- \sin \gamma \right)^2 + \left( I_q^+ - I_q^- \cos \gamma \right)^2, \\ I_b^2 &= \left( \frac{1}{2} I_p^+ + I_{Q1} \right)^2 + \left( \frac{\sqrt{3}}{2} I_p^+ + I_{Q2} \right)^2, \\ I_c^2 &= \left( \frac{1}{2} I_p^+ + I_{Q3} \right)^2 + \left( -\frac{\sqrt{3}}{2} I_p^+ + I_{Q4} \right)^2 \end{aligned} \quad (4.13),$$

where

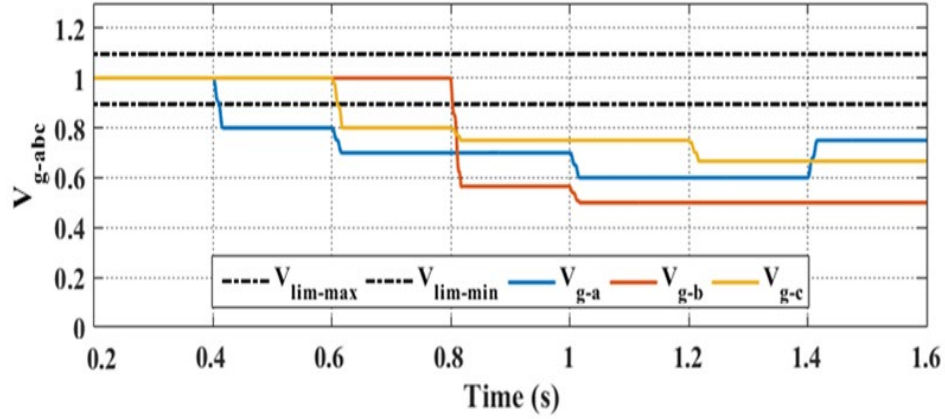
$$\begin{aligned}
I_{Q1} &= \frac{1}{2}I_q^- \sin \gamma + \frac{\sqrt{3}}{2}I_q^+ + \frac{\sqrt{3}}{2}I_q^- \cos \gamma \\
I_{Q2} &= -\frac{1}{2}I_q^+ + \frac{1}{2}I_q^- \cos \gamma - \frac{\sqrt{3}}{2}I_q^- \sin \gamma \\
I_{Q3} &= \frac{1}{2}I_q^- \sin \gamma - \frac{\sqrt{3}}{2}I_q^+ - \frac{\sqrt{3}}{2}I_q^- \cos \gamma \\
I_{Q4} &= -\frac{1}{2}I_q^+ + \frac{1}{2}I_q^- \cos \gamma + \frac{\sqrt{3}}{2}I_q^- \sin \gamma
\end{aligned} \tag{4.14}.$$

Using Eq (4.11)-(4.14), three values are respectively obtained for  $I_p^+$  ( $I_{p,a}^+$ ,  $I_{p,b}^+$ , and  $I_{p,c}^+$ ) in three cases, i.e.,  $I_a = I_{\max}^{set}$ ,  $I_b = I_{\max}^{set}$ , and  $I_c = I_{\max}^{set}$  :

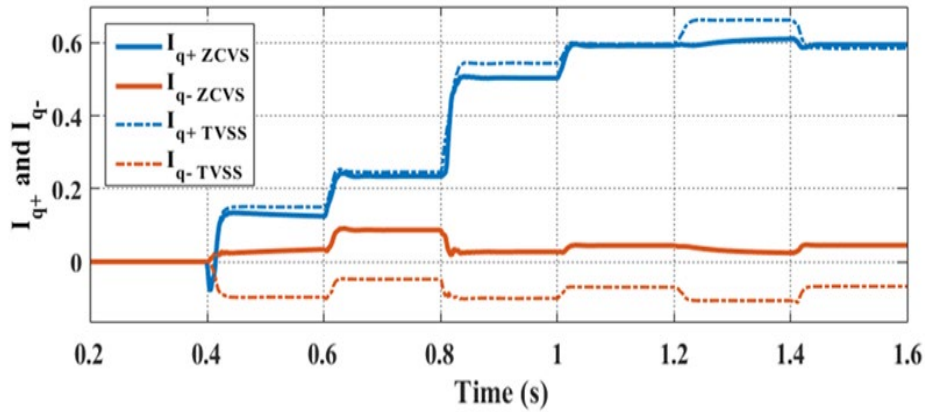
$$\begin{aligned}
I_{p,a}^+ &= \sqrt{I_{\max}^{set\ 2} - (I_q^+ - I_q^- \cos \gamma)^2} - I_q^- \sin \gamma \\
I_{p,b}^+ &= \frac{-I_{Q1} - \sqrt{3}I_{Q2} + \sqrt{(I_{Q1} + \sqrt{3}I_{Q2})^2 - 4(I_{Q1}^2 + I_{Q2}^2 - I_{\max}^{set\ 2})}}{2} \\
I_{p,c}^+ &= \frac{-I_{Q3} + \sqrt{3}I_{Q4} + \sqrt{(I_{Q3} - \sqrt{3}I_{Q4})^2 - 4(I_{Q3}^2 + I_{Q4}^2 - I_{\max}^{set\ 2})}}{2} \\
I_{p,MAPD}^+ &= \min(I_{p,a}^+, I_{p,b}^+, I_{p,c}^+)
\end{aligned} \tag{4.15}.$$

Fig 4.3 shows the control diagram of the ZCVS scheme with MAPD strategy.





(a)



(b)

Figure 4.4 Simulation test case A: (a) magnitudes of the grid phase voltages, and (b) obtained positive and negative reactive currents by TVSS and ZCVS.

#### 4.4.2 Test Case A: Traditional VSS vs Proposed ZCVS Method

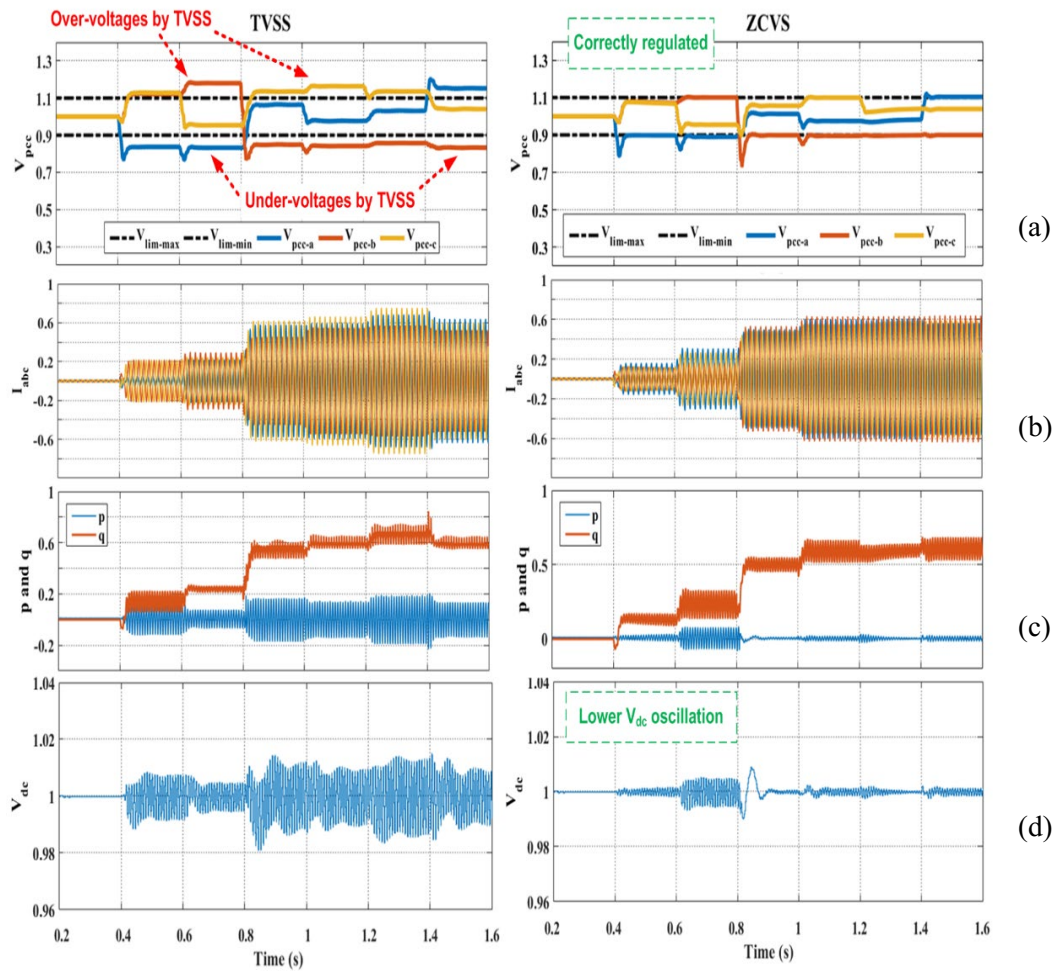
Fig 4.4(a) shows six different unbalanced faulty conditions. Fig 4.4(b) indicates the obtained  $I_q^+$  and  $I_q^-$  by the traditional VSS (i.e. TVSS) and proposed ZCVS for different fault conditions. As Fig 4.5(a)-left reveals, TVSS fails to precisely regulate the phase voltages within the pre-set voltage limits. Over-voltages up to 1.18 pu and under-voltages down to 0.83 pu occur whereas the voltage accepted limits are set to  $\pm 0.1$  pu around the nominal value. However, the proposed ZCVS method demonstrates successful results. As Fig 4.5(a)-right shows, the phase-

voltages of the PCC are precisely regulated between the  $V_{\min}^{set}$  and  $V_{\max}^{set}$ . Also, it is notable from Fig 4.5(d) that the dc voltage ripples are also considerably lower when the ZCVS is applied.

#### 4.4.3 Test Case B: ZCVS with LAPO and MAPD strategies

First, the result of the ZCVS method with LAPO strategy is presented. The maximum acceptable oscillation on the active power is set to 0.08 pu as indicated in Fig 4.6(c). The maximum negative reactive current reference value is calculated where the active power oscillations are lower than 0.08 pu. As Fig 4.6(a) demonstrates, the reference value calculated is higher than  $I_{q,LAPO}^-$ . It causes active power oscillations greater than 0.08 pu as depicted in Fig 4.6(c). To limit the oscillations, the reference value is limited to  $I_{q,LAPO}^-$  at  $t=0.5s$  and  $t=0.9s$ , as indicated in Fig 4.6(a). Therefore, the active power oscillations are limited to 0.08 pu as shown in Fig 4.6(c). As a result, the dc voltage ripples are decreased too by applying the LAPO strategy.

As another complementary strategy, the ZCVS method with MAPD strategy is also tested in this section. The value of maximum phase current is set to 1.0 pu. The suitable  $I_p$  is calculated. Fig 4.7(a) shows that an unbalanced fault occurs at  $t=0.3s$ . The pre-fault active power is 1 p.u. which causes overcurrent as Fig 4.7 illustrates. At  $t=0.5s$  the chopper in the dc-side is activated to avoid the overcurrent and the delivered active power becomes zero, as indicated in Fig 4.7(f). At  $t=0.7s$ , the active current component obtained by proposed method is applied. Thus, the MAPD strategy allows delivering maximum allowable active power (Fig 4.7(f)) while simultaneously respects the phase current limit (Fig 4.7(e)). As Fig 4.7(b) shows, the ZCVS is still operating accurately even if the MAPD strategy is applied.



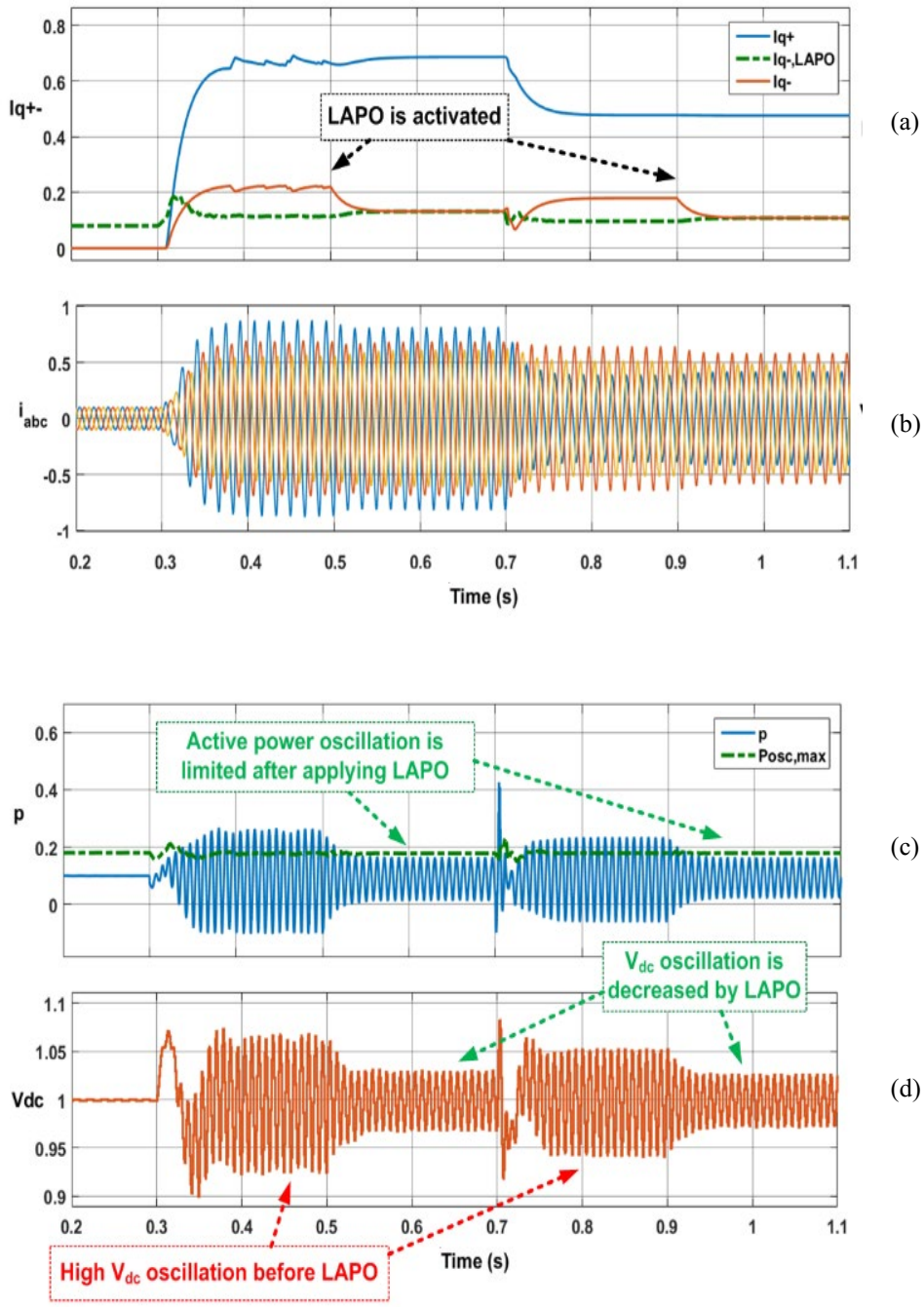


Figure 4.6 Simulation results of ZCVS with LAPO strategy: (a) obtained positive and negative reactive currents by ZCVS and LAPO, (b) phase currents, (c) active power, and (d) dc voltage.

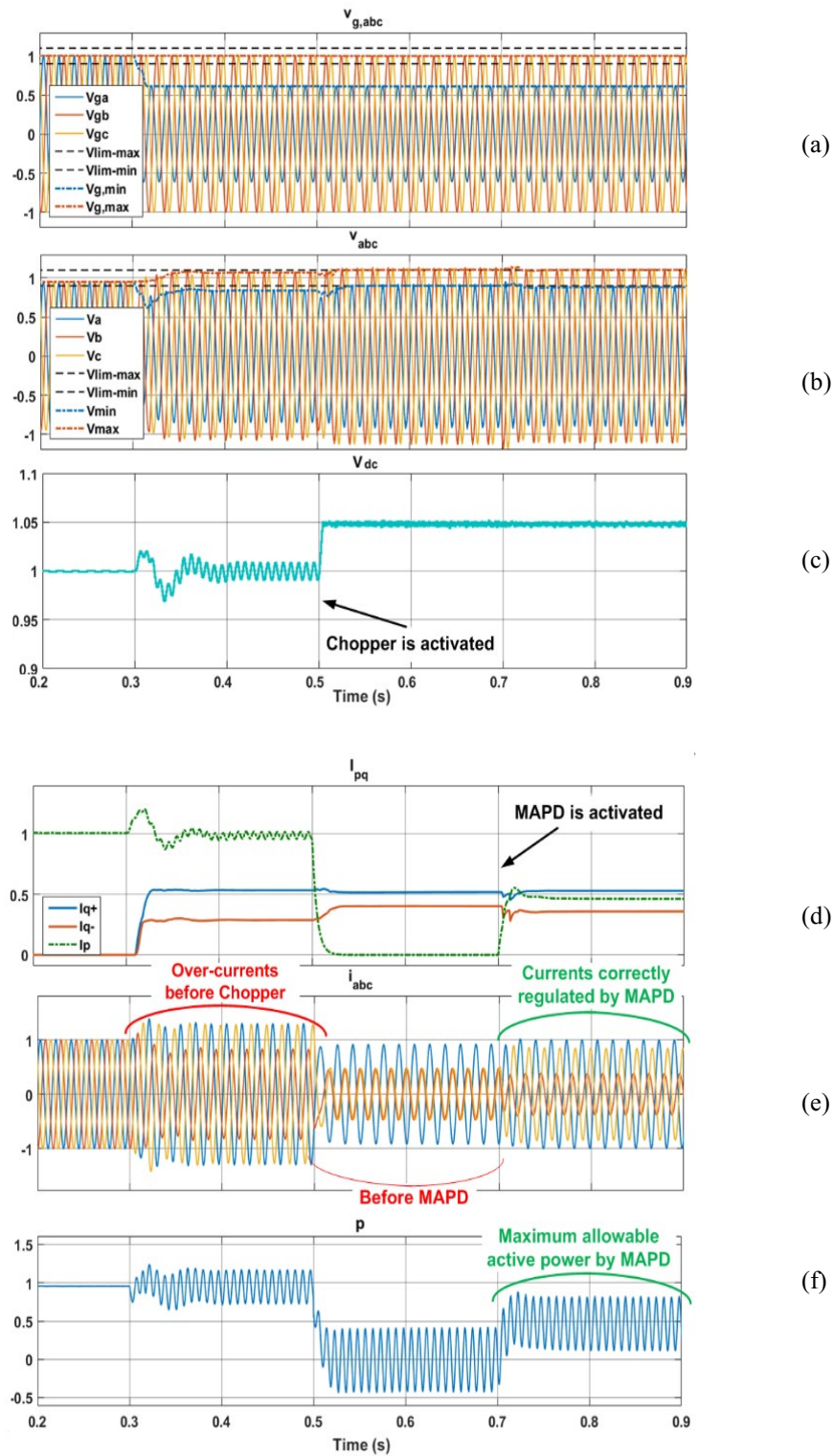


Figure 4.7 Simulation results of ZCVS with MAPD: (a) grid voltages, (b) PCC voltages, (c) dc voltage, (d) active current and positive/negative reactive currents, (e) phase currents, (f) active power.

#### 4.4.4 Test Case C: ZCVS Method under Various X/R Ratios

In the previous test cases, the ZCVS was applied to inductive grids (i.e.,  $X/R \gg 1$ ). The ZCVS is tested here in two other systems: a resistive grid and a grid with  $X/R=1$ . Fig 4.8 demonstrates the successful results of the ZCVS. As Fig 4.8(a) reveals, the ZCVS uses only the active current component in positive and negative sequences in the resistive grid. However, in the grid with  $X/R=1$ , both active and reactive currents in positive and negative sequences have been utilized, as shown in Fig 4.8(c).

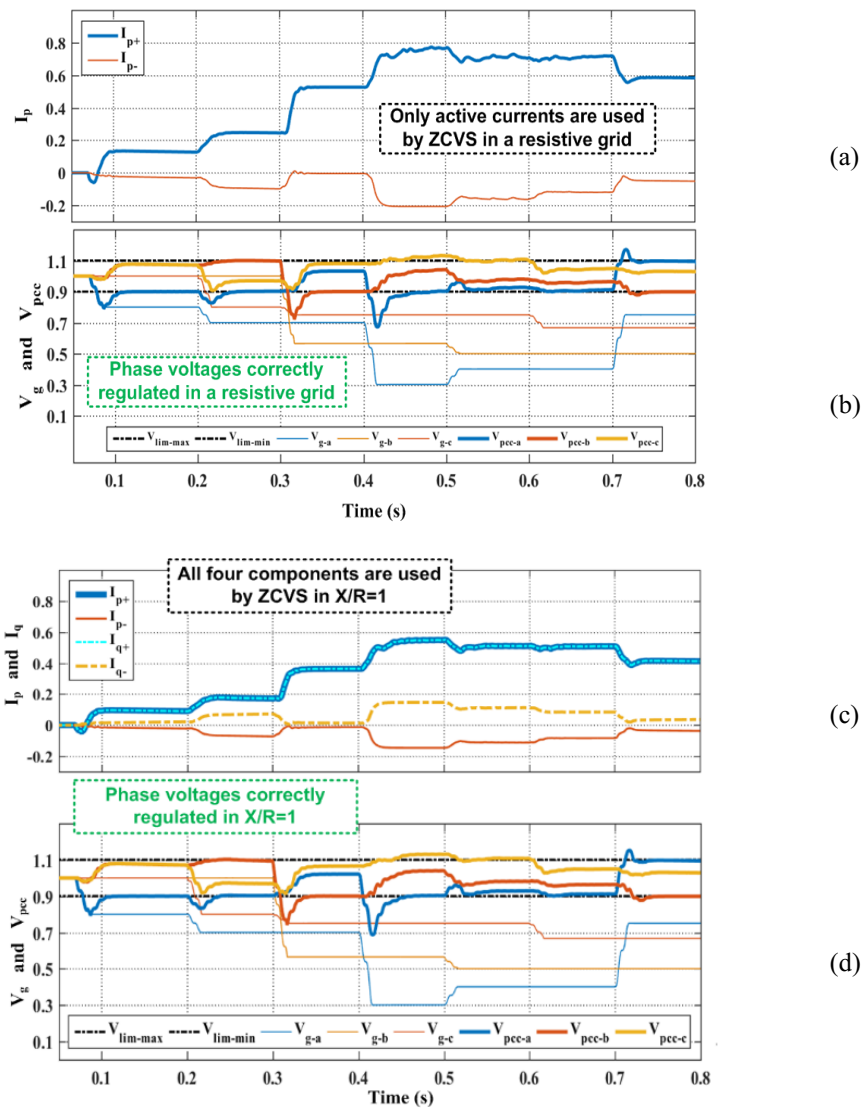


Figure 4.8 Simulation results of ZCVS in resistive and  $X/R=1$  grids: (a) injected currents in resistive grid, (b) magnitudes of grid and PCC voltages in resistive case, (c) injected currents in  $X/R=1$  grid, and (d) magnitudes of grid and PCC voltages in  $X/R=1$  case.

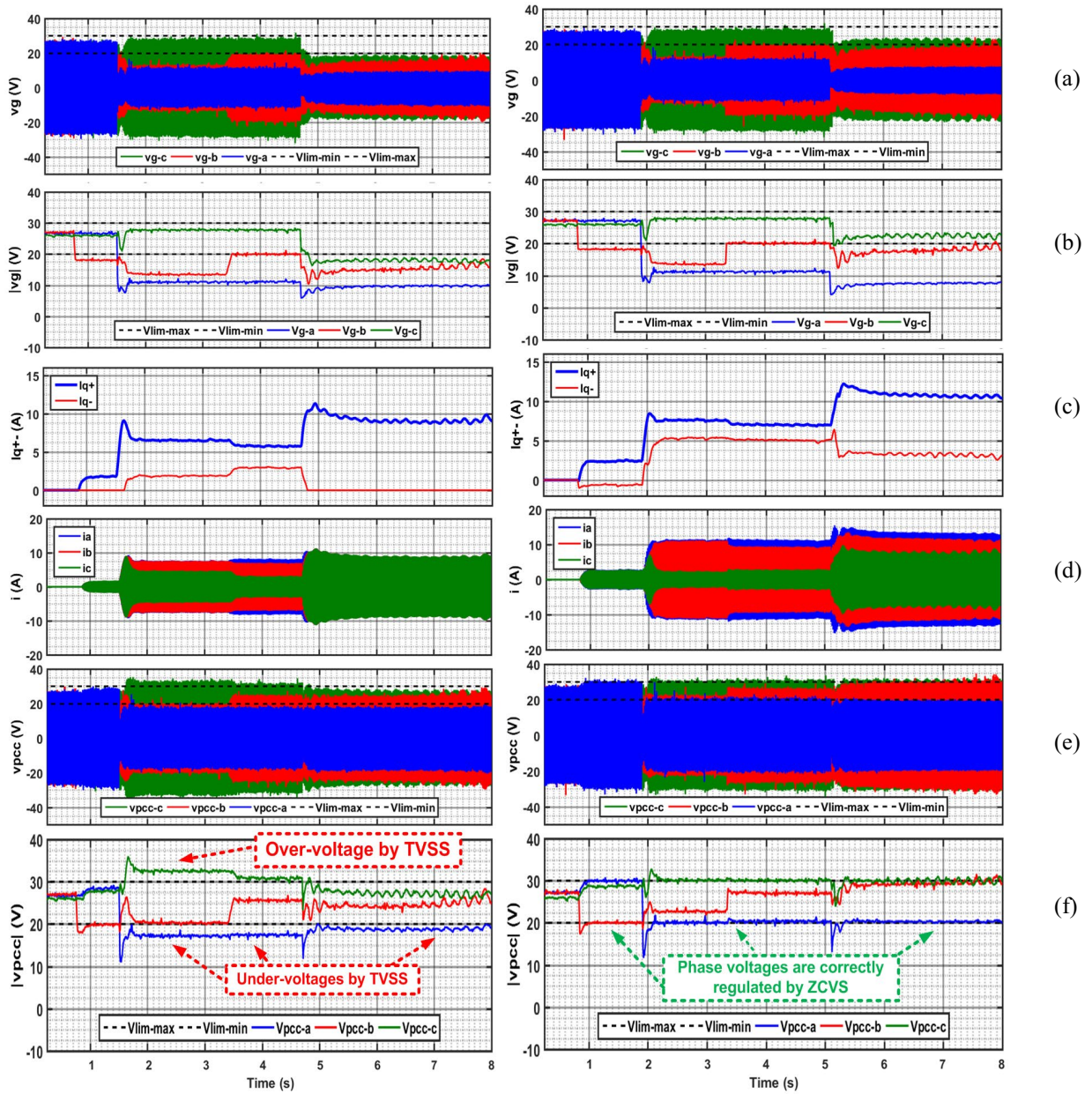


Figure 4.9 Experimental results with traditional and proposed methods, i.e. TVSS (left) and ZCVS (right): (a) grid voltages, (b) magnitudes of grid voltages, (c) obtained reactive currents by TVSS and ZCVS, (d) phase currents, (e) PCC voltages, and (f) magnitudes of PCC voltages

## 4.5 Experimental Results

To further verify the presented analytical expressions and demonstrate the performance of the proposed methods, the scaled-down test system is also employed. The experimental results of the traditional and proposed methods are obtained under different unbalanced fault conditions and presented in Fig 4.9. Fig 4.9(c) indicate the obtained positive and negative currents by the traditional VSS and proposed ZCVS. As Figs 4.9(f)-left reveals, traditional method fails to precisely regulate the phase voltages within the voltage limits. Steady-state over-voltage up to 1.32 pu and under-voltage down to 0.68 pu occur by the traditional VSS. However, the proposed method shows successful performance and accurate phase voltage regulation.

## 4.6 Conclusion

This chapter proposed an advanced MAS scheme to precisely regulate the phase voltages of a three-phase GSI within the pre-set safety limits. Conventional methods mainly suffer from three problems:

- 1) ignoring the zero-sequence voltage component;
- 2) neglecting the resistance of the grid impedance; and,
- 3) zero active power delivery assumption.

The proposed ZCVS method however addressed these three problems. Moreover, two complementary objectives were also augmented. First, the limited active power oscillation strategy provided an improved dc voltage while supporting the ac-side voltage. Second, the corresponding expressions were proposed to exploit the maximum allowable active power of a distributed energy resource even under severe unbalances while still regulating the phase voltages. The proposed voltage support scheme and two complementary strategies bring significant advantages to emerging DG units. The successful results of the proposed schemes were verified using simulation and experimental tests.

# Chapter 5

## Parallel MAS Scheme in Multiple Parallel-Operated Grid-Interactive Smart Inverters

### 5.1 Introduction

Parallel operation of converters has been continuously gaining attraction in a wide range of applications for their modular design, higher scalability, enhanced reliability, and economical benefits. As their integration increasingly rise, their contribution in sustaining the host grid stability is strongly demanded. The updating trend in the grid codes reflects that soon there will be simultaneous requirements for their LVRT capabilities as well as their effective asymmetrical voltage supports by advanced active/reactive bi-sequence power provision under unbalanced grid faults. Addressing these demands in an optimized way becomes very challenging. This chapter thus proposes a generalized MAS methodology to:

- 1) coordinate the asymmetrical ride-through and voltage support capabilities of different parallel-operated GSI units,
- 2) maximize the utilization of each unit and their collective contribution in boosting the positive-sequence voltage and reduction of the negative-

sequence voltage subject to the constraints from both DG and grid points of views.

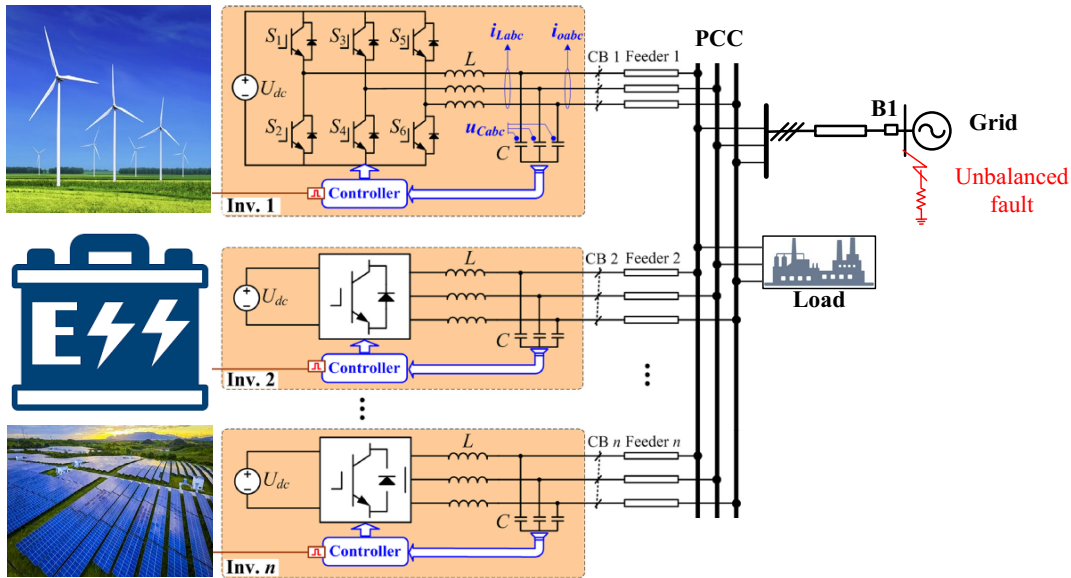


Figure 5.1 A typical POMI structure example: a grid-connected hybrid energy source system with “*n*” inverters

The simulation tests on ABB 2.0 MVA central inverters illustrate promising results of the proposed ideas.

## 5.2 Parallel-Operated Inverters

Continuously rising integration of grid-interactive converter-interfaced power units, such as DG units, microgrids, and high-voltage direct-current systems, is a vital part of the power systems evolution towards future smart energy grids. These fast developments will bring crucial reliability and stability concerns in future power grids [59]. Extensive studies have been carried out recently to present different methods for supporting the PCC voltage under unbalanced grid faults by a single DG unit, shown in Fig 2.1 [44]-[53]. Chapter 3 overviewed these voltage support strategies, and Chapter 4 introduced an advanced MAS scheme for a single GSI. Chapter 3 also introduced a combined regulation scheme, named ART scheme, for simultaneous asymmetrical voltage support and LVRT requirements

where different boundary curves are defined, specifically for asymmetric grid faults. In previous chapters, the ART and MAS schemes were provided for a single DG unit enforcing its safe operation as well as empowering its maximum grid supportive capabilities.

However, the coordination of multiple three-phase GSI units for providing maximum asymmetric grid support, also known as MAS performance, is not addressed in the literature. This gap ranges from the coordination of MAS performance for multiple distributed GSI units (e.g., in an active distribution network or in a microgrid) to effective MAS scheme for the parallel-operated multi-inverter (POMI) structures.

Most recently, parallel operation of converters has been attracting continuous attention in different applications, providing the modular converter design advantages, higher reliability, and economical benefits [93]-[95]. Fig 5.1 demonstrate a typical POMI structure widely utilized in various applications such as grid-interactive hybrid energy sources [96]-[97], interlinking applications in hybrid microgrids [98], hybrid multi-microgrid systems [99], multiple parallel-operated DG units in islanded microgrids [100]-[103] and more.

This chapter proposes an advanced methodology for optimized asymmetric support performance of a POMI system, named parallel maximum asymmetric support (PMAS) scheme. The study in this chapter shows that the MAS performance of each GSI unit inside the POMI structure does not provide the optimized overall MAS performance. On the other hand, the augmentation of the multiple GSI units will not provide the optimized overall MAS of the POMI system neither. These are analytically demonstrated in the following sections. Simply, neither individual operation nor augmentation will give optimal overall MAS since in practice multiple GSI units inside the POMI structure will have:

- 1) different MVA ratings,
- 2) different safety constraints and fault-tolerance capabilities,
- 3) more importantly, varied instantaneous operating points.

The last factor is a common scenario when hybrid energy sources (for instance wind and solar) are combined to provide complimentary power generation (e.g., during the day solar is operating at its full capacity while typically wind is operating at its high capacity during the night),

Therefore, the smart approach would be to tackle this problem by an advanced coordination scheme between the GSI units for the optimized overall MAS performance of the entire POMI structure. The proposed PMAS scheme thus aims to:

- 1) coordinate the maximum flexible asymmetrical voltage support and ride-through capabilities of individual units inside the POMI structure
- 2) maximize the collective dynamic contribution of POMI system in boosting the voltage and reducing the imbalance subject to the constraints of the plant and host system
- 3) keep the active power injection of each GSI unit intact which leads to power/cost saving in the plant operation as well as host system stability enhancement
- 4) set different objectives based on the potential requirements in future grid codes

These contributions have been illustrated using the simulation test results.

### **5.3 System Description**

The essential objectives through unbalanced faults and providing grid in riding supports by the PMAS scheme are 1) avoiding any damage or undesirable operation in each inverter, and 2) flexibly supporting the asymmetrical voltage (i.e., by boosting the positive-sequence voltage while alleviating the negative-sequence component) to the maximum capacity of each inverter. Fig 1(b) illustrates a schematic of a POMI structure with  $n$  inverters. An unbalanced grid fault or loading can cause asymmetrical voltage condition at the PCC. For any

unbalanced condition, the positive- and negative- sequence voltage vectors can be written in the  $\alpha\beta$  frame as

$$\begin{aligned} v_k^+ &= \begin{bmatrix} v_{\alpha,k}^+ \\ v_{\beta,k}^+ \end{bmatrix} = \begin{bmatrix} V_k^+ \cos(\omega t + \delta_k^+) \\ V_k^+ \sin(\omega t + \delta_k^+) \end{bmatrix}, \\ v_k^- &= \begin{bmatrix} v_{\alpha,k}^- \\ v_{\beta,k}^- \end{bmatrix} = \begin{bmatrix} V_k^- \cos(\omega t + \delta_k^-) \\ -V_k^- \sin(\omega t + \delta_k^-) \end{bmatrix} \end{aligned} \quad (5.1).$$

The total injected current by  $k^{\text{th}}$  inverter can be written in its active and reactive components as

$$i_k = i_{p,k} + i_{q,k} \quad (5.2).$$

To exploit a flexible voltage support performance from each unit, the injected reactive current vector of the  $k^{\text{th}}$  inverter,  $i_{q,k}$ , in (2) is divided into the positive and negative sequences in (3). These two current components can be written in a vector form of

$$i_{q,k} = i_{q,k}^+ + i_{q,k}^- = \begin{bmatrix} i_{\alpha,q,k} \\ i_{\beta,q,k} \end{bmatrix} = \begin{bmatrix} I_{q,k}^+ \sin(\omega t + \delta_k^+) - I_{q,k}^- \sin(\omega t + \delta_k^-) \\ -I_{q,k}^+ \cos(\omega t + \delta_k^+) - I_{q,k}^- \cos(\omega t + \delta_k^-) \end{bmatrix} \quad (5.3),$$

where the superscripts “+”/“-” and subscript “q” denote the positive/negative and reactive component, respectively.

For now, let's assume that the problem can be solved by the augmentation method. The total required reactive currents from all inverters for the unbalanced voltage support is  $i_q^{\text{aug}}$ . This current can comprise positive- negative and- sequences. The mathematical expression for the  $i_q^{\text{aug}}$  can be found by following the augmentation approach and adopting from the single DG unit structure][52, [92], as:

$$\begin{aligned} i_{q,\text{aug}} &= i_{q,\text{aug}}^+ + i_{q,\text{aug}}^- = \sum_{k=1:n} (i_{q,k}^+ + i_{q,k}^-) - (i_{q,\text{load}}^+ + i_{q,\text{load}}^-) \\ I_{q,\text{aug}}^+ &= \frac{V_{\text{ref}}^+ - V_g^+}{X_g}, \quad I_{q,\text{aug}}^- = \frac{V_g^- - V_{\text{ref}}^-}{X_g} \end{aligned} \quad (5.4),$$

where  $n$  is the number of inverters and  $i_{q,load}$  is the total reactive currents of the loads. Then, these currents can be divided among the inverters proportional to their ratings as:

$$\begin{aligned} I_{q,k}^+ &= R_k \cdot I_{q,aug}^+ = \frac{S_k}{\sum_{j=1:n} S_j} I_{q,aug}^+, \\ I_{q,k}^- &= R_k \cdot I_{q,aug}^- = \frac{S_k}{\sum_{j=1:n} S_j} I_{q,aug}^-, \end{aligned} \quad (5.5).$$

It is worth mentioning that for the augmentation approach the instantaneous operating conditions and the constraints of all inverters should be the same. The augmented notion can only be applied if the operating conditions of all units are the same at the fault instant which is not the case for most of the practical applications.

The peak current limitation of the power switches is the main constraint that must be considered in the PMAS performance. Applying this constraint ensures flexibly delivering the maximum allowable supportive currents in positive- and negative- sequences without exceeding the peak current limitation in the  $k^{\text{th}}$  unit. The analytical expressions of the phase currents can be formulated in the two-axis stationary reference frame, based on the unbalanced voltage sag characteristics of

(5.1), i.e.,  $V_k^+$ ,  $V_k^-$ ,  $\delta_k^+$ , and  $\delta_k^-$  as:

$$i_k = \begin{bmatrix} i_{\alpha,k} \\ i_{\beta,k} \end{bmatrix} = \begin{bmatrix} I_{p,k}^+ \cos(\omega t + \delta_k^+) + I_{q,k}^+ \sin(\omega t + \delta_k^+) - I_{q,k}^- \sin(\omega t + \delta_k^-) \\ I_{p,k}^+ \sin(\omega t + \delta_k^+) - I_{q,k}^+ \cos(\omega t + \delta_k^+) - I_{q,k}^- \cos(\omega t + \delta_k^-) \end{bmatrix} \quad (5.6).$$

Simplifying (5.6) gives

$$\begin{bmatrix} i_{\alpha,k} \\ i_{\beta,k} \end{bmatrix} = \begin{bmatrix} I_{\alpha 1,k}^+ & I_{\alpha 2,k}^+ \\ I_{\beta 1,k}^+ & I_{\beta 2,k}^+ \end{bmatrix} \otimes \begin{bmatrix} \cos(\omega t + \delta_k^+) \\ \sin(\omega t + \delta_k^+) \end{bmatrix} \quad (5.7),$$

where

$$\begin{aligned} I_{\alpha 1,k}^+ &= I_{p,k}^+ + I_{q,k}^- \sin \gamma_k, & I_{\alpha 2,k}^+ &= I_{q,k}^+ - I_{q,k}^- \cos \gamma_k \\ I_{\beta 1,k}^+ &= I_{p,k}^+ - I_{q,k}^- \sin \gamma_k, & I_{\beta 2,k}^+ &= -I_{q,k}^+ - I_{q,k}^- \cos \gamma_k \end{aligned}$$

Now, let's transfer the currents to the three-axis reference frame by the Clarke transformation as

$$\begin{bmatrix} I_{a,k}^2 \\ I_{b,k}^2 \\ I_{c,k}^2 \end{bmatrix} = \begin{bmatrix} (I_{\alpha 1,k})^2 + (I_{\alpha 2,k})^2 \\ (-\frac{1}{2}I_{\alpha 1,k} + \frac{\sqrt{3}}{2}I_{\beta 1,k})^2 + (\frac{1}{2}I_{\alpha 2,k} + \frac{\sqrt{3}}{2}I_{\beta 2,k})^2 \\ (-\frac{1}{2}I_{\alpha 1,k} - \frac{\sqrt{3}}{2}I_{\beta 1,k})^2 + (\frac{1}{2}I_{\alpha 2,k} - \frac{\sqrt{3}}{2}I_{\beta 2,k})^2 \end{bmatrix} \quad (5.8).$$

This gives the magnitude formulations of the current in three phases. Using (5.6) and (5.8), the following equations can be obtained

$$I_{\text{lim},a,k}^2 \geq \left( I_{p,k}^+ + I_{q,k}^- \sin \gamma_k \right)^2 + \left( I_{q,k}^+ - I_{q,k}^- \cos \gamma_k \right)^2 \quad (5.9)$$

$$\begin{aligned} I_{\text{lim},b,k}^2 \geq & \left( \frac{1}{2}I_{p,k}^+ + \frac{\sqrt{3}}{2}I_{q,k}^+ + I_{q,k}^- \sin(\gamma_k + \frac{\pi}{3}) \right)^2 \dots \\ & + \left( -\frac{\sqrt{3}}{2}I_{p,k}^+ + \frac{1}{2}I_{q,k}^+ - I_{q,k}^- \cos(\gamma_k + \frac{\pi}{3}) \right)^2 \end{aligned} \quad (5.10)$$

$$\begin{aligned} I_{\text{lim},c,k}^2 \geq & \left( -\frac{1}{2}I_{p,k}^+ + \frac{\sqrt{3}}{2}I_{q,k}^+ - I_{q,k}^- \sin(\gamma_k - \frac{\pi}{3}) \right)^2 \dots \\ & + \left( \frac{\sqrt{3}}{2}I_{p,k}^+ + \frac{1}{2}I_{q,k}^+ - I_{q,k}^- \cos(\gamma_k - \frac{\pi}{3}) \right)^2 \end{aligned} \quad (5.11),$$

where typically

$$I_{\text{lim},a,k} = I_{\text{lim},b,k} = I_{\text{lim},c,k} := I_{\text{lim},k} \quad (5.12).$$

## 5.4 Plane of Negative Reactive vs. Positive Reactive

### (NRPR)

It is proposed in this chapter to use peak-current equations and draw their dynamic boundaries in the  $I_{q,k}^-$  vs  $I_{q,k}^+$  plane, as shown Fig 5.2. This plane is called *NRPR* in this chapter. Using (5.9)-(5.11), three analytical relations are obtained between  $I_{q,k}^-$  and  $I_{q,k}^+$ . Eqs. (5.7)-(5.12) show that the relations between  $I_{q,k}^-$  and  $I_{q,k}^+$  in the peak-current limitation (PCL) constraints of each unit depend on three principal parameters:

- 1) the pre-set value of  $I_{lim,k}$  (based on the  $k^{th}$  unit's data-sheets),
- 2) the instantaneous value of the active power component of the current in that unit, i.e.,  $I_{p,k}^+$ , which can be a time-varying magnitude based on the output power of the unit at the duration of support (DOS), and
- 3) the unbalanced fault characteristics, i.e.,  $\delta_k^+$ , and  $\delta_k^-$ . For instance, if the unbalanced voltage sag occurs in phase A,  $\delta_k^+ - \delta_k^- = \pi$  and three equations of (5.9)-(5.11) are simplified as

$$I_{q,k}^- \leq \sqrt{I_{lim,k}^2 - I_{p,k}^+} - I_{q,k}^+ \quad (5.13)$$

$$I_{q,k}^{+2} + I_{q,k}^{-2} - I_{q,k}^+ I_{q,k}^- + \sqrt{3} I_{p,k}^+ I_{q,k}^+ + I_{p,k}^{+2} \leq I_{lim,k}^2 \quad (5.14)$$

$$I_{q,k}^{+2} + I_{q,k}^{-2} - I_{q,k}^+ I_{q,k}^- + \sqrt{3} I_{p,k}^+ I_{q,k}^- + I_{p,k}^{+2} \leq I_{lim,k}^2 \quad (5.15)$$

Eqs. (5.9)-(5.11) are named *EQ-Ia*, *EQ-Ib*, and *EQ-Ic*, represented in Fig 5.2 in *blue*, *orange*, and *yellow* colors, respectively. Based on these equations, the three curves representing the relationship between  $I_{q,k}^-$  and  $I_{q,k}^+$  for each of the three phases are drawn in the NRPR plane, as shown Fig 5.2.

#### 5.4.1 Allowable Current Areas in NRPR Plane

Based on the *EQ-Ia*, *EQ-Ib*, and *EQ-Ic* equations in (5.9)-(5.11), the graph of Fig 5.2 reveals important information such as the dynamic non-linear and time-varying relation between the  $I_{q,k}^-$  and  $I_{q,k}^+$  based on three varying parameters: i) setting parameters of the converters (i.e.,  $I_{lim,k}$ ), ii) instantaneous active power component of the injected currents (i.e.,  $I_{p,k}^+(t)$ ), and iii) unbalanced voltage characteristics (i.e.  $\gamma_k$ ). It is worth mentioning that Fig 5.2 is just an snapshot for the set parameters of  $I_{lim,k}$ ,  $I_{p,k}^+(t)$ , and  $\gamma_k$ . These parameters vary over time depending on the operating conditions and the fault characteristics.

One of the main information extracted from this graph is the allowable current area at each instant for the flexible combination of the  $I_{q,k}^-$  and  $I_{q,k}^+$ . The shaded green area of Fig 5.2 illustrates the snapshot of the allowable current area for the following conditions: a single-phase to ground fault occurs at phase while  $I_{lim,k}$  is set to 1.3 p.u. and  $I_{p,k}^+(t) = 0.2 p.u.$  at the time of the fault.

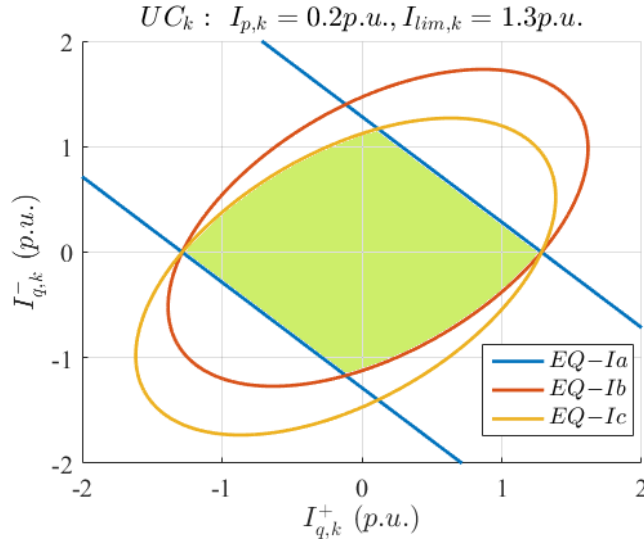


Figure 5.2 A snapshot of the dynamic allowable current area and peak-current boundaries of phases a, b, and c in the NRPR plane for  $k^{th}$  inverter at the DOS when a single-phase to ground fault occurs at phase “A”, i.e.,  $\gamma_k = \pi$  (Test Case A).

#### 5.4.1 Allowable Flexible Voltage Support Areas

The allowable flexible support areas (AFSAs) can be also identified in the NRPR plane for all units. For instance, Fig 5.3 shows the NRPR plane of similar conditions to those in Fig 5. 2 with two different values of the instantaneous active power, i.e.,  $I_{p,k}^+(t) = 0.4 p.u.$  and  $I_{p,k}^+(t) = 0.8 p.u.$ . As shown in Fig 5.3-(a), higher values of  $I_p$  will decrease the allowable current areas in the NRPR plane. For the purpose of this chapter, only the positive values of  $I_{q,k}^-$  and  $I_{q,k}^+$  are important. Fig 5. 3-(b) thus shows the zoomed view of Fig 5.3-(a) to illustrate only the positive values of  $I_{q,k}^-$  and  $I_{q,k}^+$ . This figure also shows two AFSAs for two values of the instantaneous active power. Light green and dark green areas show the AFSAs for  $I_{p,k}^+(t) = 0.4 p.u.$

and  $I_{p,k}^+(t) = 0.8 p.u.$ , respectively. As it is clear from Fig 5.3-(b) that higher instantaneous active power value shrink the AFSA area of the kth unit at the DOS resulting in lower allowable room for contribution in supporting the unbalanced voltage by positive- and negative-sequence reactive currents.

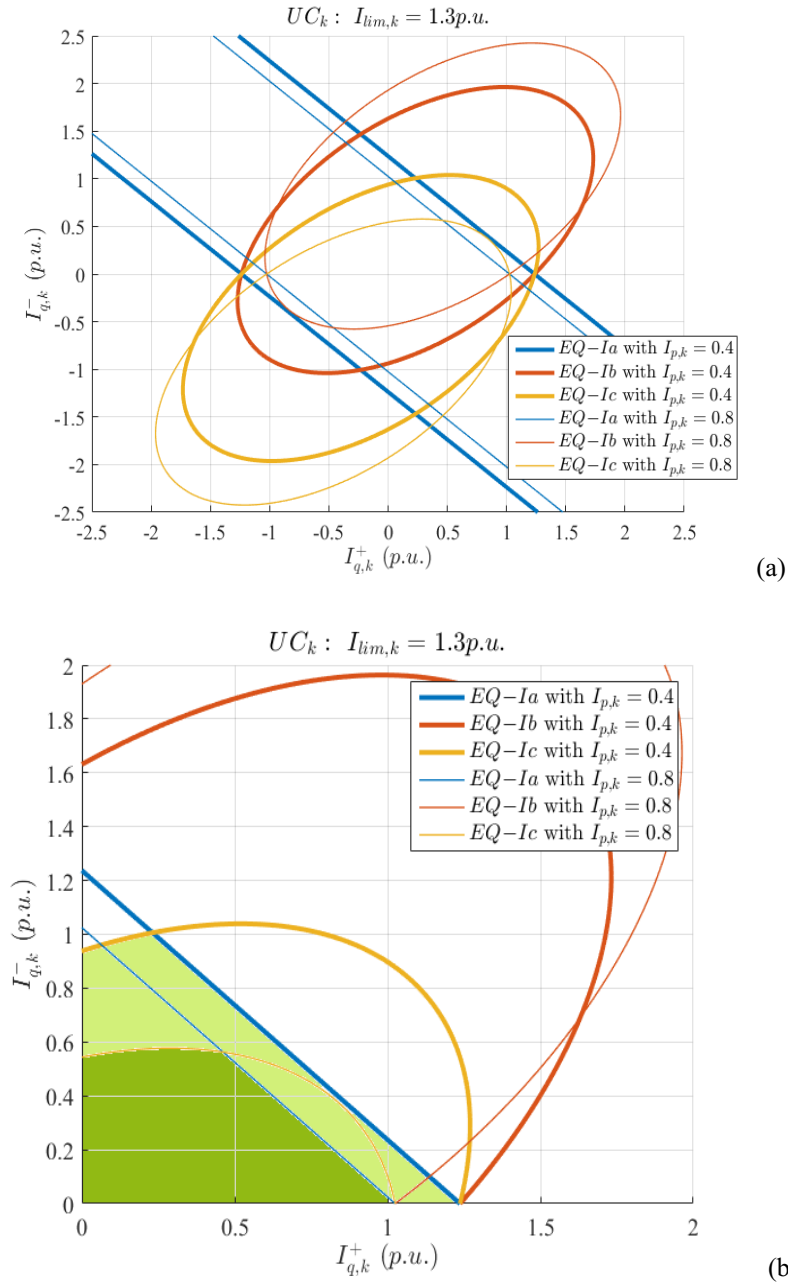


Figure 5.3 Two more snapshots of the *NRPR* plane for a similar inverter at Test Case A when the instantaneous active power has been increase to  $I_{p,k}^+(t) = 0.4 p.u.$  and  $I_{p,k}^+(t) = 0.8 p.u.$  (b) zoomed view for the flexible voltage support area.

Therefore, based on the *instantaneous* active current value at the DOS, the allowable voltage support area of the  $k^{th}$  inverter may be varied resulting in very different optimal reference values for the  $k$ th unit as well as for the entire POMI structure. These plots also show the nonlinear relation between the active current component value and the AFSA resulting in a complex optimization problem.

## 5.5 Proposed Optimized Asymmetric Support by PMAS

To find the optimal coordination between inverters inside the POMI structure, the instantaneous available capacity or AFSA characteristic of each unit should be considered. The instantaneous available current capacity of each converter during the DOS depends on the instantaneous active power injection by each unit in addition to its pre-set values (e.g., rating and maximum peak-current). All these parameters can be varied for different units at the DOS. A common example is the case of a hybrid energy source with complementary power generation units, e.g., wind and solar as shown in Fig 5.1. Typically, one of the units will have limited current capacity at the DOS since it is injecting a considerable amount of active power while other units still have extra capacities available for the flexible asymmetric voltage support since they are operating in lower active power operating points. This can provide a useful opportunity for cooperation in the PMAS optimal supportive scheme. For instance, the active power production of the solar energy system is in its high during the day while wind typically produces its high active power at night. Therefore, a smart coordination scheme would benefit from the optimum available capacity of each unit during the DOS.

Fig 5.4 illustrates the flowchart of the proposed PMAS method. As indicated, it comprises four stages. In the following sections, these four stages are discussed.

### 5.5.1 Stage I: Obtaining NRPR Equations

In this section, the current boundaries of all inverters based on the fault characteristic and their individual instantaneous active power values at the DOS are obtained using (5.9)-(5.11). As an example, Fig 5.5 indicates a case (Test Case B)

where there is 2-DG POMI structure with different settings and operating conditions. In this test case, DG1 and DG2 are rated at 40% and 60% of the total MVA of the POMI structure, respectively. Their peak-current values are set to 1.3 and 1.7 in p.u. of their own ratings (i.e., 0.52 and 1.02 in p.u. of total POMI rating). In addition, they have different amount of active power injection at the DOS. Based on these different parameters, a single-phase fault on phase “B” will result in totally different NRPR curves as illustrated in Fig 5.5-(a) and Fig 5.5-(b).

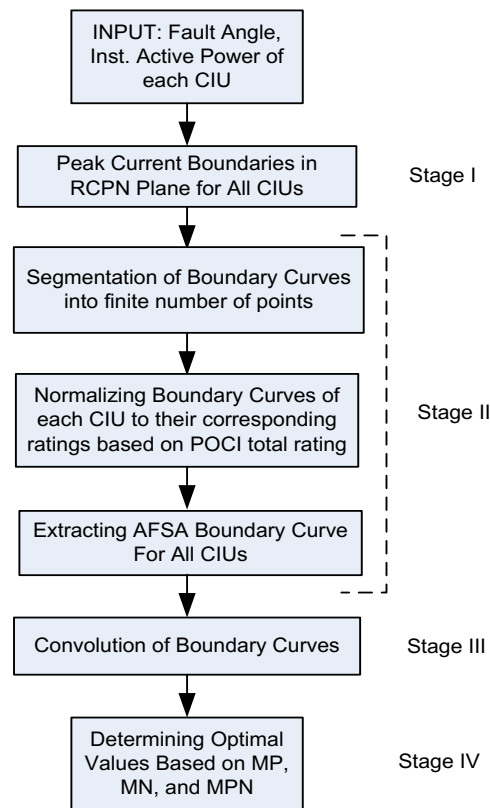


Figure 5.4 Flowchart of the proposed optimal asymmetric support by PMAS method.

### 5.5.1 Stage II: AFSA Boundary Curves

In this stage, three boundary curves will be transformed into one curve, named AFSA curve. First, the positive reactive current of the  $k$ th inverter is defined as a vector:

$$i_{q,k,AFSA}^+ = 0 : \frac{R_k \sqrt{I_{lim,k}^2 - I_{p,k}^2}}{M} : R_k \sqrt{I_{lim,k}^2 - I_{p,k}^2} \quad (5.16),$$

where “M” is the number of segments in the AFSA curves, and  $I_{q,k,m}^+$  is the mth element of the  $I_{q,k,AFSA}^+$  vector. Also using “ $R_k$ ” parameter,  $I_{q,k,AFSA}^+$  vector becomes a normalized vector of  $I_{q,k}^+$  in per unit of the total MVA of the POMI system.

Second, the following equations give the negative reactive current AFSA vector of each inverter:

$$I_{q,k,m}^- = R_k \cdot \min(y_{1,k,m}, y_{2,k,m}, y_{3,k,m}) \quad (5.17),$$

where  $I_{q,k,m}^-$  is the  $m^{\text{th}}$  element of the  $i_{q,k,AFSA}^-$  vector, and

$$y_{1,k,m} = \frac{-B_{1,k,m} + \sqrt{B_{1,k,m}^2 - 4C_{1,k,m}}}{2} \quad (5.18),$$

$$y_{2,k,m} = \frac{-B_{2,k,m} + \sqrt{B_{2,k,m}^2 - 4C_{1,k,m}}}{2}$$

$$y_{3,k,m} = \frac{-B_{3,k,m} + \sqrt{B_{3,k,m}^2 - 4C_{1,k,m}}}{2}$$

where

$$B_{1,k,m} = 2 \left( I_{p,k}^+ \sin \gamma_k - I_{q,k,m}^+ \cos \gamma_k \right)$$

$$B_{2,k,m} = I_{p,k}^+ \times \left( \sqrt{3} \cos \gamma_k - \sin \gamma_k \right) + I_{q,k,m}^+ \times \left( \cos \gamma_k + \sqrt{3} \sin \gamma_k \right)$$

$$B_{3,k,m} = I_{p,k}^+ \times \left( -\sqrt{3} \cos \gamma_k - \sin \gamma_k \right) + I_{q,k,m}^+ \times \left( \cos \gamma_k - \sqrt{3} \sin \gamma_k \right)$$

$$C_{1,k,m} = I_{p,k}^{+2} - I_{lim,k}^2 + I_{q,k,m}^{+2} \quad (5.19).$$

Fig 5.5-c and Fig 5.6-c demonstrate the results of applying the analytical methods of Stage II in two test cases.

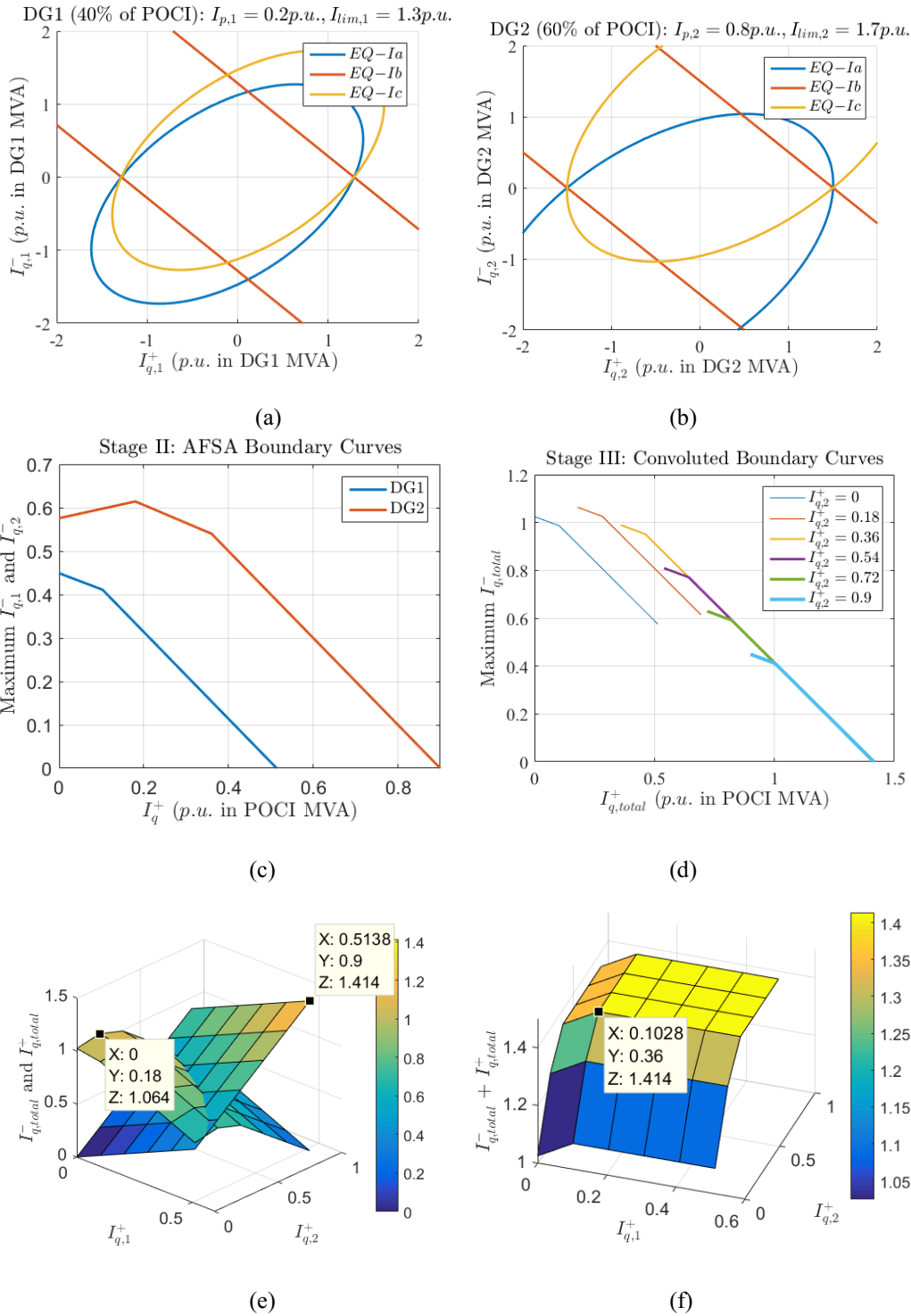


Figure 5.5 Test Case B: Single-phase fault on phase “B” and DG1 and DG2 are rated at 40% and 60% of the total MVA of the POMI structure, respectively: (a) NRPR curves for DG1, (b) NRPR curves for DG2, (c) Stage II: AFSA boundary curves for DG1 and DG2, (d) Stage III: convolted AFSA boundary curves, (e) Stage IV: optimal values of the MTP and MTN strategies, (f) Stage IV: optimal value of the MTPN strategy

### 5.5.2 Stage III: Convolution of Boundary Curves

After identifying the constraints and allowable support areas in Stage I and reducing the constraints into two smaller and normalized vectors in Stage II, this section simply convolutes AFSA vectors of all inverters into vectors of vectors or a  $m \times m$  matrix for the entire POMI system as:

$$Q_{M \times M}^+ = \begin{bmatrix} I_{q,k,1}^+ + I_{q,k+1,1}^+ & \dots & \dots & I_{q,k,0}^+ + I_{q,k+1,M}^+ \\ \vdots & \dots & \dots & \vdots \\ \vdots & \dots & \dots & \vdots \\ I_{q,k,M}^+ + I_{q,k+1,1}^+ & \dots & \dots & I_{q,k,M}^+ + I_{q,k+1,M}^+ \end{bmatrix} \quad (5.20)$$

$$Q_{M \times M}^- = \begin{bmatrix} I_{q,k,1}^- + I_{q,k+1,1}^- & \dots & \dots & I_{q,k,0}^- + I_{q,k+1,M}^- \\ \vdots & \dots & \dots & \vdots \\ \vdots & \dots & \dots & \vdots \\ I_{q,k,M}^- + I_{q,k+1,1}^- & \dots & \dots & I_{q,k,M}^- + I_{q,k+1,M}^- \end{bmatrix} \quad (5.21).$$

Fig 5.5-(d) and Fig 5.6-(d) reveal the results of applying these matrix convolutions in two test cases where each curve represents the corresponding two vectors in each column of  $Q_{M \times M}^+$  and  $Q_{M \times M}^-$  matrices. From these two figures, it is obvious that the applied number of segmentation in Stage II was  $M=6$ . The 2D matrices in Eq (5.20) and (5.21) can be generalized to  $n$ -D matrices of  $\underbrace{Q_{M \times \dots \times M}^{\pm}}_n$

where  $n$  is the number of parallel DG units.

### 5.5.3 Stage IV: Determination of the Optimal Values

This section is the final section and it explores the ways to find the optimal reference values for  $I_{q,k}^-$  and  $I_{q,k}^+$ . Having the  $Q_{M \times M}^+$  and  $Q_{M \times M}^-$  matrices, many applicable objectives can be defined to determine the  $I_{q,k}^-$  and  $I_{q,k}^+$  of all inverters to provide the global optimality in the POMI system. In this chapter, three simple objectives are defined as examples.

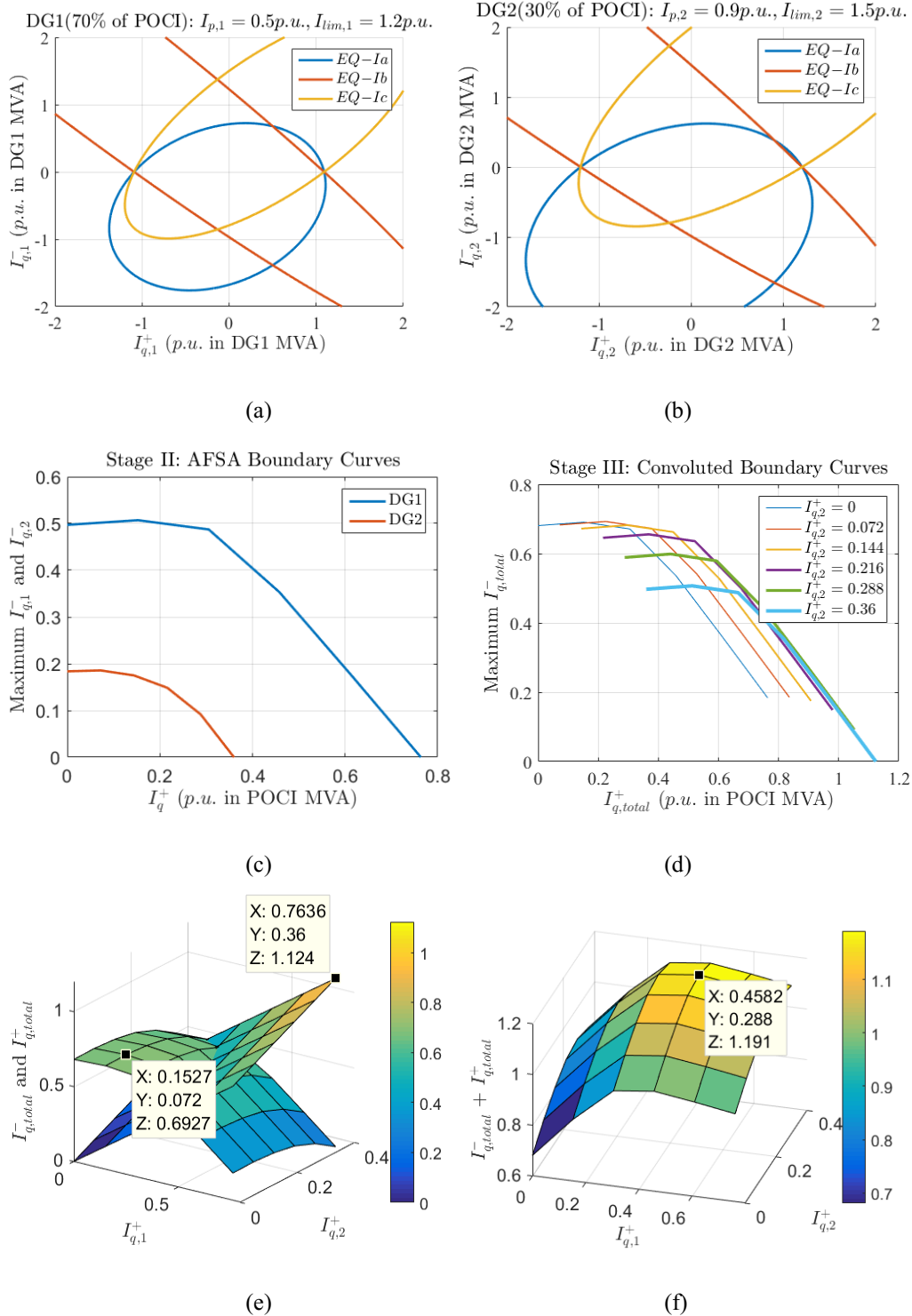


Figure 5.6 Test Case C: Arbitrary asymmetrical fault with  $\gamma = 5\pi / 12$  and DG1 and DG2 are rated at 70% and 30% of the total MVA of the POMI structure, respectively: (a) NRPR curves for DG1, (b) NRPR curves for DG2, (c) Stage II: AFSA boundary curves for DG1 and DG2, (d) Stage III: convolved AFSA boundary curves, (e) Stage IV: optimal values of the MTP and MTN strategies, (f) Stage IV: optimal value of the MTPN strategy

First, the maximum total positive-sequence (MTP) strategy finds the optimal values of the  $I_{q,k}^-$  and  $I_{q,k}^+$  for all inverters where the total positive-sequence reactive current injection of the POMI system is maximized. This can be easily determined by finding the maximum value of the  $Q_{M \times M}^+$  matrix. Since the building vectors of the  $Q_{M \times M}^+$  matrix, i.e.,  $i_{q,k,AFSA}^+$  vectors of all units, are ascending the entire matrix is ascending and the highest point is where

$$I_{q,k,M}^+ = R_k \sqrt{I_{\text{lim},k}^2 - I_{p,k}^2} \quad \text{for all } k=1:n \quad (5.22).$$

This is also clear from  $I_{q,\text{total}}^+$  surface in Fig 5.5-(e) and Fig 5.6-(e).

Another approach can be the optimal points to maximize the total negative-sequence (MTN) reactive current of the POMI system. This means the highest point in the  $Q_{M \times M}^-$  matrix. This can be also seen in Fig 5.5-(e) and Fig 5.6-(e) where the following sets for the values of the  $I_{q,k}^-$  and  $I_{q,k}^+$  of the DG1 and DG2 are obtained.

Test Case B:

$$I_{q,1,1}^+ = 0 \quad I_{q,2,2}^+ = 0.18 p.u. \quad I_{q,1,1}^- = 0.45 p.u. \quad I_{q,2,2}^- = 0.61 p.u. \quad (5.23).$$

Test Case C:

$$\begin{aligned} I_{q,1,2}^+ &= 0.153 \quad I_{q,2,2}^+ = 0.072 p.u. \\ I_{q,1,2}^- &= 0.507 p.u. \quad I_{q,2,2}^- = 0.186 p.u. \end{aligned} \quad (5.24).$$

As a third and better approach we can define our objective to maximize the following statement:

$$Q_{M \times M}^{+-} = \alpha^+ Q_{M \times M}^+ + \alpha^- Q_{M \times M}^- \quad (5.25),$$

to combine both positive and negative-sequence reactive currents and provide optimal flexible asymmetric voltage support. The result of applying this function is shown in Fig 5.5-(f) and Fig 5.6-(f) where  $\alpha^+ = \alpha^- = 1$ .

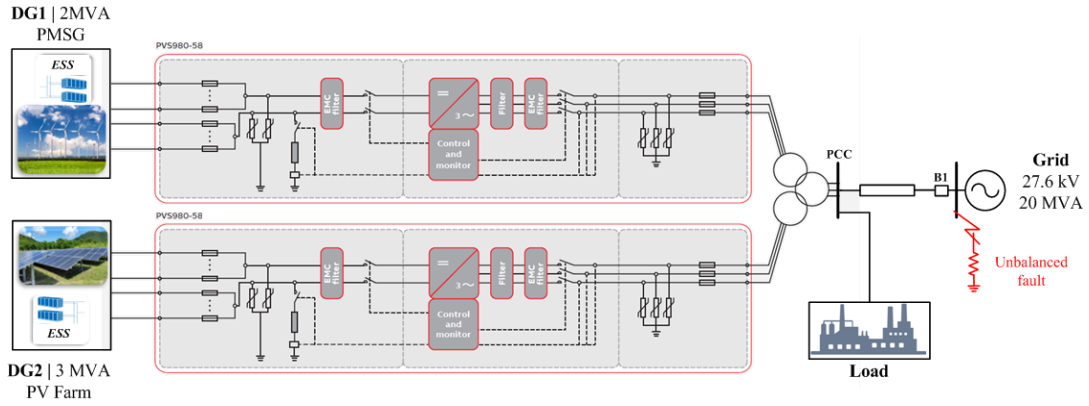


Figure 5.7 ABB PVS980 Central Inverter Model [104] block diagram interfacing two renewable DG units, i.e., 2MVA wind and 3MVA solar, to 20MVA grid

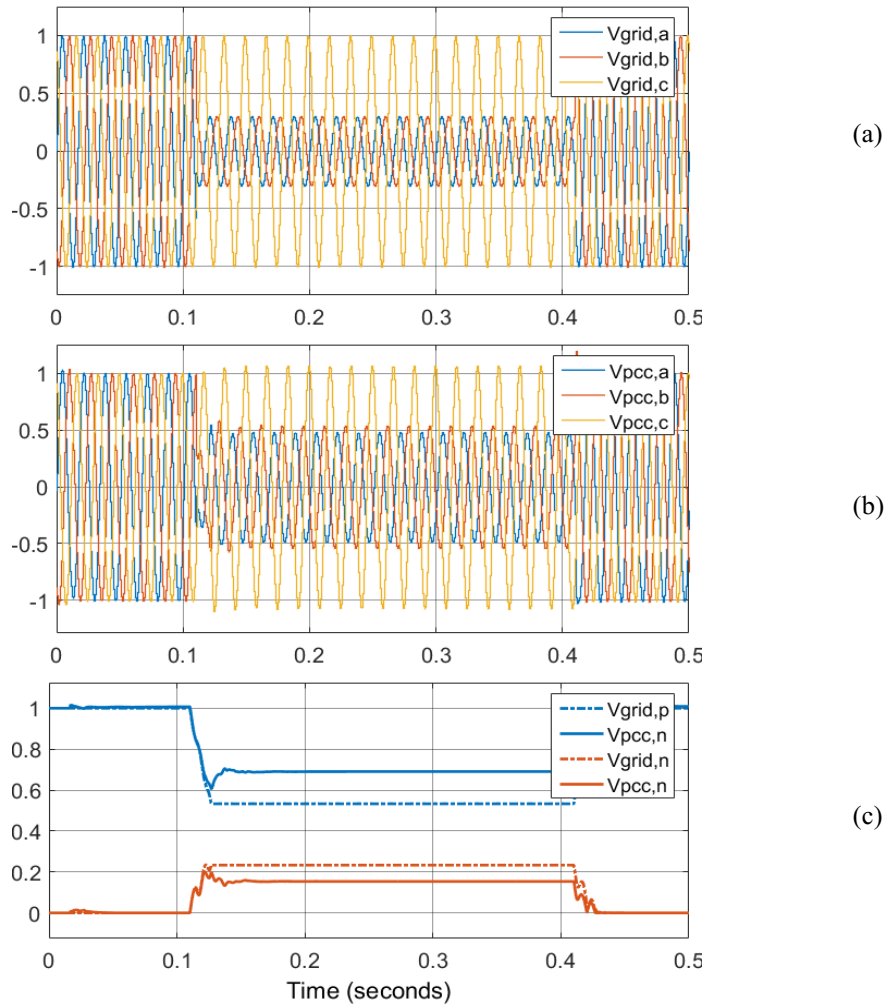


Figure 5.8 Test Case D: Conventional voltage support method [43]-[45] (a) grid voltage, (b) PCC voltage, (c) positive- and negative sequence voltages of the grid and PCC.

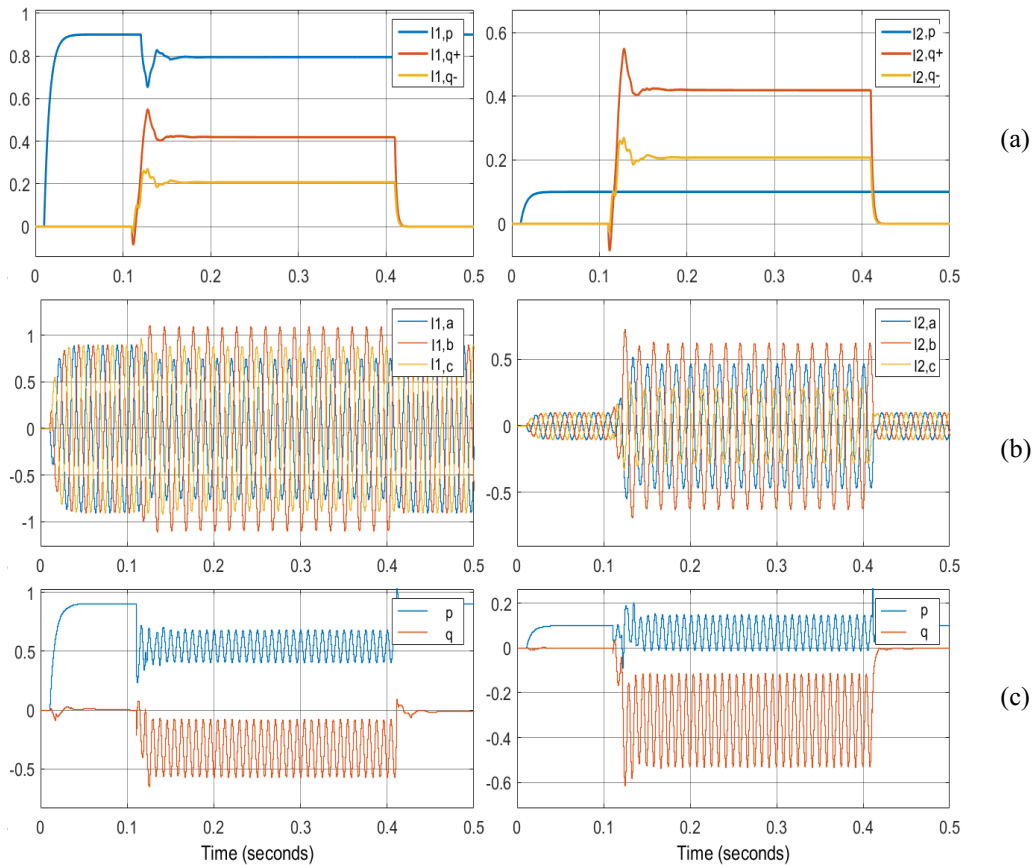


Figure 5.9 Test Case D: Conventional voltage support method [43]-[45]: (a) active and positive/negative-sequence reactive currents of DG1, DG2 (b) phase-currents of DG1, DG2, (c) active and reactive powers of DG1 and DG2.

## 5.6 Simulation Results

The proposed methods are examined on a simulated version of a practical test system, adapted from a typical ABB PVS980 Central Inverter [104], as shown in Fig 5.7. This POMI structure is connected to the medium-voltage distribution system in Ontario, Canada. The details of this distribution system are provided in Chapter 6. The system parameters are reported in Fig 5.7. The POMI system interfaces a 2MVA wind farm and a 3 MVA solar farm to a 27 kV distribution grid. Each DG has its own integrated energy storage system to balance its dc-link voltage.

Fig 5.8 shows the result of applying the conventional voltage support method [43]-[45] with constant reactive current injection under the unbalanced fault. This method has three drawbacks:

- 1) It is not a maximum unbalanced voltage support.
- 2) The active power in DG1 (see Fig 5.9-a-left and Fig 5.9-c-left) is disrupted.
- 3) There is no coordination between 2 DGs support. There is neither adjustability in the support process since it is just a constant reactive power injection based on the unbalanced voltage.

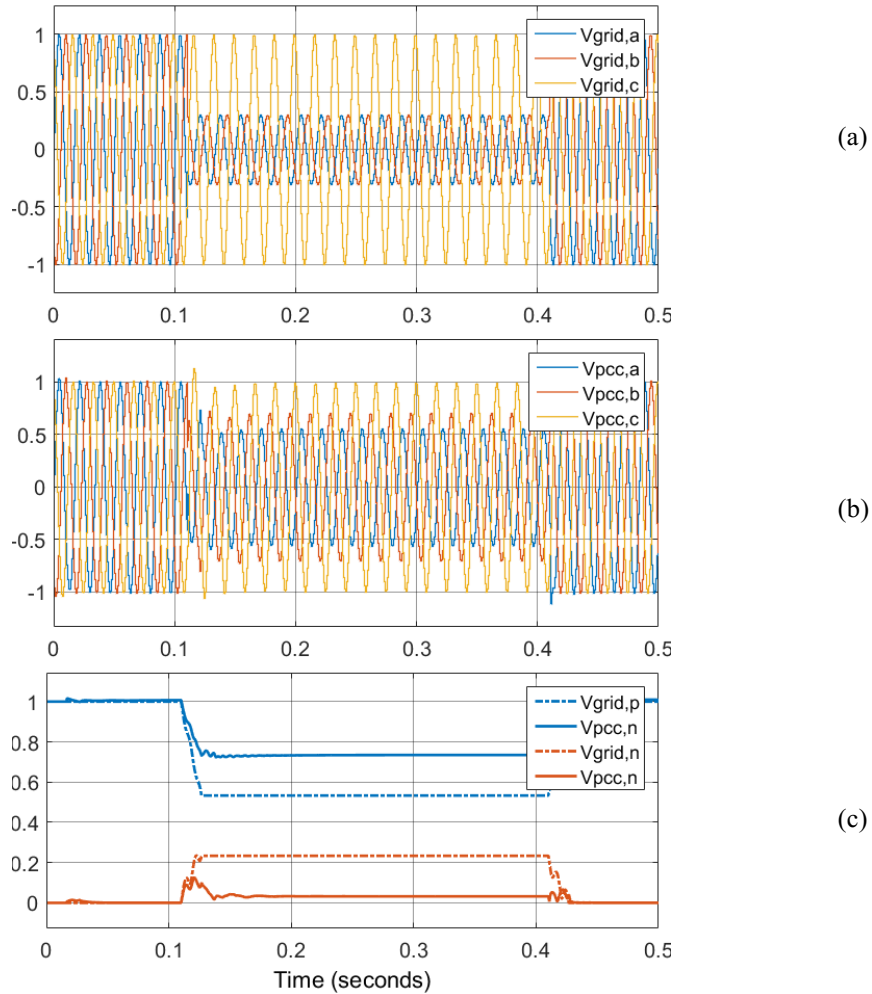


Figure 5.10 Test Case D: Proposed PMAS voltage support method (a) grid voltage, (b) PCC voltage, (c) positive- and negative sequence voltages of the grid and PCC.

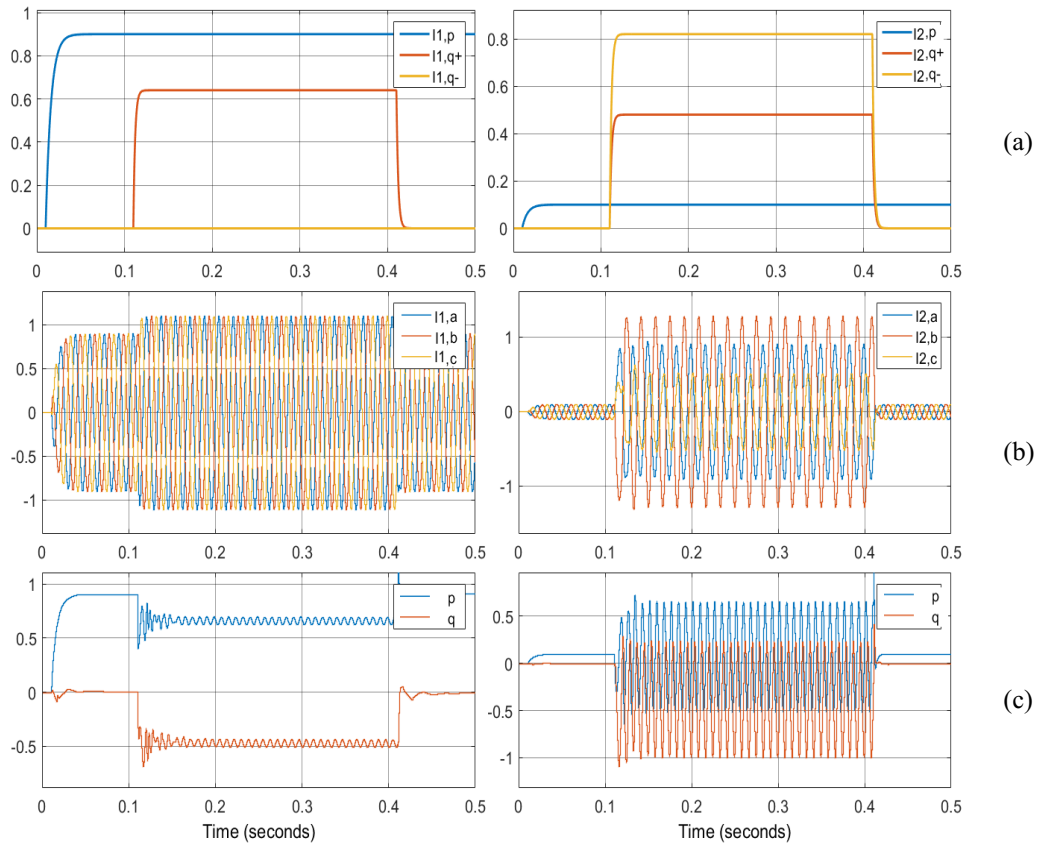


Figure 5.11 Test Case D: Proposed PMAS voltage support method: (a) active and positive/negative-sequence reactive currents of DG1, DG2 (b) phase-currents of DG1, DG2, (c) active and reactive powers of DG1 and DG2.

On the other hand, the proposed PMAS method addresses these insufficiencies as illustrated in Fig 5.10 and 5.11.

- 1) Fig 5.10 shows better positive voltage boost and more negative voltage reduction.
- 2) Furthermore, Fig 5.11 reveals the smart coordination between the two DGs. It is clear from Fig 5.11 that DG2 injects more supportive reactive currents in the positive and negative sequences since its active power injection at the DOS is relatively smaller than DG1 (see Fig 5.11-a).
- 3) Fig 5.11-a and Fig 5.11-c also show that despite higher asymmetric support by the PMAS compared to the conventional method, the proposed

method does not disrupt the active power injection of DG1 due to its coordination mechanism.

## 5.7 Conclusion

This chapter proposed an advanced methodology for optimized asymmetric support performance of a parallel-operated multi-inverter system, named the PMAS scheme. The study in this chapter shows that the maximum asymmetric support performance of each inverter unit inside the parallel structure does not provide the overall optimized performance. On the other hand, the augmentation of the multiple inverters will neither provide the optimized overall maximum asymmetric support for the parallel system. This is due to the differences on the inverters different MVA ratings, different safety constraints and fault-tolerance capabilities, and more importantly, varied instantaneous operating points. Therefore, the smart approach would be to tackle this problem by an advanced coordination scheme between the inverter units for the overall optimized asymmetric support performance. The proposed PMAS scheme thus empower the parallel multi-inverter system to:

- 1) coordinate the maximum flexible asymmetrical voltage support and ride-through capabilities of individual units inside the POMI structure,
- 2) maximize the collective dynamic contribution of POMI system in boosting the voltage and reducing the imbalance subject to the constraints of the plant and host system,
- 3) keep the active power injection of each GSI unit intact which leads to power/cost saving in the plant operation as well as host system stability enhancement, and
- 4) set different objectives based on the potential requirements in future grid codes

The simulation tests on ABB 2MVA central inverters illustrated effectiveness of the proposed ideas.

# Chapter 6

## Decentralized MAS Scheme in Multiple Distributed Grid-Interactive Smart Inverters

### 6.1 Introduction

The active power injection of DG units before and during the fault occurrence is an important factor affecting the maximum amount of allowable voltage support by individual DG units. Therefore, to allocate the supportive currents from each DG, the *instantaneous* capacity of each DG (i.e., instantaneous available capacity under the fault) plays a crucial role. The autonomy of the coordination scheme can also be highly beneficial since it eliminates (or at least reduces) the reliance on communication systems, central data acquisition/processing, and supervisory control. This leads to saving the costs while increasing the reliability of the highly-integrated active distribution networks (ADNs). However, coordinating the asymmetrical voltage support among multiple DG units while maximizing their contribution is very challenging for the autonomous/decentralized methods since there exists many constraints but no communication between the units.

The main achievement of this chapter is to propose an autonomous cooperative scheme to address these objectives. The main contributions of this chapter are the followings:

- 1) A comprehensive decentralized asymmetrical ride-through scheme is proposed in this chapter. The objective is coordinating the flexible asymmetrical voltage support contribution of multiple converter-interfaced DG units in an ADN such that their supports neither interfere with each other nor worsen the faulty situation. There is no need for the central control unit in the proposed coordination scheme, avoiding the high costs of communication infrastructures and increasing the reliability and flexibility of the ADN and DG units.
- 2) The active power injection of DG units is not affected during the support time; saving power and cost (important from the DG owner point of view) and improving the host system stability (important from the system operator point of view). This is achieved by considering both instantaneous active power injection and active power oscillation limit of individual DG units during the support in the proposed strategies.
- 3) The maximum flexible asymmetric voltage support performance is not compromised whenever one DG reaches its limits since other DG units can instantaneously compensate for that due to the cooperative nature of the proposed method. In addition, the over-voltage problem on the un-faulted phases are considered in the coordination scheme.

A new concept is proposed to build a comprehensive coordination scheme, named maximum support point tracking. This technique is achieved using the identified boundary limits and dynamic support points trajectories.

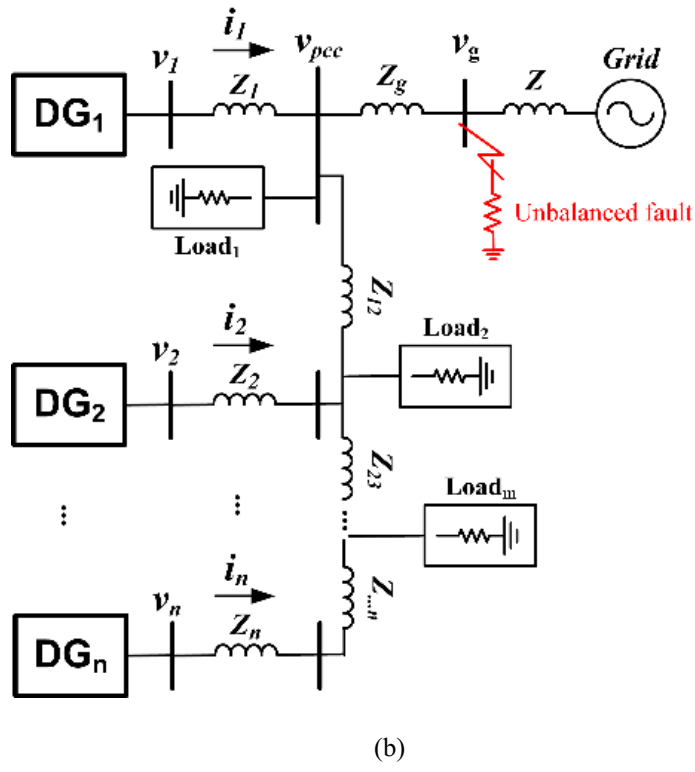
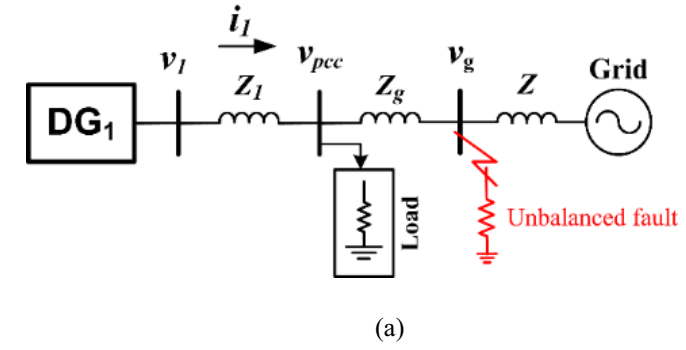


Figure 6.1 Active distribution network with (a) single and (b) multiple DG units.

## 6.2 Multi-DG Active Distribution Network

A single DG unit connected to the grid under the unbalanced condition is indicated in Fig 6.1(a). Extensive studies have been carried out recently to present different methods for supporting the PCC voltage under unbalanced grid faults by a single DG unit [36]-[53].

On the other hand, a multi-DG system under unbalanced grid faults, illustrated in Fig 6.1(b), has not been thoroughly investigated in the literature. The

voltage control techniques in active distribution networks (ADNs) proposed in the existing literature are commonly classified as centralized and decentralized methods. An in-depth literature review of these two categories is presented in [105]-[107]. The centralized voltage control methods typically use communication signals for controlling distributed loads, multiple DG units, and distributed storage systems. Such an active centralized scheme results in the accumulation of the information and requires signal processing and decision-making units as well as communication infrastructures to transmit all the signals [108]. Although the centralized methods can lead to optimal management of the ADNs and economic dispatch of DG units with high accuracy and controllability, in theory, they suffer from several important drawbacks in practice:

- 1) computation complexity in gathering and processing the information and optimal decision making;
- 2) challenges of optimal decision making based on the limited information, e.g., when the information of one area is not available;
- 3) defected operation in the entire network in the case of a failure in one control unit;
- 4) high costs of building communication infrastructures; and (5) undesirable impact on the plug-and-play feature of the distributed units [105]-[106].

Therefore, some efforts have been carried out in the recent literature to propose proper decentralized voltage control methods in microgrids [106]-[107], [109]-[114] and ADNs [105], [115] as well as distributed consensus-based control strategies in smart grids [116]-[117]. However, none of these studies has considered asymmetrical voltage support and LVRT performance improvement in ADNs with multiple DG units.

### 6.3 Proposed Decentralized Maximum Flexible Asymmetrical Support Tracking Scheme

The essential objectives in riding through unbalanced faults and providing grid supports by a single DG unit are to avoid any damage or undesirable operation in the DG unit, and flexibly support the asymmetrical voltage (i.e., by boosting the positive-sequence voltage while alleviating the negative-sequence component). Fig 6.1(b) illustrates a schematic of an ADN with  $n$  converter-interfaced DG units. An unbalanced grid fault or loading can cause asymmetrical voltage condition in the entire distribution network. For any unbalanced condition, the positive- and negative- sequence voltage vectors can be written for each unit (similar to the unbalanced voltage equations for the POMI system in the previous chapter) as

$$v_k^+ = \begin{bmatrix} v_{\alpha,k}^+ \\ v_{\beta,k}^+ \end{bmatrix} = \begin{bmatrix} V_k^+ \cos(\omega t + \delta_k^+) \\ V_k^+ \sin(\omega t + \delta_k^+) \end{bmatrix}, \quad v_k^- = \begin{bmatrix} v_{\alpha,k}^- \\ v_{\beta,k}^- \end{bmatrix} = \begin{bmatrix} V_k^- \cos(\omega t + \delta_k^-) \\ -V_k^- \sin(\omega t + \delta_k^-) \end{bmatrix} \quad (6.1).$$

The total injected current by  $k^{\text{th}}$  DG unit can be mathematically formulated as

$$i_k = i_{p,k} + i_{q,k} \quad (6.2).$$

To exploit a flexible voltage support performance from distributed units, the injected reactive current vector of the  $k^{\text{th}}$  converter,  $i_{q,k}$ , in (6.2) is divided into the positive and negative sequences in (6.3). These two current components can be written in a vector form of

$$i_{q,k} = i_{q,k}^+ + i_{q,k}^- = \begin{bmatrix} i_{\alpha,q,k} \\ i_{\beta,q,k} \end{bmatrix} = \begin{bmatrix} I_{q,k}^+ \sin(\omega t + \delta_k^+) - I_{q,k}^- \sin(\omega t + \delta_k^-) \\ -I_{q,k}^+ \cos(\omega t + \delta_k^+) - I_{q,k}^- \cos(\omega t + \delta_k^-) \end{bmatrix} \quad (6.3).$$

For now, let's assume that the augmented reactive currents from all distributed units,  $i_q^{\text{aug}}$ , for the unbalanced voltage support is available. This current can comprise positive and negative sequences and can be found by following the notions for the single DG unit structure [52]. [51] It is worth mentioning that for conventional augmented approaches the operating conditions of distributed units should be assumed to be the same.

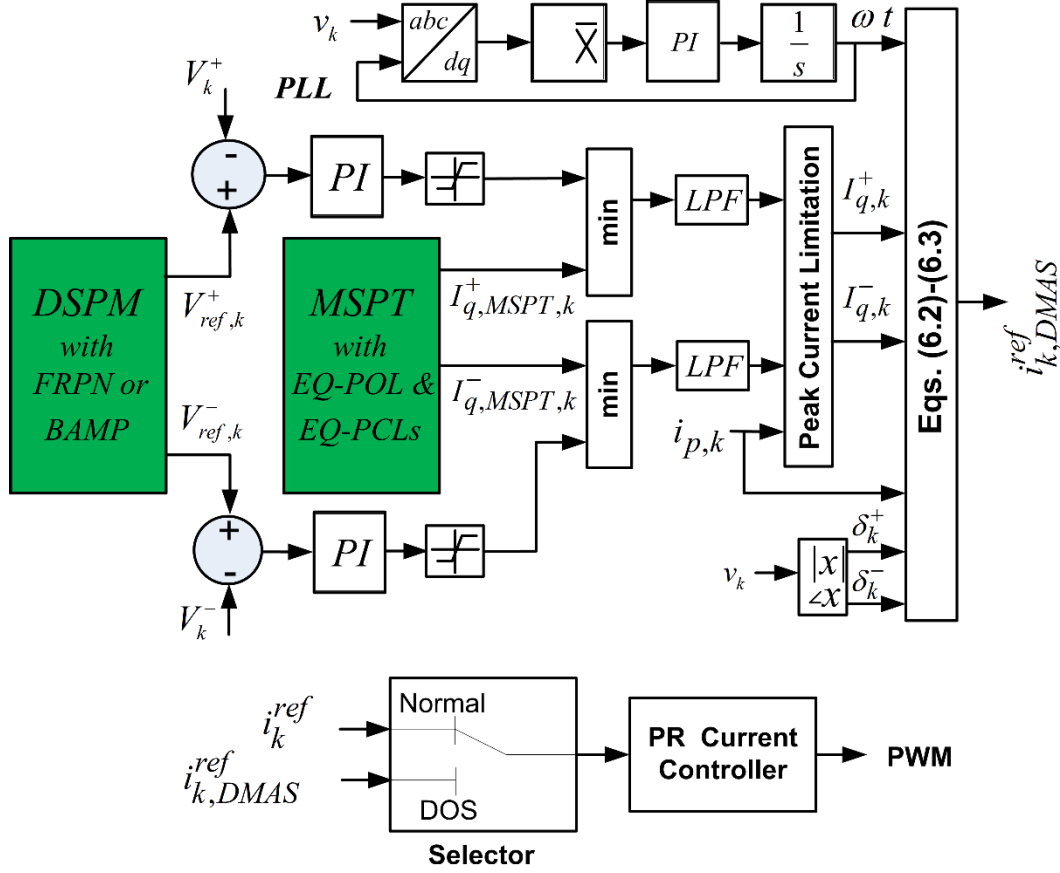


Figure 6.2 Control system diagram of the proposed DMAS scheme embracing the DSPM and MSPT blocks

After determining the total required positive- and negative-sequence currents by the augmented notion, the problem becomes dividing the total supportive currents between the distributed converters. The Kirchhoff's current law gives

$$i_q^{aug} = \sum_{k=1:n} i_{q,k} - i_{q,load}^{total} \quad (6.4),$$

where  $n$  is the number of distributed units and  $i_{q,load}^{total}$  is the total reactive currents of the loads. The positive and negative-sequence can then be divided based on the ratings of the distributed units by drop-based approaches.

For an effective distributed voltage support, the nearest converter (i.e., with the lowest line impedance) can contribute more to support the voltage, if all the converters have the same amount of the available capacity for additional reactive

current injection. Therefore, the default distributed assignment of the set-points can be realized using the following equation:

$$I_{q,k}^+ = \frac{1/X_k}{\sum_{j=1:n} 1/X_j} I_{q,g}^+, \quad I_{q,k}^- = \frac{1/X_k}{\sum_{j=1:n} 1/X_j} I_{q,g}^- \quad (6.5),$$

where  $X_i$  is the inductance of the line connecting the  $i^{\text{th}}$  converter to the PCC. The ratings of the DG units and their corresponding peak currents during the asymmetrical condition must also be considered prior to the augmentation. However, this augmented notion can only be applied if the operating conditions of all distributed units are the same at the fault instant, or there exists a central control unit. Hereinafter, the time interval in which the proposed voltage support method is applied is called the duration of support (DOS).

To find the decentralized coordination between individually optimized flexible asymmetric voltage supports of multi-DG structure in Fig 6.1(b), the following points should also be considered in addition to the rating and maximum peak current of each unit:

- 1) Available capacity of each converter during the DOS: There might be a case that one unit reaches its maximum current capacity at the DOS since it is injecting a considerable amount of active power while other units still have extra capacities available for the support (since they are operating in lower active power operating points). This is a common scenario in ADNs with both solar and wind energy units which can create a useful opportunity for cooperation. During the day, the active power production of the solar energy system is typically in its high while during the night wind produces its high active power. Therefore, a smart coordination scheme would benefit from the optimum available capacity of each unit during the DOS.
- 2) Active power oscillation of each converter during the DOS: This parameter should be kept under control for a stable operation and reliable distributed support. High active power oscillation (due to the severe unbalanced faults)

harms the frequency stability of the ac-side as well as dc-side voltage stability.

- 3) Un-faulted phase voltage magnitudes: The over-voltage on the un-faulted phases must be avoided. This can be achieved by the dynamic nature of the proposed method.
- 4) Maximum utilization of the  $k^{\text{th}}$  unit in a dynamic and autonomous manner.

The proposed coordination scheme is named decentralized maximum asymmetrical support tracking (DMAS) which encompasses two core blocks:

- 1) dynamic support point movement (DSPM), and
- 2) maximum support point tracking (MSPT).

Fig 6.2 illustrates the control system of the proposed DMAS scheme with its DSPM and MSPT blocks. These control blocks are explained in the following sections.

## 6.4 Identified Constraints for MSPT Method

This section explains how to find the maximum allowable support of  $k^{\text{th}}$  DG unit. The MSPT method defines two criteria: maximum tolerable active power oscillation limit (POL) and peak current limit (PCL). Then, the appropriate reference values for the positive- and negative-sequence reactive currents will be determined.

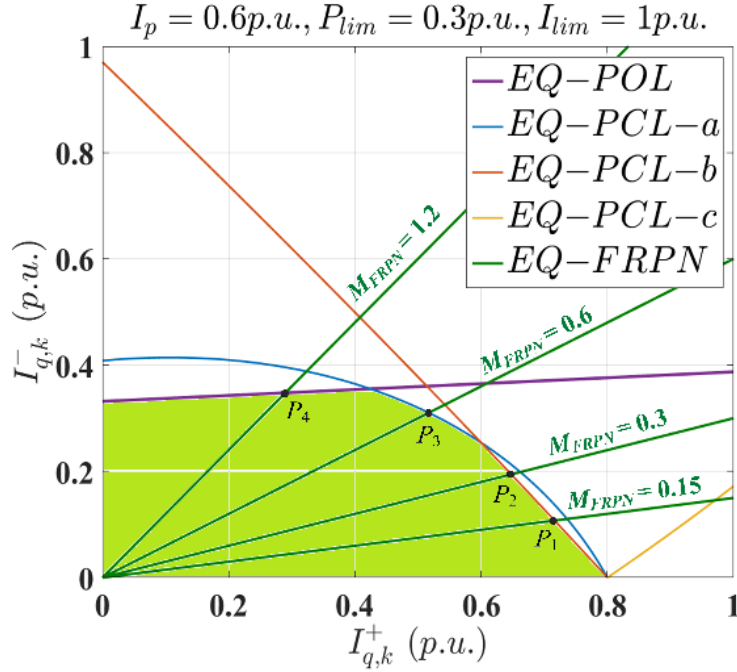


Figure 6.3 Proposed MSPT approach with FRPN strategy

#### 6.4.1 Active Power Oscillation Limit (POL) Constraint

Based on the instantaneous power theory, the output active power oscillation terms of the  $k^{th}$  DG unit is calculated as

$$\tilde{p} = v_k^+ \cdot i_k^- + v_k^- \cdot i_k^+ \quad (6.6).$$

The maximum active power oscillation of the  $k^{th}$  unit can be formulated as

$$\tilde{p}_{\max,k} = \sqrt{(V_k^+ I_{q,k}^- - V_k^- I_{q,k}^+)^2 + (V_k^- I_{p,k}^+)^2} \quad (6.7).$$

Therefore, depending on the instantaneous amount of  $I_p^+$  in the  $k^{th}$  unit, the following relation between the  $I_{q,k}^-$  and  $I_{q,k}^+$  is obtained:

$$I_{q,k}^- \leq \frac{\sqrt{\tilde{P}_{\lim,k}^2 - (V_k^- I_{p,k}^+)^2} + V_k^- I_{q,k}^+}{V_k^+} \quad (6.8).$$

This is the first obtained constrain between  $I_{q,k}^-$  and  $I_{q,k}^+$ . Eq (8) is named *EQ-POL* for representing the POL constrains the MSPT graphs. The *EQ-POL* boundary

is sketched as a straight line in Fig 6.3 in *magenta* color. This analytical equation does not allow the active power oscillation of  $k^{\text{th}}$  unit exceeds its corresponding limitation,  $\tilde{P}_{\text{lim},k}$ . The value of  $\tilde{P}_{\text{lim},k}$  is set by the converter's manufacturer or owner. This feature thus avoids any undesired damage to the converter and the control system of the  $k^{\text{th}}$  unit. Furthermore, it enhances the ac-side frequency stability and dc-side voltage stability during severe unbalanced grid faults.

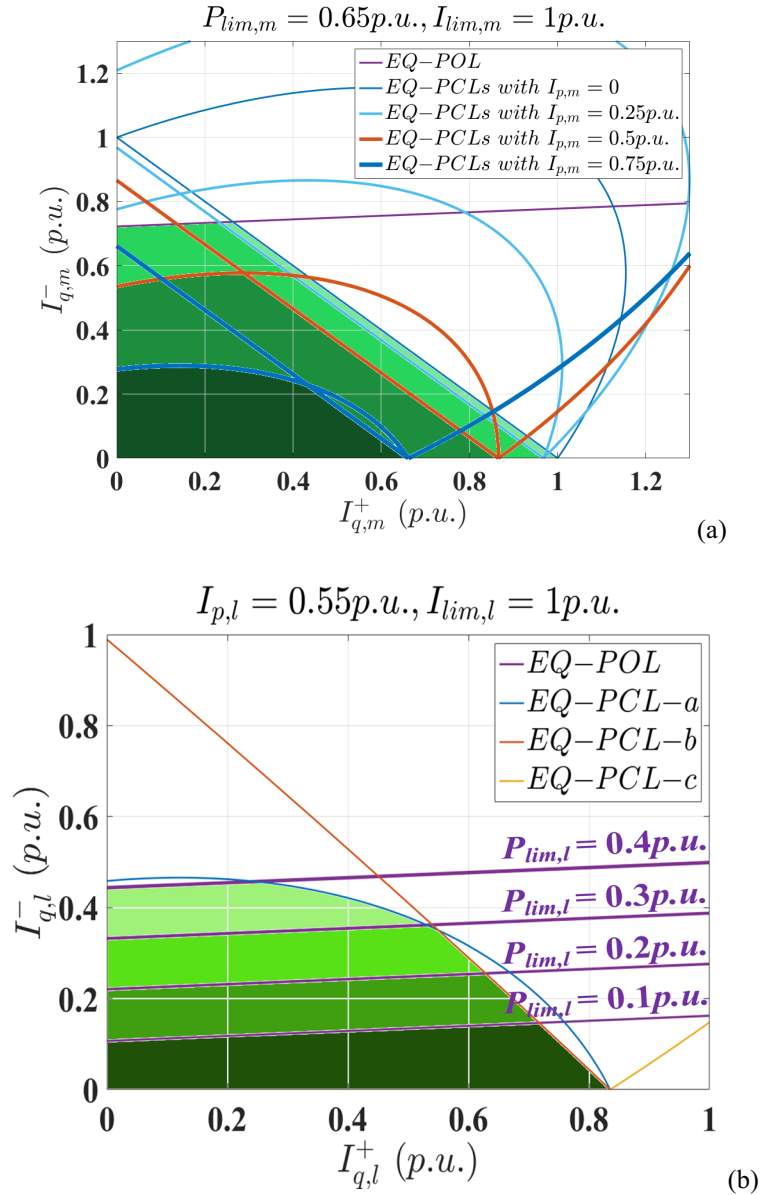


Figure 6.4 Allowable flexible voltage support areas of (a)  $m^{\text{th}}$  DG unit with four different values of  $I_{p,m}$  at the DOS, and (b)  $l^{\text{th}}$  DG unit with four different values of  $P_{\text{lim},l}$  at the DOS

It is worth mentioning that the *EQ-POL* boundary may be time varying during the DOS featuring the dynamic characteristic of the proposed MSPT since (8) indicates that the relation between  $I_{q,k}^-$  and  $I_{q,k}^+$  in the POL constraint of the  $k^{\text{th}}$  unit depends on:

- 1) the instantaneous value of the active power component of the current in that unit, i.e.,  $I_{p,k}^+$ , during the DOS, and
- 2) the unbalanced fault characteristics, i.e.,  $V_k^+$  and  $V_k^-$ .

#### 6.4.2 Peak-Current Limitation (PCL) Constraint

The peak current limitation of the power switches is another important constraint that must be considered in the MSPT method. Applying this constraint ensures i) flexibly delivering the maximum allowable supportive currents in positive- and negative- sequences and ii) autonomously setting the reference values of  $I_{q,k}^-$  and  $I_{q,k}^+$  without exceeding the peak current limitation in the  $k^{\text{th}}$  unit. The analytical expressions of the phase currents can be formulated in the two-axis stationary reference frame, based on the unbalanced voltage sag characteristics. Similar analysis to the parallel system in the previous chapter can also be carried out here. Eq (5.9)-(5.11) can be also used here for the peak current limitation constrains in distributed GSI units. These equations are respectively named *EQ-PCL-a*, *EQ-PCL-b*, and *EQ-PCL-c*, represented in Fig 6.3 in *blue*, *orange*, and *yellow* colors, respectively. Based on these three equations the graph of Fig 6.3 becomes complete. These three equations besides the *EQ-POL* determine the non-linear and time-varying constraint boundaries for  $I_{q,k}^-$  and  $I_{q,k}^+$ . In summary, these boundaries depend on three factors: i) setting parameters of the converters (i.e.,  $I_{lim,kS}$  and  $p_{lim,kS}$ ), ii) unbalanced voltage characteristics, and iii) instantaneous active power component of the injected currents. Based on these three factors, the four curves representing the relationship between  $I_{q,k}^-$  and  $I_{q,k}^+$  are drawn in Fig 6.3 to better illustrate the proposed MSPT approach.

### 6.4.3 Allowable Flexible Voltage Support Areas

Based on the proposed ideas in this chapter, the allowable flexible support areas (AFSAs) can be identified in the *NRPR* plane for all units. As a first example, the AFSA of the  $k^{\text{th}}$  DG unit is shown with the green area in Fig 6.4 considering its pre-set configurations as well as instantaneous operating points at the DOS. The green areas of Fig 6.4 show other examples of AFSAs. Fig 6.4(a) illustrates four different AFSAs (from light green to dark green) for four different values of the active current of the  $m^{\text{th}}$  DG unit at the DOS. Therefore, based on the *instantaneous* active current value at the DOS, the allowable voltage support area of the  $m^{\text{th}}$  DG unit may be varied resulting in very different optimal reference values for the positive- and negative-sequence reactive currents of that specific unit. It is clear from Fig 6.4(a) that higher active current values of the DG unit at the DOS results in lower allowable room for contribution in supporting the unbalanced voltage by positive- and negative-sequence reactive currents. These plots clearly show the nonlinear relation between the active current component value and the permissible values for the supportive reactive currents in positive- and negative sequences.

Fig 6.4(b) also demonstrates four different AFSAs (from light green to dark green) for another DG unit based on four different values of the maximum tolerable active power oscillation. Based on Fig 6.4(b), if the maximum tolerable active power oscillation amount of the  $l^{\text{th}}$  DG unit decreases, the available area of its flexible voltage support contribution will shrink. Therefore, other DG units shall compensate for the shrunk area of support in the  $l^{\text{th}}$  DG unit in the collaborative MSPT approach within their own available green areas. The introduced AFSAs give useful insights on how to drive appropriate strategies in a decentralized manner to achieve coordinated flexible support by multiple distributed units.

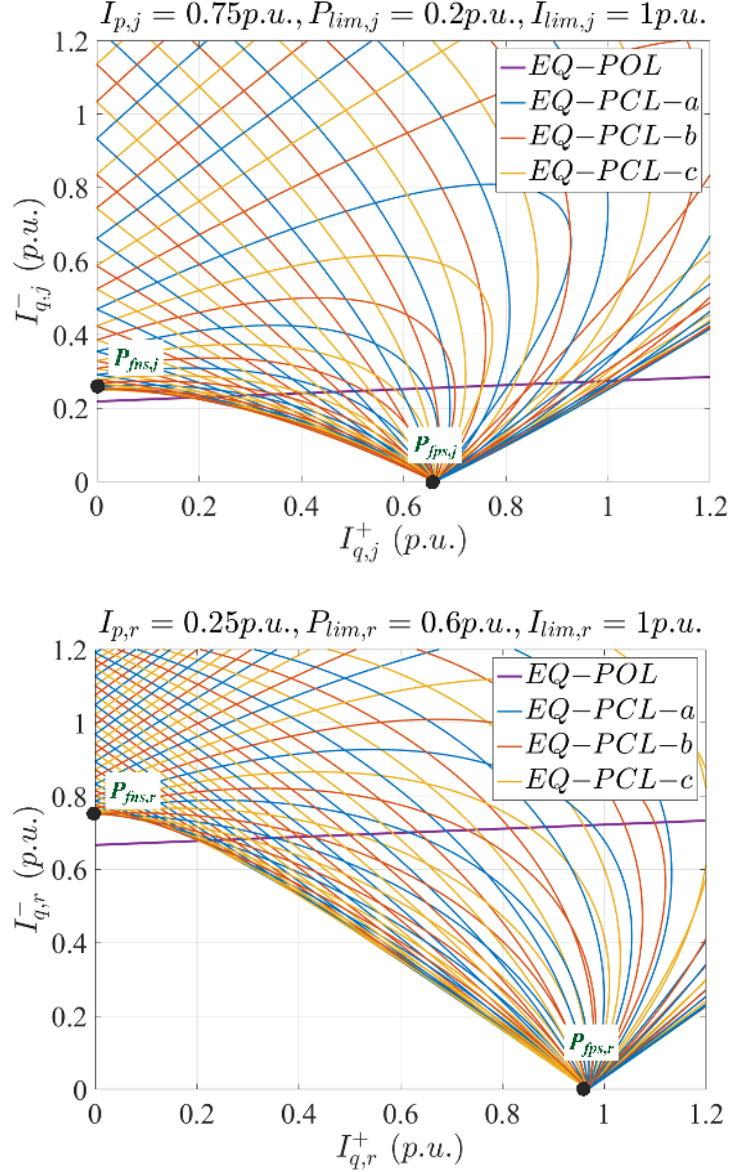


Figure 6.5 PCL equations for the entire range of possible asymmetrical fault types, i.e.,

$$\gamma_k = 0 : \frac{\pi}{12} : 2\pi \text{ for two different cases.}$$

### 6.4.1 Simplified MSPT

We can also use a simplified version of the MSPT approach in the control system (i.e., MSPT block of Fig 6.2) to reduce the computational complexity. Fig 6.5 demonstrates all possible EQ-PCLs for any type of asymmetrical faults. Fig 6.5 reveals an interesting feature in the  $NRPR$  plane: for any type of asymmetrical faults we can find two useful points (i.e., full positive support point,  $P_{fps}$ , and full negative

support point,  $P_{fns}$ ) such that a line connecting these two points gives a good estimation of the all possible EQ-PCLs boundaries. This simplification approach effectively removes the dependency of the PCL equations (5.9)-(5.11) to the asymmetrical fault type. Manipulating (5.9)-(5.11) gives

$$\begin{aligned} P_{fps} : I_{q,k}^- &= 0, & I_{q,k,fps}^+ &= \sqrt{I_{lim,k}^2 - I_{p,k}^2} \\ P_{fns} : I_{q,k}^+ &= 0, & I_{q,k,fns}^- &= I_{lim,k} - I_{p,k} \end{aligned} \quad (6.9).$$

Using this simple approach enormously expedites the calculation and can be very efficient in the case of real applications with low-speed processing units.

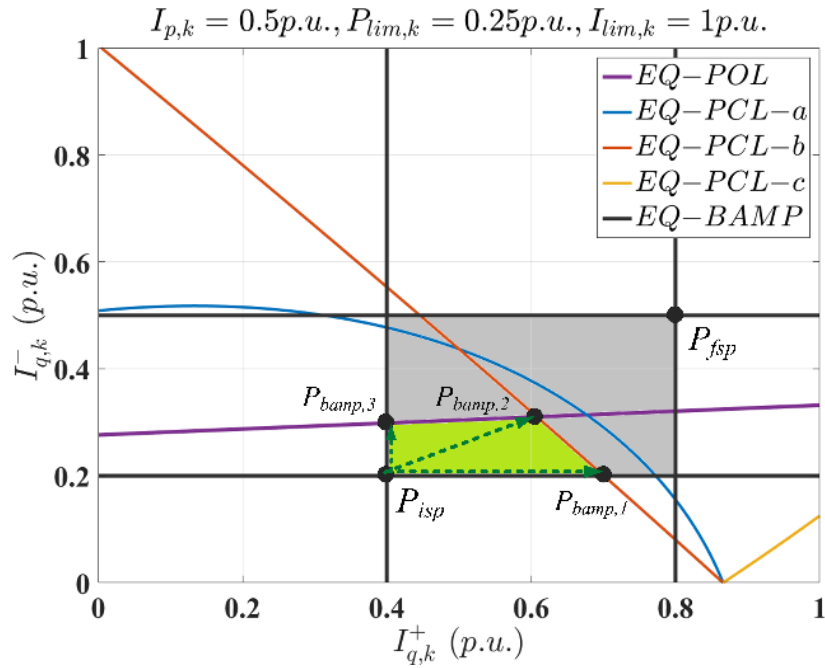


Figure 6.6 Maximum support point tracking with BAMP

## 6.5 Proposed Strategies to Determine Maximum Support Points by DSPM

Now that we have identified the constraints and allowable support areas, the final stage of the MSPT approach is to find the optimal reference values for  $I_{q,k}^+$  and  $I_{q,k}^-$  in an autonomous way for individual units. The following subsections introduce

two strategies to track and find the optimal values for  $I_{q,k}^+$  and  $I_{q,k}^-$  without any communication between the distributed units.

### 6.5.1 MSPT with Flexible Ratio between Positive- and Negative-Sequences (FRPN)

The relation between the desired  $I_{q,k}^-$  and  $I_{q,k}^+$  values can be defined by:

$$\frac{I_{q,k}^-}{I_{q,k}^+} = \frac{V_g^- - V_{ref,k}^-}{V_{ref,k}^+ - V_g^+} = \frac{\Delta V_k^-}{\Delta V_k^+} = M_{FRPN,k} \quad (6.10).$$

This equation governs the ratio between the desired positive and negative voltage supports, i.e.,  $M_{FRPN}$ , and it is named *EQ-FRPN*. The *EQ-FRPN* is the line sketched in *green* color in Fig 6.3. The maximum support points are thus determined by the intersection of *EQ-FRPN* line and one of the boundary curves, i.e., *EQ-POL*, *EQ-PCL-a*, *EQ-PCL-b*, and *EQ-PCL-c*. For example, points  $P_1$  and  $P_2$  in Fig 6.3 indicate the peak-current limitation of phase *B* and the maximum values for the positive- and negative-sequence reactive currents respectively for  $M_{FRPN} = 0.15$  and  $M_{FRPN} = 0.3$ . Point  $P_3$  shows the peak-current limitation of phase *A* and the maximum values for the positive- and negative-sequence reactive currents for  $M_{FRPN} = 0.6$ . The slope of the *EQ-FRPN* line can vary flexibly during the DOS to reach the equilibrium point between the distributed units in an autonomous way.

### 6.5.2 MSPT with Bounded Autonomous Moving Points (BAMP) Approach

As opposed to the FRPN strategy, the MSPT with the bounded autonomous moving points (BAMP) does not require a ratio between  $I_{q,k}^+$  and  $I_{q,k}^-$ . Instead, it suggests defining one initial support point ( $P_{isp}$ ) and one final support point ( $P_{fsp}$ ). The corresponding  $I_{q,k}^+$  and  $I_{q,k}^-$  for the initial and final points can be obtained by

$$\begin{aligned}
I_{q,k,isp}^+ &= \frac{1/X_k}{\sum_{j=1:n} 1/X_j} \times \frac{\Delta V_{isp}^+}{X_g}, & I_{q,k,isp}^- &= \frac{1/X_k}{\sum_{j=1:n} 1/X_j} \times \frac{\Delta V_{isp}^-}{X_g} \\
I_{q,k,fsp}^+ &= \frac{1/X_k}{\sum_{j=1:n} 1/X_j} \times \frac{\Delta V_{fsp}^+}{X_g}, & I_{q,k,fsp}^- &= \frac{1/X_k}{\sum_{j=1:n} 1/X_j} \times \frac{\Delta V_{fsp}^-}{X_g}
\end{aligned} \tag{6.11}.$$

These expressions are named *EQ-BAMP* and depicted in Fig 6.6. According to Fig 6.6, the voltage support area for this case (i.e., without constraints) includes both green and gray areas. However, if the MSPT constraints are applied, then the moving points will be limited to just the green area. Two very useful features can be extracted from Fig 6.6.

- 1) Generally, if the positive-sequence reactive current increases during the dynamic voltage support (e.g., starting from point  $P_{isp}$ ), it is most likely to hit the PCL constraint boundaries.
- 2) Generally, if the negative-sequence reactive current increases during the bounded moving points strategy, it is most likely to hit the POL constraint.

Based on these useful features obtained from the *NRPR* plane, we can properly design our MSPT approach with BAMP strategy (see Fig 6.2). It is thus proposed in this chapter that the MSPT with POL constraint is applied to adjust the negative-sequence reactive current while the equations of the PCL constraints are considered for regulating the positive-sequence reactive current. The simulation results will better clarify the proposed concepts

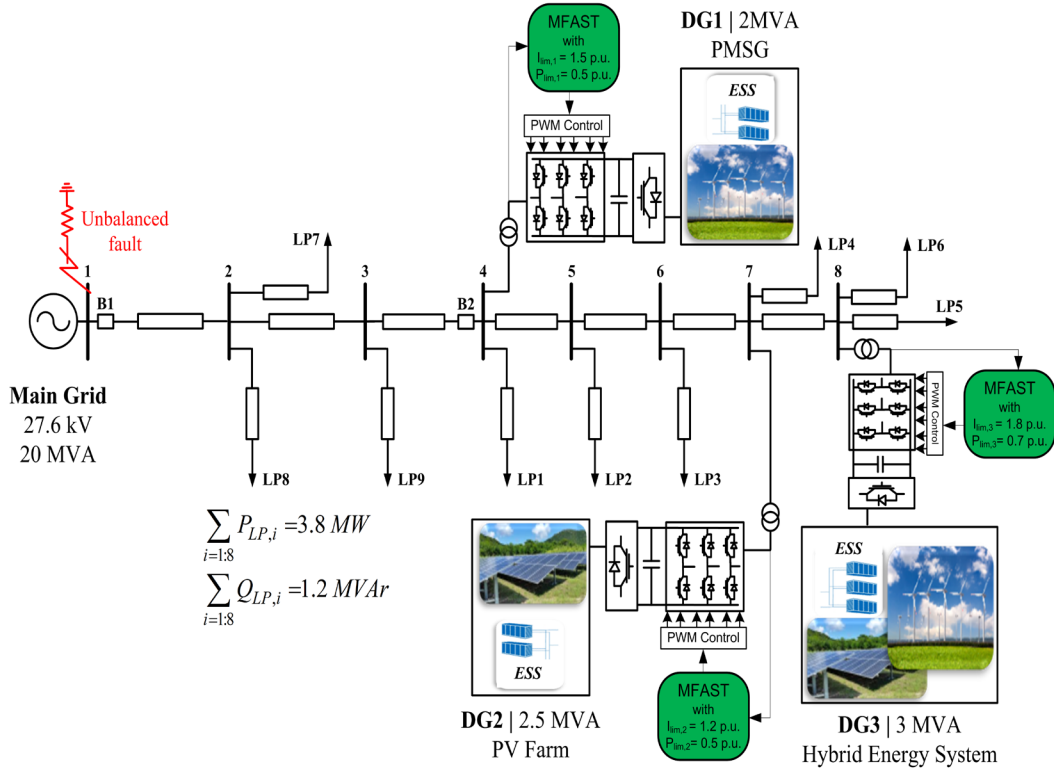


Figure 6.7 Studied Test System: A typical medium-voltage distribution system in Ontario, Canada

## 6.6 Simulation Results

The proposed methods are examined on a practical test system, adapted from a typical Hydro One system, the medium-voltage distribution system in Ontario, Canada [118]. The system parameters are reported in Fig 6.7. This 27-kV distribution network consists of three large renewable plants (2MVA wind farm, 2.5 MVA solar farm, and 3MVA hybrid plant). As Fig 6.7 also indicates, the pre-set PCL/POL values of three DGs are different ( $I_{peak,1}=1.5 \text{ p.u.}$ ,  $I_{peak,2}=1.2 \text{ p.u.}$ ,  $I_{peak,3}=1.8 \text{ p.u.}$ ,  $P_{lim,1}=0.5 \text{ p.u.}$ ,  $P_{lim,2}=0.5 \text{ p.u.}$ , and  $P_{lim,3}=0.7 \text{ p.u.}$ ).

### 6.6.1 Test Case A: Conventional vs Proposed

A double-phase fault occurs at  $t=0.1\text{s}$  and clears at  $t=0.4\text{s}$ , as shown in Figs 6.8 and 6.10. Fig 6.8 and 6.9 show the results of the conventional asymmetrical voltage support method [44], [83], [91]. In the conventional approach, all three DGs inject similar amount of positive- and negative- sequence currents, respectively,

proportional to the positive-sequence voltage reduction (from a specific value, e.g., 0.9 p.u. [44]) and negative-sequence voltage rise (from a specific value, e.g., 0.05 p.u. [44]). Although there are huge differences between the *instantaneous* supportive capacity of each DG (in addition to differences between their pre-set values, i.e., ratings and PCL/POL constraints), they inject both sequences with respect to two simple droop control techniques. Due to the simplicity of the conventional method, some grid codes have adopted it [83]. However, the results obtained from the conventional approaches are neither sufficient nor coordinated. This is clear by comparing Fig 6.8(b)-(c) with Fig 6.10(b)-(c).

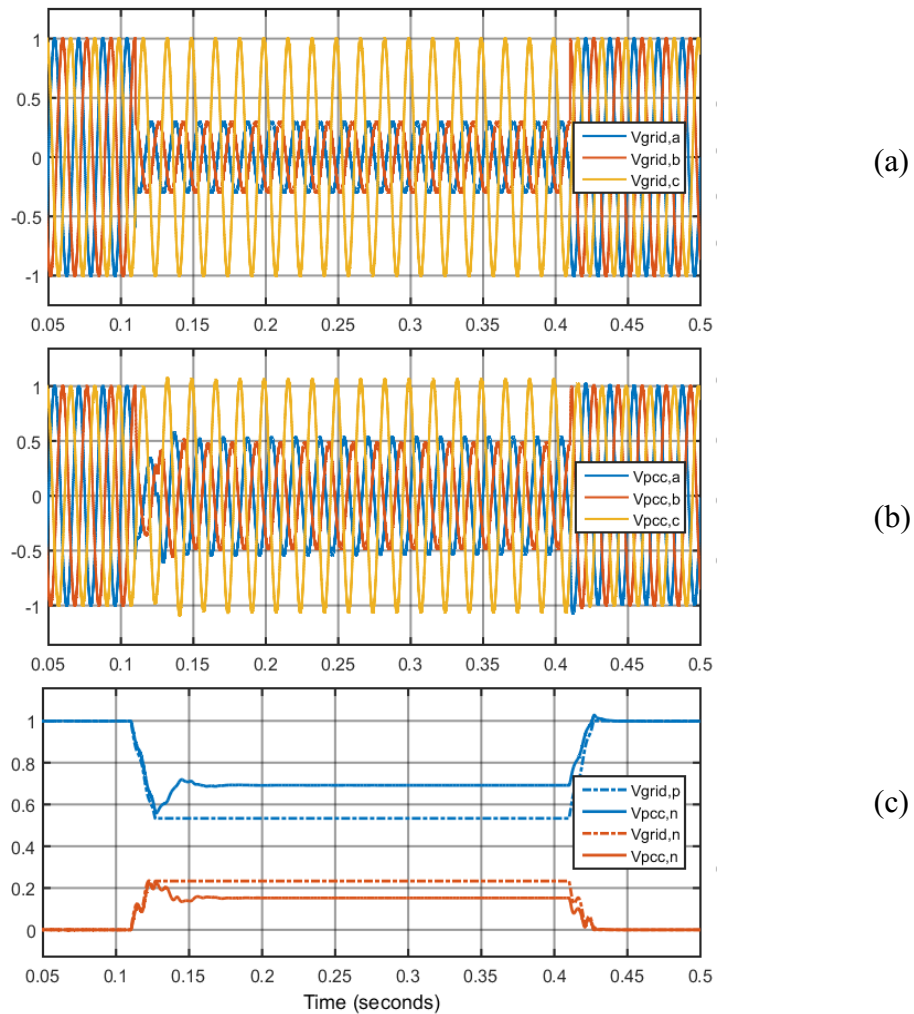


Figure 6.8 Test Case A: Conventional voltage support method [44], [83], [91] (a) grid voltage, (b) PCC voltage, (c) positive- and negative sequence voltages of the grid and PCC.

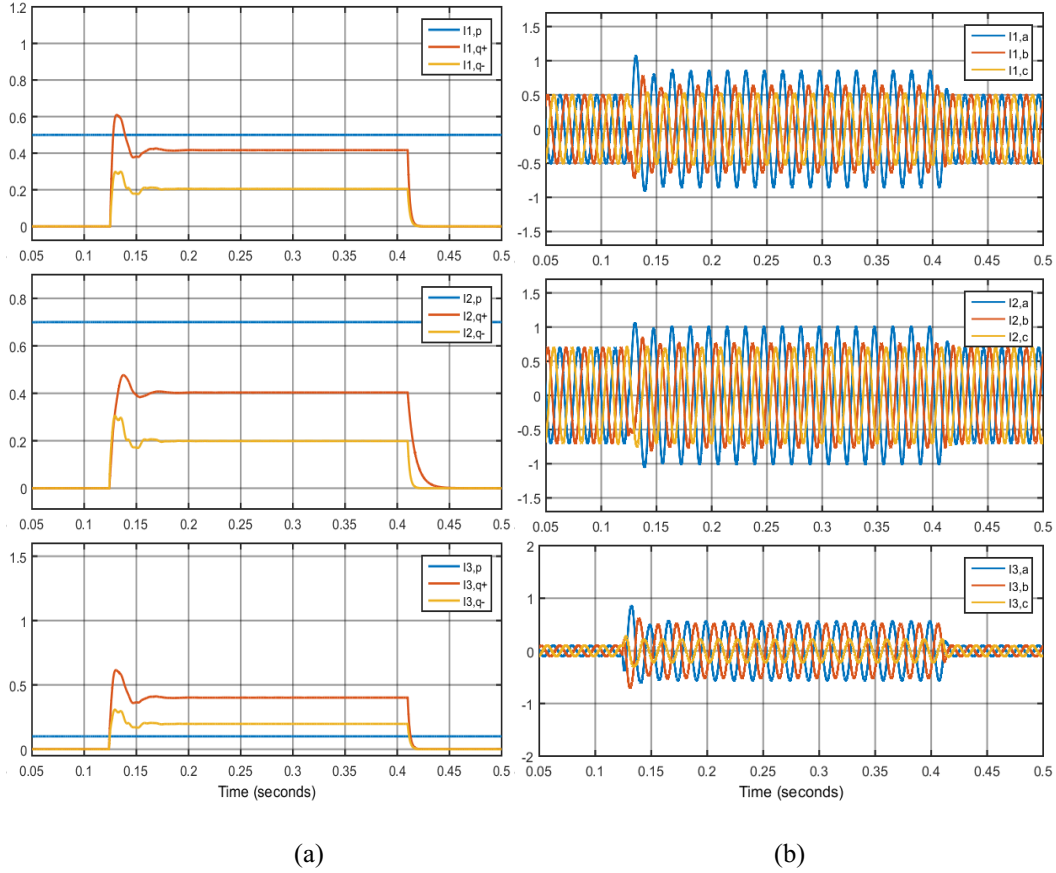


Figure 6.9 Test Case A: Conventional voltage support method [44], [83], [91]: (a) active and positive/negative-sequence reactive currents of DG1, DG2, and DG3, (b) phase-currents of DG1, DG2, and DG3

On the other hand, Figs 6.10 and 6.11 illustrate the results of the proposed scheme. The active current components of DG1 and DG2 are high during the DOS. **Event-1:** According to Fig 6.11(b), in the first milliseconds after the fault occurrence, the peak-current in phase *A* in DG2 hits the limitation. Therefore, the proposed MSPT method tries to autonomously and dynamically adjust the positive-sequence reactive current of the DG2 (see Fig 6.11(a), event-2) so that the peak-current limitation criterion is satisfied while still contributing to the distributed voltage support (to the maximum capability of DG2). **Event-3:** To compensate for this shortage, DG1 autonomously tries to inject more positive-sequence reactive current as it is clear from  $t=0.2$ s to  $t=0.32$ s in Fig 6.11(a). **Event-4:** At this point, DG1 also hits the peak-current limitation in phases *A* and *B*, as shown in Fig 6.11(b). Therefore, the proposed MSPT method autonomously keeps its positive-

sequence reactive current constant, as indicated in Fig 6.11(a), event-5. **Event-6:** From this point, DG3 autonomously tries to inject even more positive-sequence reactive current, as accelerated increase is observable in Fig 6.11(a), to compensate for the shortcomings of positive-sequence support in DG1 and DG2.

Comparing Fig 6.8(b)-(c) with Fig 6.10(b)-(c) clearly illustrates the superior performance of the proposed DMAS scheme in supporting the phase voltages as well as in improving positive- and negative-sequences of the voltage.

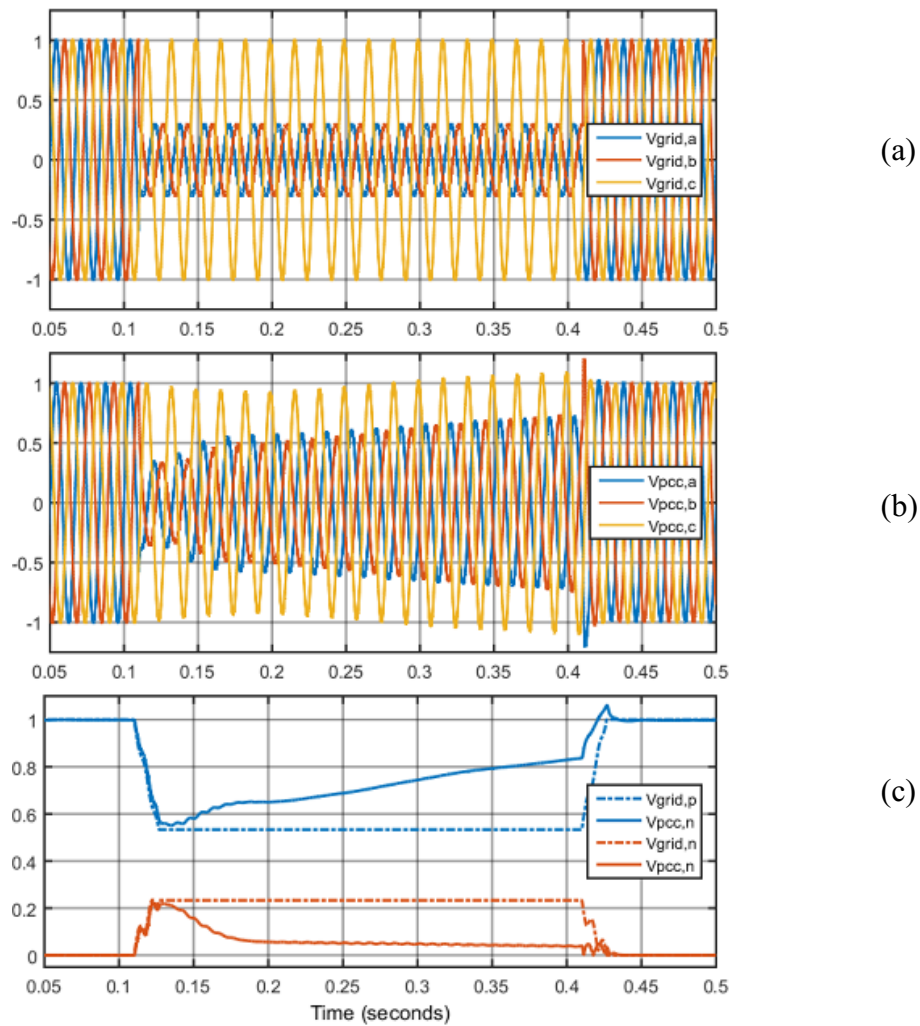


Figure 6.10 Test Case A: the proposed DMAS scheme, (a) grid phase-voltages, (b) PCC phase-voltages, (c) positive- and negative- sequence voltages of the grid and PCC.

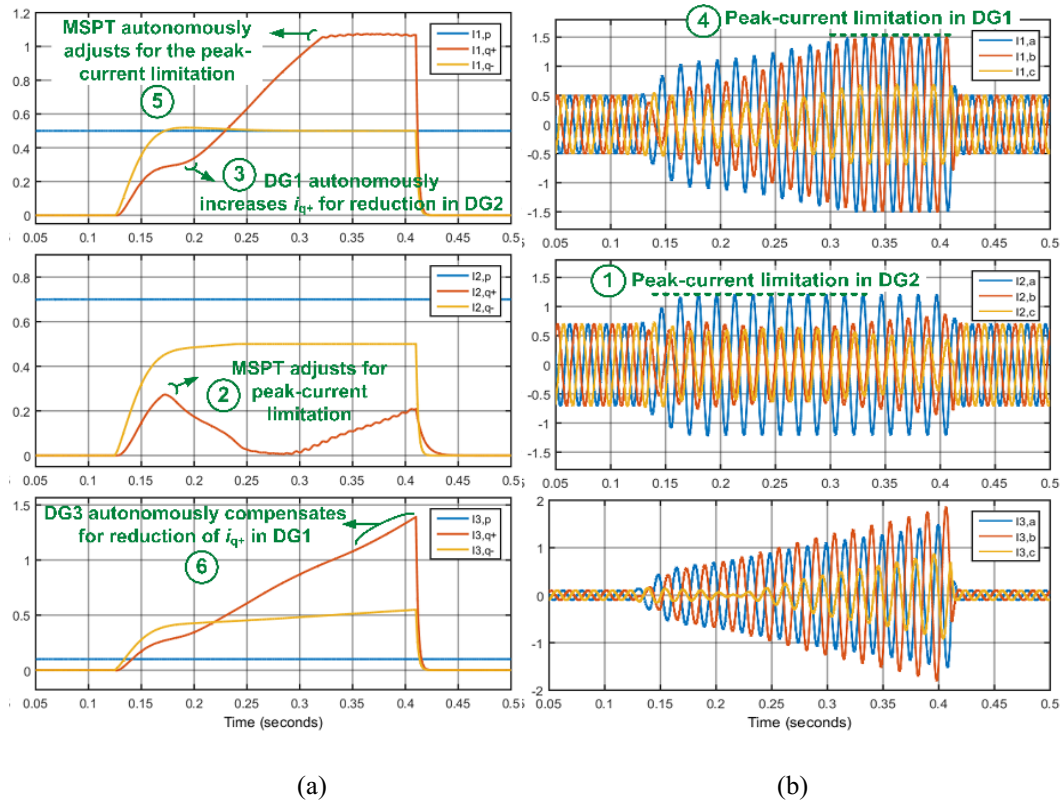


Figure 6.11 Test Case A: the proposed DMAS scheme: (a) active and positive/negative-sequence reactive currents of DG1, DG2, and DG3, (b) phase-currents of DG1, DG2, and DG3

### 6.6.2 Test Case B: Proposed Scheme under Severe Conditions

In this test case, two different voltage drops 100% on phases *A* and 50% on phase *B* (as shown in Fig 6.12(a)) have been applied to test the proposed coordination scheme. The result of the DMAS voltage support is presented in Fig 6.12(b). Fig 6.12(c) also illustrates the improvements in positive- and negative-sequence voltages. During the dynamic and autonomous operation of the proposed DMAS method in this test case, five noticeable MSPT events happen (i.e., first in DG2, then in DG1, and finally in DG3). **Event-1:** At  $t=0.15s$ , the peak-current limitation of DG2 (Fig 6.13(b)) causes to reduce the positive-sequence reactive current (Fig 6.13(a), event-2). This event is autonomously compensated by accelerated increase in positive support contributions from DG1 and DG3 from  $t=0.15s$ , event-3. **Event-4:** Another main MSPT event occurs at 0.22s in DG1 due to peak-current limitation. **Event-6:** A few milliseconds later, another MSPT constraint occurs at  $t=0.32s$

where the active power oscillation of the DG1 hits the pre-set maximum allowable limit (Fig 6.13(b)). Therefore, the DMAS immediately reduces the negative-sequence reactive current in DG1 (Fig 6.13(a), event-7). **Event-8:** As expected, DG3 autonomously and quickly respond to this shortcoming by an accelerated increase in its contribution in injecting negative-sequence reactive current (Fig 6.13 (a)). **Event-9:** Finally, at  $t=0.35$ s the fourth MSPT constraint happens in DG3 due to its peak-current limitation. These nine events all happen autonomously without having any communication between three units. This test case clearly demonstrates the main contributions of this chapter: 1) the decentralized nature of the proposed coordination scheme; 2) maximum flexible asymmetrical voltage support of individual DG units and their cooperative support; 3) intact active power injection of all DG units during the DOS; 4) effective performance of the proposed DSPM and MSPT concepts while respecting the important boundary limits.

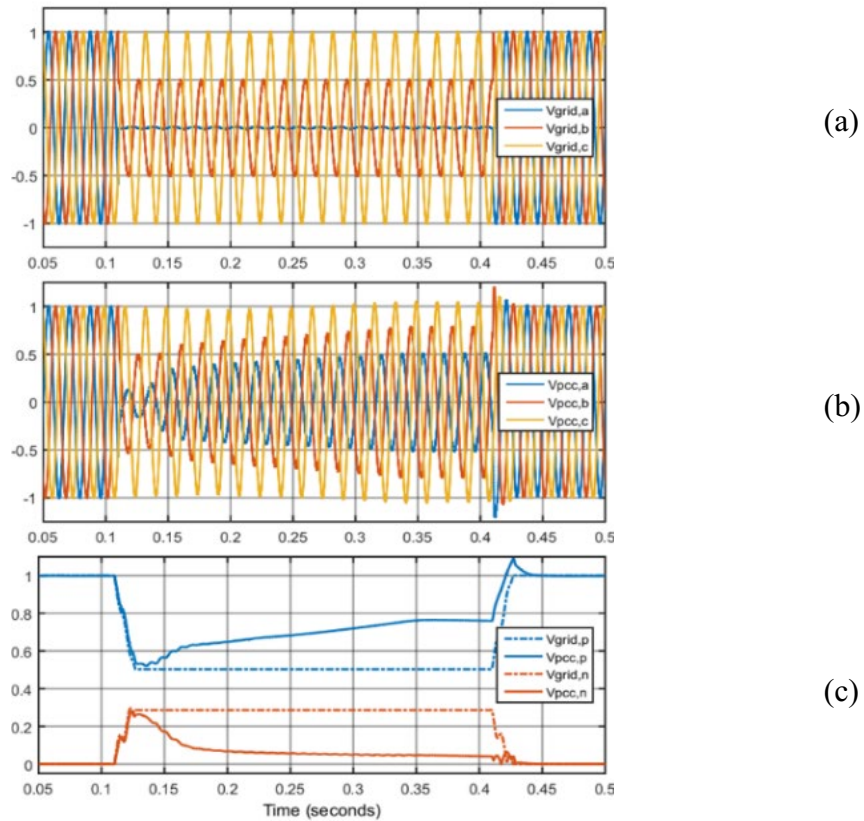


Figure 6.12 Test Case B: the proposed DMAS scheme, (a) grid phase-voltages, (b) PCC phase-voltages, (c) positive- and negative sequence voltages of the grid and PCC.

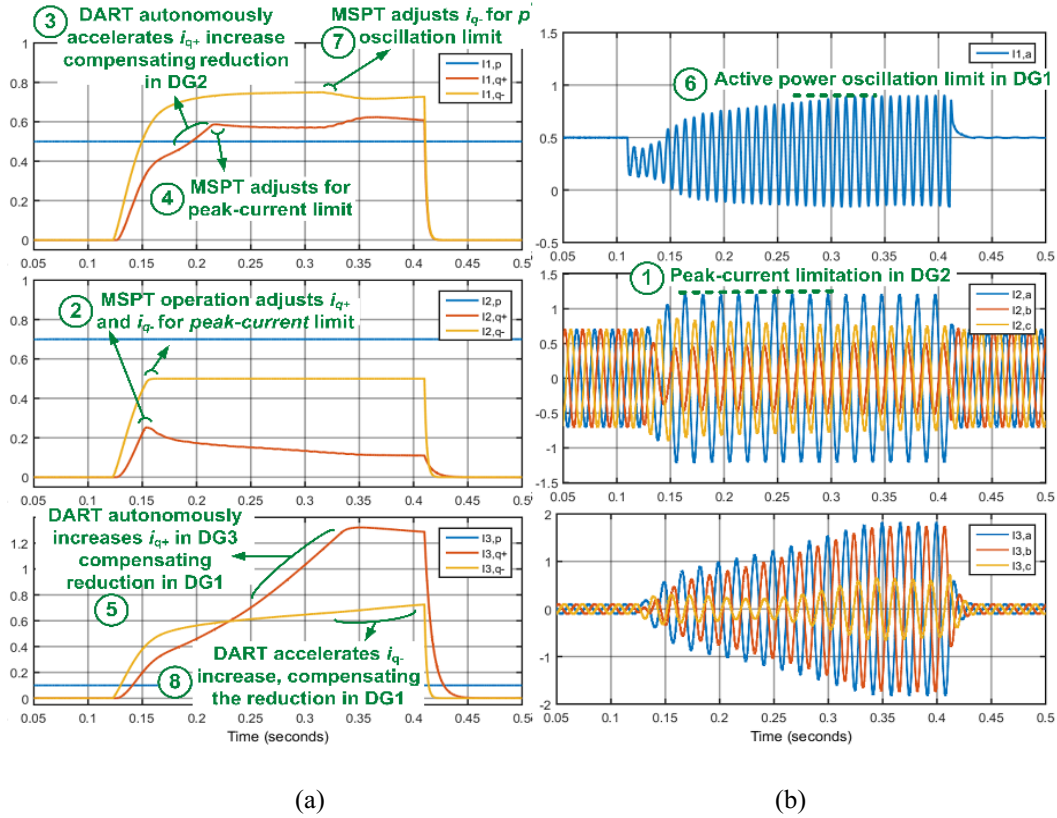


Figure 6.13 Test Case B: the proposed DMAS scheme: (a) active and positive/negative-sequence reactive currents of DG1, DG2, and DG3, (b) phase-currents of DG1, DG2, and DG3

## 6.7 Conclusion

This chapter presented a comprehensive coordination control scheme for maximized and flexible asymmetrical grid support by multiple DG units in an active distribution network. In addition to being decentralized, the proposed coordination scheme benefits from three additional features:

- 1) a maximized flexible asymmetrical voltage support that does not affect the active power injection of individual units at the time of the support,
- 2) maximum support point tracking of each unit considering current, voltage, and power constraints, and
- 3) wise dynamic support points movement. Furthermore, this chapter introduced new concepts including allowable flexible support areas and support points trajectories represented in the *negative-reactive-current* vs.

*positive-reactive-current* plane. These concepts were applied in the proposed scheme.

They are also useful for further research in this area. The proposed comprehensive scheme was tested in the simulated version of a distribution network in Ontario, Canada. Test results illustrated the superiority of the proposed techniques compared to the existing methods in the literature.

# Chapter 7

## Conclusion and Future Work

In this chapter, the main findings of the thesis are summarized, and future work suggestions are presented.

### 7.1 Thesis Achievements

The achievements of this research project can be summarized as:

- 1) The available control strategies under asymmetric grid conditions for a grid-interactive inverter was thoroughly studied.
- 2) A novel maximum asymmetric support control scheme (i.e., MAS scheme) was proposed based on the analytical methods. This scheme enables grid-interactive inverters to use their full potential to flexibly and optimally support the asymmetric grid voltage.
- 3) An advanced reference current generation scheme was suggested. This scheme has multiple objectives such as minimizing the power oscillations, maximizing the average active or reactive power delivery, and minimizing asymmetric fault currents.
- 4) A comprehensive guideline for riding through asymmetric faults and simultaneously supporting the grid (i.e., ART scheme) is introduced. This

scheme enforces large DGs to properly regulate the phase voltages within the pre-set dynamic limits under short-term asymmetric low voltages.

- 5) A novel dynamic voltage regulation method is also proposed to accurately address the ART specifications.
- 6) A new voltage support scheme with improved accuracy in regulating the phase voltages at the PCC within the pre-set safety limits was introduced. This method addresses the drawbacks of the existing approach by considering the zero-sequence voltage compensation, the output active power and being adaptive to complex grid impedance (i.e. with resistive and inductive parts). Two complementary strategies are also augmented to this method: the adjustable limited active power oscillation and the maximum active power delivery strategies. These strategies enabled the proposed voltage support method to have MAS capability.
- 7) A unique MAS scheme was proposed for multiple GSI units in the parallel structure which enables the maximum collaboration between the units in flexible and optimal asymmetric voltage support. This method was called parallel MAS (PMAS) technique. In addition to ordinary MAS capabilities, PMAS added the following advantages to the parallel multi-inverter structure:
  - a. coordinating the maximum flexible asymmetrical voltage support and ride-through capabilities of individual units inside the parallel structure,
  - b. maximizing the collective dynamic contribution of parallel structure in boosting the voltage and reducing the imbalance subject to the constraints of the plant and host system,
  - c. retaining the active power injection of each inverter unit intact which leads to power/cost saving in the plant operation as well as host system stability enhancement, and

- d. setting different objectives based on the potential requirements in future grid codes.
- 8) Another unique MAS scheme was proposed for the autonomous coordination control of multiple inverters in the distributed structure. This scheme is named decentralized MAS tracking (DMAS). While achieving the optimal coordination between the MAS performance of each inverter, the DMAS eliminates the dependency of the control system to communication infrastructure. The DMAS scheme is realized using two core concepts:
- a. The maximum support areas were introduced in the positive negative reactive currents plane.
  - b. The dynamic support points movement were proposed by two autonomous strategies.

## 7.2 Future Works

The proposed control and regulatory schemes (i.e., ART, MAS, PMAS, and DMAS) can be examined and applied in different applications such as different types of converter-interfaced DG units, grid-interactive converter-interfaced microgrids, interlinking converters inside hybrid AC/DC microgrids, and modular multi-level converter-based HVDC systems. They can be further explored for various type of energy resources such as permanent magnet synchronous generator-based wind turbines or converter-based photovoltaic systems, squirrel cage induction generators, and doubly-fed induction generators. Further investigation is required for the application of the proposed schemes for micro-units, such as small roof-top solar panels and electric vehicles. Since the voltage support in most cases is obtained using the reactive current, the nature of the energy source (that is responsible for generating the active power) does not affect the effectiveness of the proposed schemes in theory. However, further study is needed to validate this. Also, the algorithms can be extended to utilize the active current component in the supportive techniques. The specification on the active power limitation during the

fault and its restoration after the fault is an important area which needs similar comparative research. These specifications vary in different grid codes based on system characteristics such as grid strength. Although the imposed specifications on active power restoration by different grid codes can be adopted by the proposed supportive and regulation schemes, it is an interesting area for future research on specific requirements of active power restoration (from the system operator point of view) under unbalanced grid faults.

### **7.3 Expected Significance**

This research intends to identify the critical challenges of emerging grid-interactive smart inverters under asymmetric grid conditions. Some of the most significant benefits of this project are as follows: (1) tackling the reliability challenges brought by the increasing integration of distributed inverters into the existing power grids, (2) enforcing large DGs and microgrids to provide maximum support to the grid under abnormal conditions to guarantee the stable operation of the host system, (3) applying the advanced control schemes in different configuration (i.e., parallel- and distributed structures), and in various application, i.e., a single DG system, hybrid ac/dc microgrids, and active distribution networks, (4) facilitating the booming growth of high renewable and clean energies integration.

## References

- [1] International Energy Agency, *Energy and Climate Change*, World Energy Outlook Special Report, 75739, Paris, Cedex 15, France, 2015. [E-Book] Available: [www.iea.org/publications](http://www.iea.org/publications).
- [2] R. Quitzow, S. Roehrkasten, M. Jaenicke, “The German Energy Transition in International Perspective”, Institute for Advanced Sustainability Studies (IASS) Potsdam, March 2016. [E-Book] Available: [www.iass-potsdam.de](http://www.iass-potsdam.de).
- [3] The Danish Ministry of Climate and Energy, “Energy strategy 2050 - from coal, oil and gas to green energy”, Copenhagen, Denmark, Feb. 2011. [E-Book] Available: <http://www.danishwaterforum.dk>.
- [4] “Microgrid Deployment Tracker 4Q12”, 2015, [Online]. Available: [www.navigantresearch.com/newsroom](http://www.navigantresearch.com/newsroom). [Accessed Nov 2017].
- [5] “List of HVDC projects”, [Online]. Available: [en.wikipedia.org/wiki/List\\_of\\_HVDC\\_projects](http://en.wikipedia.org/wiki/List_of_HVDC_projects). [Accessed Nov 2017].
- [6] J. Jia, G. Yang and A. H. Nielsen, "A Review on Grid-connected Converter Control for Short Circuit Power Provision under Grid Unbalanced Faults," in *IEEE Transactions on Power Delivery*, vol. 33, no. 2, pp. 649-661, 2018.
- [7] Measurement and assessment of power quality characteristics of grid connected wind turbines, IEC Std. 61400-21:2008, Aug. 2008.
- [8] “The massive integration of power electronic devices”, Sept 2016. [Online]. Available: <https://www.h2020-migrate.eu>.
- [9] “Application of synchronous condensers”, Sept 2016. [Online]. Available: <http://www.scapp.dk>.
- [10] “Prosmart, kpn-project energix”, Sept 2016. [Online]. Available: <http://www.ntnu.edu/prosmart>.

- [11] S. Mortazavian, M. M. Shabestary and Y. A. R. I. Mohamed, "Analysis and Dynamic Performance Improvement of Grid-Connected Voltage–Source Converters Under Unbalanced Network Conditions," in *IEEE Transactions on Power Electronics*, vol. 32, no. 10, pp. 8134-8149, Oct. 2017.
- [12] Remus Teodorescu; Marco Liserre; Pedro Rodriguez, "Control of Grid Converters under Grid Faults," in *Grid Converters for Photovoltaic and Wind Power Systems*, 1, Wiley-IEEE Press, 2011, pp.237-287
- [13] K. Ma, W. Chen, M. Liserre and F. Blaabjerg, "Power Controllability of a Three-Phase Converter with an Unbalanced AC Source," in *IEEE Transactions on Power Electronics*, vol. 30, no. 3, pp. 1591-1604, March 2015.
- [14] A. Moawwad, M. S. El Moursi and W. Xiao, "Advanced Fault Ride-Through Management Scheme for VSC-HVDC Connecting Offshore Wind Farms," in *IEEE Transactions on Power Systems*, vol. 31, no. 6, pp. 4923-4934, Nov. 2016.
- [15] A. Moawwad, M. S. El Moursi and W. Xiao, "A Novel Transient Control Strategy for VSC-HVDC Connecting Offshore Wind Power Plant," in *IEEE Transactions on Sustainable Energy*, vol. 5, no. 4, pp. 1056-1069, Oct. 2014.
- [16] Remus Teodorescu; Marco Liserre; Pedro Rodriguez, "Control of Grid Converters under Grid Faults," in *Grid Converters for Photovoltaic and Wind Power Systems*, 1, Wiley-IEEE Press, 2011, pp.237-287
- [17] S. Sang, N. Gao, X. Cai and R. Li, "A Novel Power-Voltage Control Strategy for the Grid-Tied Inverter to Raise the Rated Power Injection Level in a Weak Grid," in *IEEE Journal of Emerging and Selected Topics in Power Electronics*, vol. 6, no. 1, pp. 219-232, March 2018.
- [18] T. Chen, C. K. Lee and R. Hui, "A General Design Procedure for Multi-parallel Modular Grid-tied Inverters System to Prevent Common and

- Interactive Instability," in *IEEE Transactions on Power Electronics*, Early Access, 2019.
- [19] S. R. Mohapatra and V. Agarwal, "Model Predictive Controller with Reduced Complexity for Grid-Tied Multilevel Inverters," in *IEEE Transactions on Industrial Electronics*, Early Access, 2019.
- [20] M. Shahparasti, M. Mohamadian, P. T. Baboli and A. Yazdianp, "Toward Power Quality Management in Hybrid AC–DC Microgrid Using LTC-L Utility Interactive Inverter: Load Voltage–Grid Current Tradeoff," in *IEEE Transactions on Smart Grid*, vol. 8, no. 2, pp. 857-867, March 2017.
- [21] J. Lamb and B. Mirafzal, "Grid-Interactive Cascaded H-Bridge Multilevel Converter PQ Plane Operating Region Analysis," in *IEEE Transactions on Industry Applications*, vol. 53, no. 6, pp. 5744-5752, Nov.-Dec. 2017.
- [22] C. H. Ng, L. Ran and J. Bumby, "Unbalanced-Grid-Fault Ride-Through Control for a Wind Turbine Inverter," in *IEEE Transactions on Industry Applications*, vol. 44, no. 3, pp. 845-856, May-June 2008.
- [23] S. Alepuz *et al.*, "Control Strategies Based on Symmetrical Components for Grid-Connected Converters Under Voltage Dips," in *IEEE Transactions on Industrial Electronics*, vol. 56, no. 6, pp. 2162-2173, June 2009.
- [24] A. Junyent-Ferre, O. Gomis-Bellmunt, T. C. Green and D. E. Soto-Sanchez, "Current Control Reference Calculation Issues for the Operation of Renewable Source Grid Interface VSCs Under Unbalanced Voltage Sags," in *IEEE Transactions on Power Electronics*, vol. 26, no. 12, pp. 3744-3753, Dec. 2011.
- [25] Z. R. Ivanović, E. M. Adžić, M. S. Vekić, S. U. Grabić, N. L. Čelanović and V. A. Katić, "HIL Evaluation of Power Flow Control Strategies for Energy Storage Connected to Smart Grid Under Unbalanced Conditions," in *IEEE Transactions on Power Electronics*, vol. 27, no. 11, pp. 4699-4710, Nov. 2012.

- [26] F. Wang, J. L. Duarte and M. A. M. Hendrix, "Design and analysis of active power control strategies for distributed generation inverters under unbalanced grid faults," in *IET Generation, Transmission & Distribution*, vol. 4, no. 8, pp. 905-916, August 2010.
- [27] F. Wang, J. L. Duarte and M. A. M. Hendrix, "Pliant Active and Reactive Power Control for Grid-Interactive Converters Under Unbalanced Voltage Dips," in *IEEE Transactions on Power Electronics*, vol. 26, no. 5, pp. 1511-1521, May 2011.
- [28] X. Guo, X. Zhang, B. Wang, W. Wu and J. M. Guerrero, "Asymmetrical Grid Fault Ride-Through Strategy of Three-Phase Grid-Connected Inverter Considering Network Impedance Impact in Low-Voltage Grid," in *IEEE Transactions on Power Electronics*, vol. 29, no. 3, pp. 1064-1068, March 2014.
- [29] M. Castilla, J. Miret, A. Camacho, L. García de Vicuña and J. Matas, "Modeling and Design of Voltage Support Control Schemes for Three-Phase Inverters Operating Under Unbalanced Grid Conditions," in *IEEE Transactions on Power Electronics*, vol. 29, no. 11, pp. 6139-6150, Nov. 2014.
- [30] A. Camacho, M. Castilla, J. Miret, A. Borrell and L. G. de Vicuña, "Active and Reactive Power Strategies With Peak Current Limitation for Distributed Generation Inverters During Unbalanced Grid Faults," in *IEEE Transactions on Industrial Electronics*, vol. 62, no. 3, pp. 1515-1525, March 2015.
- [31] X. Guo, W. Liu, X. Zhang, X. Sun, Z. Lu and J. M. Guerrero, "Flexible Control Strategy for Grid-Connected Inverter Under Unbalanced Grid Faults Without PLL," in *IEEE Transactions on Power Electronics*, vol. 30, no. 4, pp. 1773-1778, April 2015.
- [32] F. Nejabatkhah, Y. W. Li and B. Wu, "Control Strategies of Three-Phase Distributed Generation Inverters for Grid Unbalanced Voltage

- Compensation," in *IEEE Transactions on Power Electronics*, vol. 31, no. 7, pp. 5228-5241, July 2016.
- [33] A. Camacho *et al.*, "Reactive power control for voltage support during type C voltage-sags," *IECON 2012 - 38th Annual Conference on IEEE Industrial Electronics Society*, Montreal, QC, 2012, pp. 3462-3467.
- [34] Z. Dai, H. Lin, H. Yin and Y. Qiu, "A novel method for voltage support control under unbalanced grid faults and grid harmonic voltage disturbances," in *IET Power Electronics*, vol. 8, no. 8, pp. 1377-1385, 8 2015.
- [35] J. Miret, A. Camacho, M. Castilla, J. L. García de Vicuña and J. de la Hoz, "Reactive current injection protocol for low-power rating distributed generation sources under voltage sags," in *IET Power Electronics*, vol. 8, no. 6, pp. 879-886, 6 2015.
- [36] A. Calle-Prado, S. Alepuz, J. Bordonau, J. Nicolas-Apruzzese, P. Cortés and J. Rodriguez, "Model Predictive Current Control of Grid-Connected Neutral-Point-Clamped Converters to Meet Low-Voltage Ride-Through Requirements," in *IEEE Transactions on Industrial Electronics*, vol. 62, no. 3, pp. 1503-1514, March 2015.
- [37] D. Shin, K. J. Lee, J. P. Lee, D. W. Yoo and H. J. Kim, "Implementation of Fault Ride-Through Techniques of Grid-Connected Inverter for Distributed Energy Resources With Adaptive Low-Pass Notch PLL," in *IEEE Transactions on Power Electronics*, vol. 30, no. 5, pp. 2859-2871, May 2015.
- [38] K. Kawabe and K. Tanaka, "Impact of Dynamic Behavior of Photovoltaic Power Generation Systems on Short-Term Voltage Stability," in *IEEE Transactions on Power Systems*, vol. 30, no. 6, pp. 3416-3424, Nov. 2015.
- [39] M. Mirhosseini, J. Pou and V. G. Agelidis, "Single- and Two-Stage Inverter-Based Grid-Connected Photovoltaic Power Plants With Ride-Through

- Capability Under Grid Faults," in *IEEE Transactions on Sustainable Energy*, vol. 6, no. 3, pp. 1150-1159, July 2015.
- [40] A. Calle-Prado, S. Alepuz, J. Bordonau, P. Cortes and J. Rodriguez, "Predictive Control of a Back-to-Back NPC Converter-Based Wind Power System," in *IEEE Transactions on Industrial Electronics*, vol. 63, no. 7, pp. 4615-4627, July 2016.
- [41] M. Shabestary, M. (2015). A Comparative Analytical Study on Low-Voltage Ride-Through Reference-Current-Generation (LVRT-RCG) Strategies in Converter-Interfaced DER Units (Master's thesis), University of Alberta.
- [42] M. M. Shabestary and Y. A. R. I. Mohamed, "An Analytical Method to Obtain Maximum Allowable Grid Support by Using Grid-Connected Converters," in *IEEE Transactions on Sustainable Energy*, vol. 7, no. 4, pp. 1558-1571, Oct. 2016.
- [43] A. Camacho, M. Castilla, J. Miret, J. C. Vasquez and E. Alarcon-Gallo, "Flexible Voltage Support Control for Three-Phase Distributed Generation Inverters Under Grid Fault," in *IEEE Transactions on Industrial Electronics*, vol. 60, no. 4, pp. 1429-1441, April 2013.
- [44] Kamran Sharifabadi; Lennart Harnfors; Hans-Peter Nee; Staffan Norrga; Remus Teodorescu, "Control under Unbalanced Grid Conditions," in *Design, Control and Application of Modular Multilevel Converters for HVDC Transmission Systems*, 1, Wiley-IEEE Press, 2016, pp.416-
- [45] R. Kabiri, D. G. Holmes and B. P. McGrath, "Control of Active and Reactive Power Ripple to Mitigate Unbalanced Grid Voltages," in *IEEE Transactions on Industry Applications*, vol. 52, no. 2, pp. 1660-1668, March-April 2016.
- [46] J. Miret, A. Camacho, M. Castilla, L. G. de Vicuña and J. Matas, "Control Scheme With Voltage Support Capability for Distributed Generation

- Inverters Under Voltage Sags," in *IEEE Transactions on Power Electronics*, vol. 28, no. 11, pp. 5252-5262, Nov. 2013.
- [47] T. L. Lee, S. H. Hu and Y. H. Chan, "D-STATCOM With Positive-Sequence Admittance and Negative-Sequence Conductance to Mitigate Voltage Fluctuations in High-Level Penetration of Distributed-Generation Systems," in *IEEE Transactions on Industrial Electronics*, vol. 60, no. 4, pp. 1417-1428, April 2013.
- [48] M. Castilla, J. Miret, A. Camacho, J. Matas and L. García de Vicuña, "Voltage Support Control Strategies for Static Synchronous Compensators Under Unbalanced Voltage Sags," in *IEEE Transactions on Industrial Electronics*, vol. 61, no. 2, pp. 808-820, Feb. 2014.
- [49] A. Camacho, M. Castilla, J. Miret, R. Guzman and A. Borrell, "Reactive Power Control for Distributed Generation Power Plants to Comply With Voltage Limits During Grid Faults," in *IEEE Transactions on Power Electronics*, vol. 29, no. 11, pp. 6224-6234, Nov. 2014.
- [50] Salvador Revelo, César A. Silva, "Current reference strategy with explicit negative sequence component for voltage equalization contribution during asymmetric fault ride through", *International Transactions on electrical Energy Systems*, Int. Trans. Electr. Energ. Syst. 2015; 25:3449–347
- [51] M. M. Shabestary and Y. A. R. I. Mohamed, "Analytical Expressions for Multiobjective Optimization of Converter-Based DG Operation Under Unbalanced Grid Conditions," in *IEEE Transactions on Power Electronics*, vol. 32, no. 9, pp. 7284-7296, Sept. 2017.
- [52] M. M. Shabestary and Y. A-R. I. Mohamed, "Advanced Voltage Support and Active Power Flow Control in Grid-Connected Converters under Unbalanced Conditions," in *IEEE Transactions on Power Electronics*, vol. 33, no. 2, pp. 1855-1864, Feb. 2018.
- [53] N. R. Merritt, C. Chakraborty and P. Bajpai, "New Voltage Control Strategies for VSC-Based DG Units in an Unbalanced Microgrid," in *IEEE*

*Transactions on Sustainable Energy*, vol. 8, no. 3, pp. 1127-1139, July 2017.

- [54] S. F. Chou, C. T. Lee, H. C. Ko and P. T. Cheng, "A Low-Voltage Ride-Through Method With Transformer Flux Compensation Capability of Renewable Power Grid-Side Converters," in *IEEE Transactions on Power Electronics*, vol. 29, no. 4, pp. 1710-1719, April 2014.
- [55] A. K. Pathak, M. P Sharma, Mahesh Bundele, "A critical review of voltage and reactive power management of wind farms", *Renewable and Sustainable Energy Reviews*, vol. 51, 2015.
- [56] M. Nasiri, J. Milimonfared, S.H. Fathi, "A review of low-voltage ride-through enhancement methods for permanent magnet synchronous generator-based wind turbines", *Renewable and Sustainable Energy Reviews*, vol. 47, 2015.
- [57] Abdul Motin Howlader, Tomonobu Senjyu, "A comprehensive review of low voltage ride through capability strategies for the wind energy conversion systems", *Renewable and Sustainable Energy Reviews*, vol. 56, p.p. 643-658, 2016.
- [58] X. Du, Y. Wu, S. Gu, H. M. Tai, P. Sun and Y. Ji, "Power oscillation analysis and control of three-phase grid-connected voltage source converters under unbalanced grid faults," in *IET Power Electronics*, vol. 9, no. 11, pp. 2162-2173, 9 7 2016.
- [59] X. Zhao, J. M. Guerrero, M. Savaghebi, J. C. Vasquez, X. Wu and K. Sun, "Low-Voltage Ride-Through Operation of Power Converters in Grid-Interactive Microgrids by Using Negative-Sequence Droop Control," in *IEEE Transactions on Power Electronics*, vol. 32, no. 4, pp. 3128-3142, April 2017.
- [60] D. Zhu, X. Zou, L. Deng, Q. Huang, S. Zhou and Y. Kang, "Inductance-Emulating Control for DFIG-Based Wind Turbine to Ride-Through Grid

- Faults," in *IEEE Transactions on Power Electronics*, vol. 32, no. 11, pp. 8514-8525, Nov. 2017.
- [61] T. Kauffmann, U. Karaagac, I. Kocar, S. Jensen, J. Mahseredjian and E. Farantatos, "An Accurate Type III Wind Turbine Generator Short Circuit Model for Protection Applications," in *IEEE Transactions on Power Delivery*, vol. 32, no. 6, pp. 2370-2379, Dec. 2017.
- [62] G. Rashid and M. H. Ali, "Nonlinear Control-Based Modified BFCL for LVRT Capacity Enhancement of DFIG-Based Wind Farm," in *IEEE Transactions on Energy Conversion*, vol. 32, no. 1, pp. 284-295, March 2017.
- [63] K. Oguma and H. Akagi, "Low-Voltage-Ride-Through (LVRT) Control of an HVDC Transmission System Using Two Modular Multilevel DSCC Converters," in *IEEE Transactions on Power Electronics*, vol. 32, no. 8, pp. 5931-5942, Aug. 2017.
- [64] I. Erlich, C. Feltes and F. Shewarega, "Enhanced Voltage Drop Control by VSC-HVDC Systems for Improving Wind Farm Fault Ride-Through Capability," in *IEEE Transactions on Power Delivery*, vol. 29, no. 1, pp. 378-385, Feb. 2014.
- [65] "E. ON-Netz, Grid Code, High and extra high voltage", April 2006. [Online] Available: <http://www.eon-netz.com>
- [66] R. K. Varma and E. M. Siavashi, "Enhancement of Solar Farm Connectivity with Smart PV Inverter PV-STATCOM," in *IEEE Transactions on Sustainable Energy*.
- [67] J. W. Smith, W. Sunderman, R. Dugan and B. Seal, "Smart inverter volt/var control functions for high penetration of PV on distribution systems," in Proc. IEEE PSCE, 2011, pp. 1-6.
- [68] "Common Functions for Smart Inverters, Version 3", EPRI Palo Alto, CA, Report No. 3002002233, Feb. 2014

- [69] B. Mather, “NREL/SCE High-Penetration PV Integration Project: Report on Field Demonstration of Advanced Inverter Functionality in Fontana, CA”, NREL Report NREL/TP-5D00-62483, 2014.
- [70] M. Morjaria, D. Anichkov, V. Chadliev, and S. Soni, “A Grid-Friendly Plant”, IEEE Power and Energy Magazine, May-June 2014, pp. 87-95
- [71] A. Kirakosyan, M. S. El Moursi, P. Kanjiya, V. Khadkikar, "A Nine Switch Converter-Based Fault Ride Through Topology for Wind Turbine Applications," in IEEE Transactions on Power Delivery, vol. 31, no. 4, pp. 1757-1766, Aug. 2016.
- [72] A. K. Pathak, M. P Sharma, M. Bundele, “A critical review of voltage and reactive power management of wind farms”, Renewable and Sustainable Energy Reviews, vol. 51, 2015.
- [73] M. Nasiri, J. Milimonfared, S.H. Fathi, “A review of low-voltage ride-through enhancement methods for permanent magnet synchronous generator-based wind turbines”, Renewable and Sustainable Energy Reviews, vol. 47, 2015.
- [74] A. M. Howlader, T. Senjyu, “A comprehensive review of low voltage ride through capability strategies for the wind energy conversion systems”, Renewable and Sustainable Energy Reviews, vol. 56, 2016.
- [75] Energinet, “Wind turbines connected to grids with voltages below 100 kV” Regulation TF 3.2.6., May 2004.
- [76] Industry, Tourism and Commerce Spanish Ministry, “Operation Procedure O.P. 12: Response requirements in front of voltage dip at wind farms utilities. BOE 254, 37017- 37019”, October, 2006.
- [77] “The grid code, issue 3, rev. 24”, National Grid Electricity Transmission plc, UK, October 2008.
- [78] ”Grid code–version 3.0”, ESB National Grid, Ireland, September 2007.

- [79] Beijing General Administration of Quality Supervision Inspection and Quarantine and Standardization Administration of China, “Technical Rule for Connecting Wind Farm to Power System: GB/T 19963”, China, 2011.
- [80] M. Tsili and S. Papathanassiou, "A review of grid code technical requirements for wind farms," in *IET Renewable Power Generation*, vol. 3, no. 3, pp. 308-332, Sept. 2009.
- [81] General Electric Energy, “Technical Requirements for Wind Generation Interconnection and Integration-New England Wind Integration Study”, Schenectady, New York, 2009.
- [82] W. Lasher, “Summary of Significant Wind-Plant Requirements in ERCOT”, North American Electric Reliability Corporation, 2010.
- [83] “VDE-AR-N 4120, Technical requirements for the connection and operation of customer installations to the high voltage network (TAB high voltage)”, Germany, Jan. 2015.
- [84] T. Neumann, T. Wijnhoven, G. Deconinck, I. Erlich, "Enhanced Dynamic Voltage Control of Type 4 Wind Turbines During Unbalanced Grid Faults," in *IEEE Trans. on Energy Conversion*, vol. 30, no. 4, Dec. 2015.
- [85] X. Liang and J. Hofman, "Trip Curves and Ride-Through Evaluation for Power Electronic Devices in Power System Dynamic Studies," in *IEEE Trans. on Industry Applications*, vol. 52, no. 2, March-April 2016.
- [86] *Nordic Grid Code*, 15 January 2007. [Online]. Available: [www.entsoe.eu](http://www.entsoe.eu)
- [87] L. Asiminoaei, R. Teodorescu, F. Blaabjerg, U. Borup, “A digital controlled PV inverter with grid impedance estimation for ENS detection,” *IEEE Trans. Power Electron.*, vol. 20, no. 11, Nov. 2005.
- [88] S. Cobreces, E. Bueno, D. Pizarro, F. Rodriguez, F. Huerta, “Grid impedance monitoring system for distributed power generation electronic interfaces,” *IEEE Trans. Instrum. Meas.*, vol. 58, no. 9, Sep. 2009.

- [89] N. Hoffmann and F. W. Fuchs, "Minimal invasive equivalent grid impedance estimation in inductive-resistive power-networks using extended Kalman-filter," *IEEE Trans. Power Electron.*, vol. 29, no. 2, pp. 631–641, Feb. 2014.
- [90] Bernard S., Beaulieu D., Trudel G.: 'Hydro-Que'bec grid code for wind farm interconnection'. Proc. IEEE Power Engineering Society General Meeting, San Francisco, 2005.
- [91] M. M. Shabestary, S. Mortazavian and Y. I. Mohamed, "Overview of Voltage Support Strategies in Grid-Connected VSCs under Unbalanced Grid Faults Considering LVRT and HVRT Requirements," 2018 IEEE International Conference on Smart Energy Grid Engineering (SEGE), Oshawa, ON, 2018, pp. 145-149.
- [92] M. M. Shabestary, Y. A-R. I. Mohamed, "Asymmetrical Ride-Through (ART) and Grid-Support in Converter-Interfaced DG Units under Unbalanced Conditions," *IEEE Transactions on Industrial Electronics*, vol. 66, no. 2, pp. 1130-1141, Feb. 2019.
- [93] Y. Zhang and H. Ma, "Theoretical and experimental investigation of networked control for parallel operation of inverters," *IEEE Trans. Ind. Electron.*, vol. 59, no. 4, pp. 1961–1970, Apr. 2012.
- [94] Z. Chen, X. Pei, M. Yang and L. Peng, "An Adaptive Virtual Resistor (AVR) Control Strategy for Low-Voltage Parallel Inverters," in *IEEE Transactions on Power Electronics*, vol. 34, no. 1, pp. 863-876, Jan. 2019.
- [95] M. Hua, H. B. Hu, Y. Xing, and J. M. Guerrero, "Multilayer control for inverters in parallel operation without intercommunications," *IEEE Trans. Power Electron.*, vol. 27, no. 8, pp. 3651–3663, Aug. 2012.
- [96] M. S. Taha, H. H. Abdeltawab and Y. A. I. Mohamed, "An Online Energy Management System for a Grid-Connected Hybrid Energy Source," in *IEEE Journal of Emerging and Selected Topics in Power Electronics*, vol. 6, no. 4, pp. 2015-2030, Dec. 2018.

- [97] P. Shanthi, G. Uma and M. S. Keerthana, "Effective power transfer scheme for a grid connected hybrid wind/photovoltaic system," in *IET Renewable Power Generation*, vol. 11, no. 7, pp. 1005-1017, 7 6 2017.
- [98] K. Sun, X. Wang, Y. W. Li, F. Nejabatkhah, Y. Mei and X. Lu, "Parallel Operation of Bidirectional Interfacing Converters in a Hybrid AC/DC Microgrid Under Unbalanced Grid Voltage Conditions," in *IEEE Transactions on Power Electronics*, vol. 32, no. 3, pp. 1872-1884, March 2017.
- [99] C. Wang, P. Yang, C. Ye, Y. Wang and Z. Xu, "Voltage Control Strategy for Three/Single Phase Hybrid Multimicrogrid," in *IEEE Transactions on Energy Conversion*, vol. 31, no. 4, pp. 1498-1509, Dec. 2016.
- [100] Y. Han, P. Shen, X. Zhao and J. M. Guerrero, "An Enhanced Power Sharing Scheme for Voltage Unbalance and Harmonics Compensation in an Islanded AC Microgrid," in *IEEE Transactions on Energy Conversion*, vol. 31, no. 3, pp. 1037-1050, Sept. 2016.
- [101] J. He, Y. W. Li and F. Blaabjerg, "An Enhanced Islanding Microgrid Reactive Power, Imbalance Power, and Harmonic Power Sharing Scheme," in *IEEE Transactions on Power Electronics*, vol. 30, no. 6, pp. 3389-3401, June 2015.
- [102] H. Dong, S. Yuan, Z. Han, X. Ding, S. Ma and X. Han, "A Comprehensive Strategy for Power Quality Improvement of Multi-Inverter-Based Microgrid With Mixed Loads," in *IEEE Access*, vol. 6, pp. 30903-30916, 2018.
- [103] Y. Han, H. Li, P. Shen, E. A. A. Coelho and J. M. Guerrero, "Review of Active and Reactive Power Sharing Strategies in Hierarchical Controlled Microgrids," in *IEEE Transactions on Power Electronics*, vol. 32, no. 3, pp. 2427-2451, March 2017.
- [104] SOLAR INVERTERS, ABB central inverters, PVS980 – 1818 to 2091 kVA. Available: <https://library.e.abb.com/public>

- [105] M. Bahramipناه, et al., "A Decentralized Adaptive Model-Based Real-Time Control for Active Distribution Networks Using Battery Energy Storage Systems," *IEEE Transactions on Smart Grid*, vol. 9, no. 4, July 2018.
- [106] Q. Xu, et al., "A Decentralized Control Strategy for Economic Operation of Autonomous AC, DC, and Hybrid AC/DC Microgrids," in *IEEE Transactions on Energy Conversion*, vol. 32, no. 4, pp. 1345-1355, Dec. 2017.
- [107] Q. Xu, et al., "A Decentralized Power Management Strategy for Hybrid Energy Storage System With Autonomous Bus Voltage Restoration and State-of-Charge Recovery," in *IEEE Trans. on Industrial Electronics*, vol. 64, 9, 2017.
- [108] T. Tsuji et al., "A study of centralized voltage profile control of distribution network considering dynamics of distributed generator," *Elect. Eng. Japan*, vol. 179, no. 1, pp. 29–39, Apr. 2012.
- [109] Q. Fu et al., "Microgrid generation capacity design with renewables and energy storage addressing power quality and surety," *IEEE Transactions on Smart Grid*, vol. 3, no. 4, pp. 2019–2027, Dec. 2012.
- [110] X. Zhao, et al, "LVRT Operation of Converters in Grid-Interactive Microgrids Using Negative-Seq. Droop Control," *IEEE Trans. Power Elect.*, 32, 4, 2017.
- [111] M. Hamzeh, et al, "Harmonic and Negative-Sequence Current Control in an Islanded Multi-Bus Microgrid," *IEEE Transactions on Smart Grid*, 5, 1 2014.
- [112] M. Savaghebi, et al, "Secondary Control Scheme for Voltage Unbalance Compensation in an Islanded Droop-Controlled Microgrid," *IEEE Transactions on Smart Grid*, vol. 3, no. 2, pp. 797-807, June 2012.

- [113] M. Hamzeh, et al, "A New Control Strategy for a Multi-Bus MV Microgrid Under Unbalanced Conditions," *IEEE Trans. on Power Systems*, 27, 4, 2012.
- [114] L. Meng *et al.*, "Distributed Voltage Unbalance Compensation in Islanded Microgrids by Using a Dynamic Consensus Algorithm," in *IEEE Transactions on Power Electronics*, vol. 31, no. 1, pp. 827-838, Jan. 2016.
- [115] F. Berthold, et al, "A multi-agent approach to radial feeder voltage control of PEBB-based converter: A real time simulation test," in Proc. IEEE Energy Convers. Congr. Expo. (ECCE), Raleigh, NC, USA, 2012.
- [116] F. Guo, et al, "Distributed economic dispatch for smart grids with random wind power," *IEEE Trans. on Smart Grid*, vol. 7, no. 3, pp. 1572–1583, May 2016.
- [117] G. Binetti, et al, "Distributed consensus-based economic dispatch with transmission losses," *IEEE Trans. on Power Syst.*, vol. 29, no. 4, Jul. 2014.
- [118] M. Arani, and Y. A.-R. I. Mohamed "Assessment and Enhancement of a Full-Scale PMSG-Based Wind Power Generator Performance Under Faults," in *IEEE Transactions on Energy Conversion*, vol. 31, no. 2, pp. 728-739, June 2016.